AN INVESTIGATION OF NATIVE COPPER IN PLAGIOCLASE, LAKE AND HARNEY COUNTIES, OREGON

By

Çisil Bengisu Badur

A thesis submitted to the Graduate Faculty of
Auburn University
in partial fulfillment of the
requirements for the Master of Science
Degree in Geology

Auburn, Alabama

May 7th, 2022

Keywords: Sunstone, copper, Columbia River Basalt Group, Steens Basalt

Copyright 2022 by Çisil Bengisu Badur

Approved by

Dr. Willis Hames (Chair), Professor, Geosciences
Dr. Laura Bilenker, Assistant Professor, Geosciences
Dr. Haibo Zou, Professor, Geosciences

ABSTRACT

Mafic igneous rocks are commonly associated with various metals and there are many examples of basalts that host small amounts of native copper. Such copper is more common among the matrix phases of basalts and could represent a final stage of a melt or a secondary alteration. Worldwide, there are only a few occurrences of copper within early-crystallizing phenocrysts of plagioclase, and this fact makes the 'sunstones' of Oregon as interesting as they are spectacularly beautiful. The native copper in these 'sunstones' occurs as thin platelets (copper schiller) with crystallographically-controlled orientations. These copper platelets appear to have formed via the exsolution of metallic copper and are typically found in the cores of the highest-grade gemstones. The age of the sunstone host basalts has previously been uncertain. Also, there has been little petrographic or geochemical characterization of the basalts hosting the sunstones. The objectives of this thesis were to determine the age and provide an improved petrographic, petrologic and geochemical characterization of the host basalt. These labradorite megacrysts (~An_{67}) have strikingly homogeneous major and trace element distributions and internally homogeneous $^{87}Sr/^{86}Sr$ ratios, similar to those observed in plagioclase phenocrysts of the Columbia River Basalt Group's Steens Basalt (~16.7 Ma). The homogeneous nature of all these data suggests that following copper exsolution, the crystals have not experienced significant chemical change (diffusive mass transport, alteration, weathering). This research determined the age of the basalt hosting sunstones. The means of four matrix plateaus is 9.16±0.12 Ma (95% c.l., MSWD=1.13). These late Miocene plateau ages are comparable to lavas of the High Lava Plains Trend but are distinctly younger than the Steens Basalt. In addition, this research illustrated a simple sunstone development hypothesis.

ACKNOWLEDGMENTS

I would like to thank the following people, who have helped me immeasurably in my research and academics during my master's degree at Auburn University. First and foremost, I would like to offer my profound thanks to my advisor professor, Dr. Willis E. Hames, for his assistance in the learning, experimentation, and thesis-writing phase of my research. Furthermore, he also provided me with the valuable technical know-how of using the Electron Microprobe Analyzer (EMPA) which will help me greatly in my future research career. I would like to express my gratitude to Dr. Laura Bilenker and Dr. Haibo Zou for agreeing to serve on my thesis committee. Their contributions and suggestions to my research, considering their all-encompassing knowledge of geochemistry and petrology have benefitted me greatly. I also would like to thank Dr. Emily Cahoon for her contributions to the samples used in this research, guidance, and support. I wish to thank Dr. George Kamenov for contributing not only samples and valuable data, but also his inspiring ideas to my thesis. I also thank various miners that have shared samples. I would like to thank my lab mate, Dogancan Yasar, who provided his support and his assistance in the laboratory and thank Marisa Barefoot for her assistance during the thesis-writing process and her kind friendship. I also thank Ved Soni from Auburn University Graduate Writing Partners (GWP) program for his assistance. I also wish to thank the Department of Geosciences of Auburn University and acknowledge the partial funding that was provided through Auburn University Geosciences Advisory Board (GAB). I would like to express my gratitude to the Turkish Ministry of National Education, and the General Directorate of Mineral Research and Exploration for supporting my graduate studies and research. Finally, I am very much thankful to my parents - Hülya and Hilmi Badur - for their love and sacrifices for educating and preparing me for my future.

TABLE OF CONTENTS

ABSTRACT 2
ACKNOWLEDGMENTS 3
TABLE OF CONTENTS 4
LIST OF FIGURES 6
LIST OF TABLES 8
LIST OF ABBREVIATIONS 9
INTRODUCTION 10
  Background 10
    Sunstone locations, geologic setting, and possible associated basalt flows 10
    Oregon Sunstones 17
    Concerning Native Copper and Ionic Copper in Minerals 24
    Concerning Plagioclase, and Huttenlocher Exsolution 26
    Previous Research Relevant to Copper Diffusion, and Al-Si Ordering in Lake County and Harney County Plagioclase 27
  Objectives of this Study 30
MATERIALS AND METHODS 31
RESULTS 32
  Petrology 32
    Electron Microprobe Data 32
  Geochemistry 39
    $^{87}Sr/^{86}Sr$ Data 39
    REE/Trace Element Data 41
  Age Determinations 42
    $^{40}Ar/^{39}Ar$ Data 42
DISCUSSION 48
PROPOSED ADDITIONAL RESEARCH 50
  Hypothesis of Sunstone Development 51
CONCLUSION 52
REFERENCES 53
APPENDIX 1 56
  EMPA Methods for Feldspar and Pyroxene 56

Oxide Weight Percent Values for Wollastonite and Diopside Standards Used for the Preceding Analyses ... 57
EMPA Data from Plagioclase Megacrysts ... 58
EMPA Data from Fine Matrix Plagioclase ... 60
EMPA Data from Finely Grained Pyroxene Crystals of Matrix ... 64
APPENDIX 2 ... 68
Laboratory Description and Monitors ... 68
J-Values used for layers 2 and 3 on the basis of GA-1550 and FCS analyses ... 71
Analysis of Air During This Project ... 71
Result of Matrix $^{40}Ar/^{39}Ar$ Dating ... 72
Result of Broken Pieces Plagioclase $^{40}Ar/^{39}Ar$ Dating ... 74
Result of Single Megacryst Plagioclase $^{40}Ar/^{39}Ar$ Dating ... 76

LIST OF FIGURES

Figure 1. This map indicates three regions of occurrence for samples of copper-bearing plagioclase in eastern Oregon. Modified illustration by Larry Lavitt ("Three Occurrences of Oregon Sunstone | Gems & Gemology")... 11

Figure 2: Map of the region for eruption of the Middle Miocene Columbia River Basalt (CRB) Province of the Yellowstone Hotspot. The light gray shaded region shows the approximate extent of mid-Miocene flood basalts. The (x) indicates the region of occurrence for samples of copper-bearing plagioclase (sunstone occurrences), within the western younging High Lava Plains Trend (HLPT) (from Hames et al., 2009). (Other abbreviations for the region are defined in Hames et al., 2009). 12

Figure 3. Map of the region Oregon High Lava Plains (HLP). The four stars, Sunstone occurrences, illustrate where four basalt matrix samples (LEB-001, LEB-003, and DE16-001, SW19-DD01) were taken from. Figure Legend: The High Cascade stratovolcanoes (A), flood basalts (B), volcanic calderas (C), renewed activity (D), Newberry Caldera (N), Yellowstone supervolcano (Y), Abert Rim (AR), Steens Mountain (SM), Snake River Plain (SRP), Illustration by Larry Lavitt, adapted from Long (2009) and Grunder and Meigs (2009). ("Three Occurrences of Oregon Sunstone | Gems & Gemology") 14

Figure 4. Samples of basalt porphyry from Dust Devil #16 Mine. 4A: A gem quality sunstone crystal surrounded by small and non-gem quality feldspar crystals. 4B: A highly altered porphyry basalt consisting of large crystals of non-gem quality labradorite crystals. 15

Figure 5. Microscope images of altered basalt and groundmass labradorite crystals. 5A. LEB-003 - Little Eagle Butte (the southern Plush area) - Whole-rock sample. 5B. DE16-001 - Double Eagle (the southern Plush area) - Whole-rock sample.. 16

Figure 6. Gem-quality Oregon Sunstones collected from Double Eagle #16 Mine. 6A: The reddish copper core is surrounded by the green color of protoenstatite. 6B: Blocky labradorite feldspar crystal within the host basalt. 6C: Some of the highest quality Oregon Sunstones have differed in the color pink (champagne), red, green... 18

Figure 7. Gem-quality Oregon Sunstone looking down along the normal of (001), and along b-axis [010]. Notice the extremely clear rim in image 7A along with the color zoning. In some crystals, a green border becomes brownish-red when looking down along the normal of (001). The inset in 7A illustrates the specifics of the red to green transition (~4 mm thick) (Modified from (Xu et al., 2017). 7B: Labradoritic 'sunstone' samples from the Dust Devil Mine (samples of this study). (*****) Some crystals contain a green rim (protoenstatite) or a cloudy zone around the copper core.. 19

Figure 8. Double Eagle #16 Mine. 8A: Some of the top-quality schiller Oregon Sunstones. 8B: Digging area with Mr. Aldrich who is the owner of the Double Eagle Mine.............................. 22

Figure 9. Ponderosa Mine. 9A: The mine operations. 9B: Digging area with Dr. Emily Cahoon (flow is outlined). 9C: Note that it contains angular plagioclase crystal fragments and "bombs" of basalt (black). Vertical gouges and scour marks are from mining equipment. 9D: The close image of basaltic rock fragment that contains Oregon Sunstone (white arrow)........................... 23

Figure 10. Native copper inclusions in Oregon Sunstone crystal (PMC-2) taken from Ponderosa Mine. Magnification level increases from 10A to 10D.This section is cut parallel to (010)........ 24

Figure 11. Higher magnification images of plagioclase megacrysts (PMC-2). 11A & 11B have different local planes of the same area, as do 11C & 11D... 25

Figure 12. 12A: Transmitted-light photomicrographs of polished single-crystals of plagioclase. 12B: Corresponding Cu diffusion profiles were determined along with three perpendicular directions. 12C: Measured Cu diffusion coefficients in plagioclase compared to published diffusion coefficients of other elements (Audétat et al., 2018).. 28

Figure 13. Lake County sunstone structures before (13A) and after (13B) heating treatment. The center of the I1-like domain is shown by the red planes (Jin et al., 2019). 29

Figure 14. 14A: Photograph of a plagioclase crystal (from Dust Devil Mine (GK-DD-1), the southern Plush area) mounted in epoxy, showing the copper ‘schiller’ effect created by thin lamellae of copper. The approximate area for ‘Cu Lamellae’ is shown (exaggerated). This study sample was provided by Dr. George Kamenov of the University of Florida. 14B: Electron microprobe WDS map for the distribution of copper, in and around a single copper lamellae. .. 33

Figure 15. Electron microprobe analyses of plagioclase and copper, with atoms per formula unit (pfu) indicated along section x-x' of figure 14. Electron microprobe data were obtained by using the AU Geosciences Department EMPA... 34

Figure 16. Auburn University Electron Microprobe Analyzer (AU-EMPA).............................. 35

Figure 17. A feldspar ternary diagram of EMPA analyses for plagioclase megacrysts (n=11). The data were obtained by analyses of core and rim show no distinct differences in composition. ... 36

Figure 18. A feldspar ternary diagram of EMPA analyses for fine matrix plagioclase (n=160). Note that the matrix plagioclase composition varies from labradorite to andesine/oligoclase in the same samples. 37

Figure 19. Backscattered Electron (BSE) images of sample of LEB-003. 'Image-J' was used in order to assign false color. Note that increasing Na and decreasing Al contents of matrix plagioclase from core to rim. These variations are responsible for the variations shown in Figure 18.. 37

Figure 20. Pyroxene ternary diagram of 39 pyroxene analyses from the microprobe data. Wo: wollastonite, En: enstatite, Fs: ferrosillite... 38

Figure 21. Measurement locations for the $^{87}Sr/^{86}Sr$ variation diagram in figure 21B (from A to A´) that was obtained at the University of Florida with the plagioclase crystal sample provided by Dr. George Kamenov. 21B: $^{87}Sr/^{86}Sr$ variation diagram obtained by TIMS and LA-ICP-MS analysis of a sunstone from its Cu-free rim to Cu-bearing core. This is the same crystal that microprobe data is presented for in Figure 15. 40

Figure 22. Chondrite-normalized REE diagram. 41

Figure 23. $^{40}Ar/^{39}Ar$ data from LEB-001. A: Data are shown on an inverse isochron plot. B: Apparent $^{40}Ar^{*}$ - Ca/K plot. C: $^{40}Ar/^{39}Ar$ incremental heating age spectrum for about 20 plagioclase crystal fragments from matrix. Results of individual age spectra are quoted at the 1-sigma confidence level. 44

Figure 24. $^{40}Ar/^{39}Ar$ data from LEB-003. A: Data are shown on an inverse isochron plot. B: Apparent $^{40}Ar^{*}$ - Ca/K plot, C: $^{40}Ar/^{39}Ar$ incremental heating age spectrum for about 20 plagioclase crystal fragments from matrix. 45

Figure 25. $^{40}Ar/^{39}Ar$ data from DE16-001. A: Data are shown on an inverse isochron plot. B: Apparent $^{40}Ar^{*}$ - Ca/K plot. C: $^{40}Ar/^{39}Ar$ incremental heating age spectrum for about 20 plagioclase crystal fragments from matrix. 46

Figure 26. $^{40}Ar/^{39}Ar$ data from SW19-DD01. A: Data are shown on an inverse isochron plot. B: Apparent $^{40}Ar^{*}$ - Ca/K plot. C: $^{40}Ar/^{39}Ar$ incremental heating age spectrum for about 20 plagioclase crystal fragments from matrix. 47

Figure 27. Magma chamber wherein the phenocrysts were grown and hypothesis of sunstone development. 52

LIST OF TABLES

Table 1. Physical Properties of Oregon Sunstones (“Oregon Sunstone Value, Price, and Jewelry Information - Gem Society”). 21

Table 2. Whole-rock and plagioclase samples used for the analyses. 32

LIST OF ABBREVIATIONS

ANIMAL	Auburn Noble Isotope Mass Analysis Lab
CRBG	Columbia River Basalt Group
Cu	copper
cm	centimeter
D	partition coefficients
EMPA	Electron Microprobe Analyzer
g	gram
HLP	High Lava Plains
LA-ICP-MS	Laser Ablation Inductively Coupled Plasma Mass Spectrometry
m	meter
NGB	Northern Great Basin
ppm	parts per million
REE	Rare Earth Element
SM	Steens Mountain
WDS	Wavelength-Dispersive Spectroscopy
yr	year

INTRODUCTION

Although feldspar is one of the most abundant minerals found in the Earth's crust, gem-quality feldspars are rare. Moonstone, amazonite, andesine, orthoclase, and sunstone are some of the most well-known feldspar gemstones. Labradorite megacrysts (sunstones) which include macroscopic inclusions of native copper are locally hosted in basaltic lavas across Central and Eastern Oregon. As noted by Hofmeister and Rossman, (1985), the native copper forms as thin platelets (copper schiller) with crystallographically controlled orientations in these sunstones. These copper platelets appear to have formed by exsolution and are commonly observed in the centers of high-quality gemstones. The research goals of this thesis are to determine the age and provide a basic petrographic, petrologic and geochemical characterization of the host basalt in order to enhance the understanding of the copper-bearing plagioclase.

Background

Sunstone locations, geologic setting, and possible associated basalt flows

There are currently three important gem-quality labradorite deposits in Oregon (Fig. 1). One of the sunstone deposits is the Ponderosa Mine which is smaller and occurs in south-central Oregon near the White Horse Ranch, in northwest Harney County (Johnston et al., 1991). The other two deposits are the Dust Devil and Sunstone Butte mines, both of which are nearly 120 miles further south, in Lake County. These last two deposits are referred to in the literature as the Plush, Lakeview, Lake County, Rabbit Hills, or Rabbit Basin occurrences (Johnston et al., 1991).

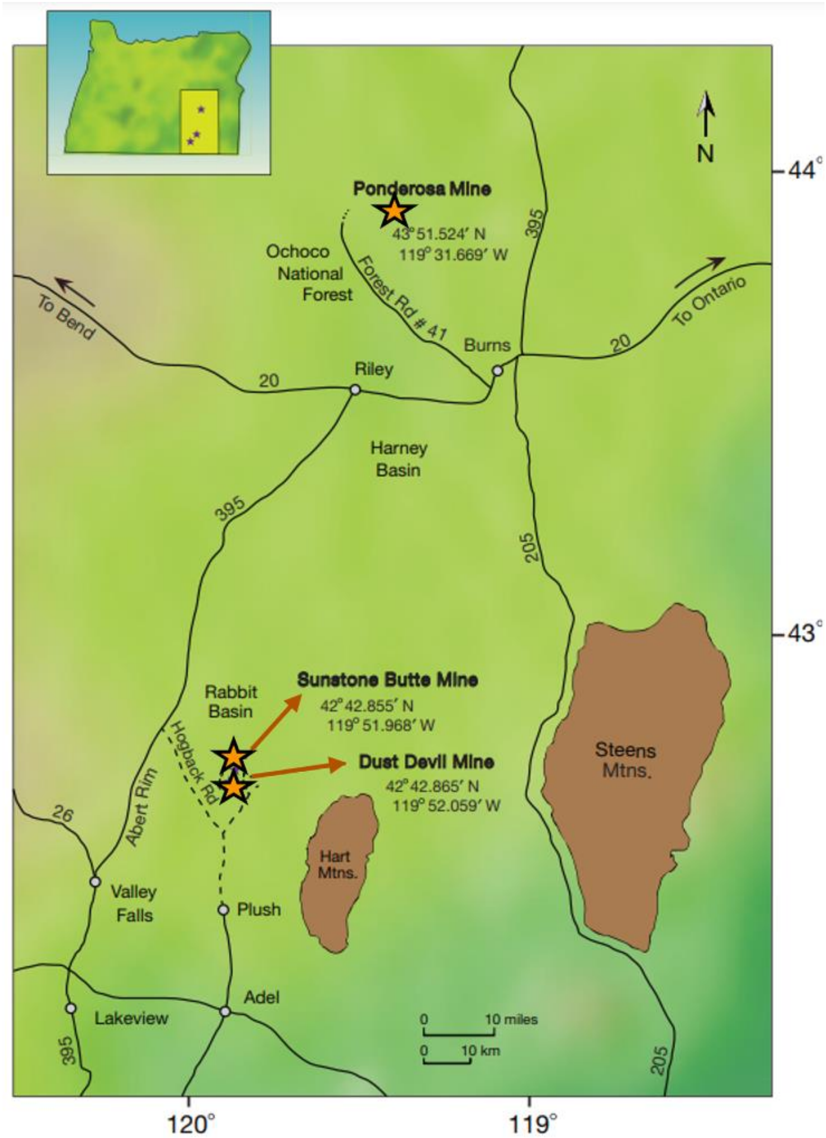

Figure 1. This map indicates three regions of occurrence for samples of copper-bearing plagioclase in eastern Oregon. Modified illustration by Larry Lavitt ("Three Occurrences of Oregon Sunstone | Gems & Gemology").

Oregon Sunstones are copper-bearing feldspar most commonly found in highly porphyritic basaltic lavas previously associated with the Columbia River Basalt Group (CRBG). The Columbia River Basalt Group (Fig. 2) is the youngest, smallest and most well preserved continental flood basalt province on Earth occupying more than 210,000 km^2, primarily in eastern Oregon and Washington, western Idaho and part of northern

Nevada. The Northern Great Basin (NGB) is associated with bimodal volcanism in the middle Miocene, which is related to a mantle plume that has now migrated to the Yellowstone Region (Brueseke et al., 2007).

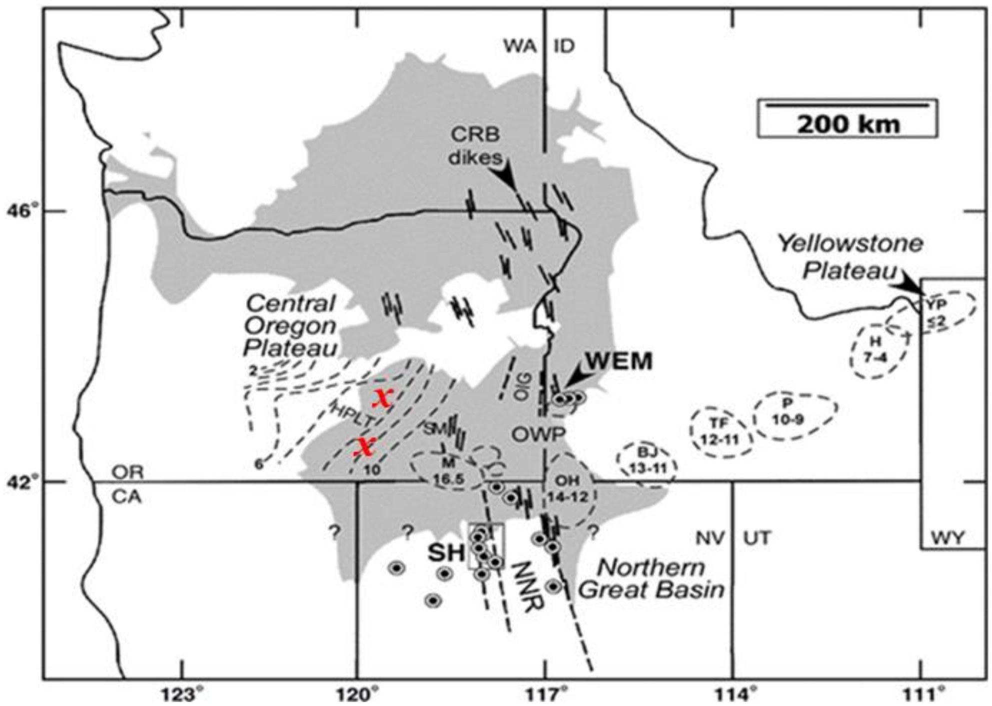

Figure 2: Map of the region for eruption of the Middle Miocene Columbia River Basalt (CRB) Province of the Yellowstone Hotspot. The light gray shaded region shows the approximate extent of mid-Miocene flood basalts. The (x) indicates the region of occurrence for samples of copper-bearing plagioclase (sunstone occurrences), within the western younging High Lava Plains Trend (HLPT) (from Hames et al., 2009). (Other abbreviations for the region are defined in Hames et al., 2009).

The Steens Basalt is a member of the Columbia River Basalt Group, with lava flows reaching ~50,000 km^2 on the Oregon Plateau (Jarboe et al., 2008) that comprises tholeiitic to slightly alkaline basalt and basaltic andesites. Some of the products of the oldest eruptions of this magmatic episode have been seen in this basaltic region. (Fig. 2). The Steens Basalt is a ~16.7 Ma flood basalt sequence that erupted through the Oregon Plateau prior to shifting to the central location of Steens Mountain, Oregon (Brueseke et al., 2007; Camp et al., 2013). Lavas of the Steens Basalt vary from aphyric to coarsely plagioclase phyric with some basalts that include up to 50 percent plagioclase mega-crystals (Johnston et al., 1991; Brueseke et al., 2007; Camp et al., 2013). Jarboe et al. (2008) showed that many erupted lava flows of the Steens Basalt formed in a short time interval and permit detailed observations of the magnetic field direction and paths. Comparison of $^{40}Ar/^{39}Ar$ ages and the geomagnetic polarity timescale suggests one reversal of the geomagnetic field during the Steens Basalt's eruption. The combined studies of Brueseke et al. (2007) and Jarboe et al. (2008) suggest that the Steens Basalt erupted during just a few hundred thousand years on the Oregon Plateau at approximately 16.7 Ma.

The High Lava Plains (HLP) is a volcanic province that has a westward younging trend of silicic volcanism and is characterized by bimodal volcanism (Fig. 3) (Jordan et al., 2004). The High Lava Plains trends emerged from the axis of the Steens Basalts middle Miocene basaltic volcanism. These basalts have been identified in varying time periods ranging from 2 to 10 Ma. Thus, the HLP and middle Miocene flood basalts appear to be closely related. The geochronologic results obtained by Jordan et al. (2004) confirm that the pattern of HLP silicic volcanism has a westward migration.

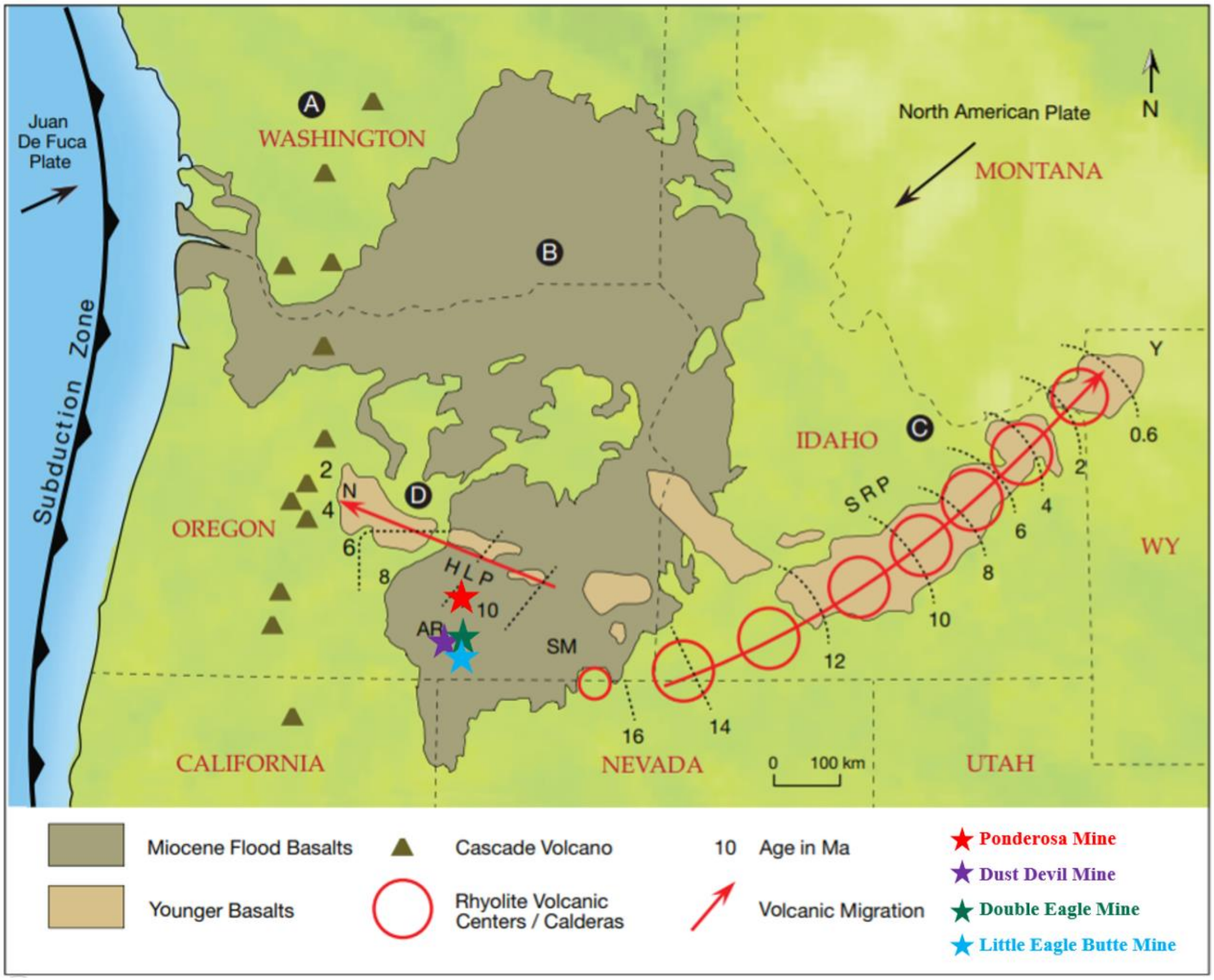

Figure 3. Map of the region Oregon High Lava Plains (HLP). The four stars, Sunstone occurrences, illustrate where four basalt matrix samples (LEB-001, LEB-003, and DE16-001, SW19-DD01) were taken from. Figure Legend: The High Cascade stratovolcanoes (A), flood basalts (B), volcanic calderas (C), renewed activity (D), Newberry Caldera (N), Yellowstone supervolcano (Y), Abert Rim (AR), Steens Mountain (SM), Snake River Plain (SRP), Illustration by Larry Lavitt, adapted from Long (2009) and Grunder and Meigs (2009). ("Three Occurrences of Oregon Sunstone | Gems & Gemology")

The basaltic lavas hosting sunstones are highly altered and oxidized (Fig. 4 and Fig. 5) and as noted previously, the timing of extrusion for the host basalts of the sunstones is currently unconstrained. Many plagioclase megacrysts of ~2-4 cm diameter in these basaltic lavas host noticeable native copper inclusions (Hofmeister and Rossman, 1985a; Wierman, 2018). In addition to plagioclase megacrysts, altered and oxidized basaltic lavas also include non-gem quality plagioclase crystals of several sizes.

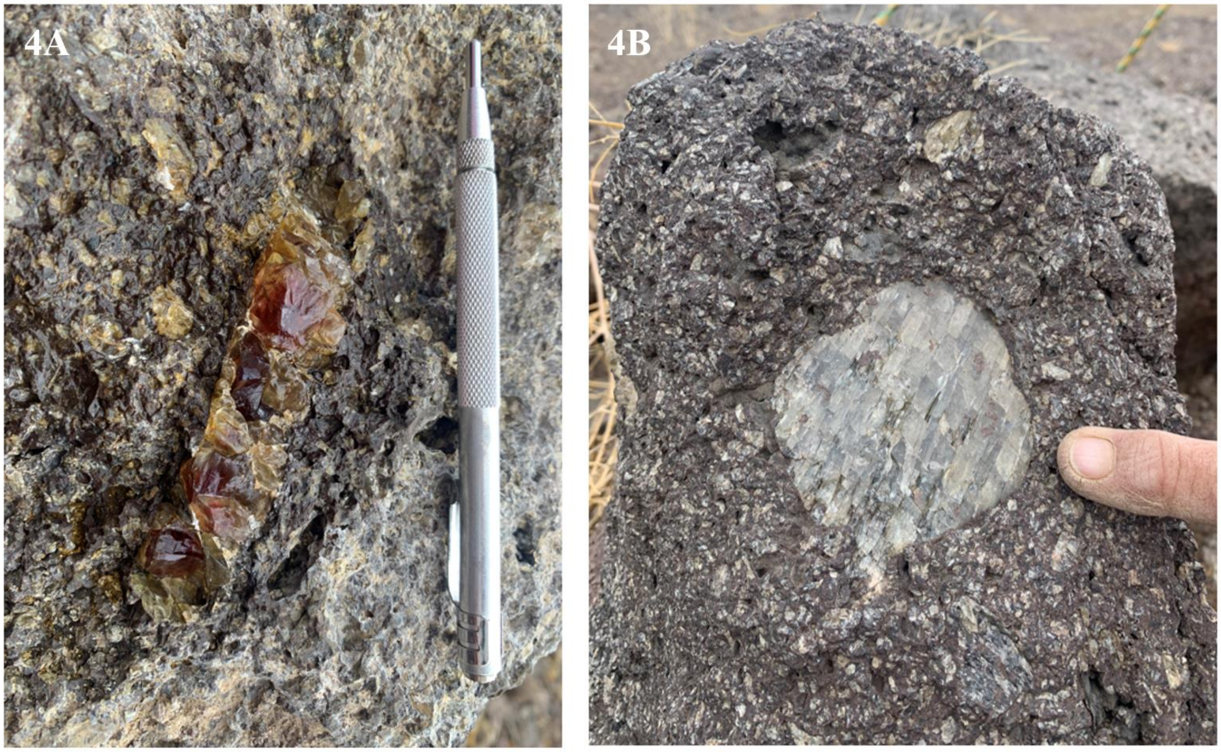

Figure 4. Samples of basalt porphyry from Dust Devil #16 Mine. 4A: A gem quality sunstone crystal surrounded by small and non-gem quality feldspar crystals. 4B: A highly altered porphyry basalt consisting of large crystals of non-gem quality labradorite crystals.

Figure 5 shows microscope images of altered basalt and groundmass labradorite crystals taken from the southern Plush area. While these fine pieces of groundmass plagioclase range from labradorite to andesine (majorly labradorite), the megacrysts in basaltic lavas are labradorite (Hofmeister and Rossman, 1985a). Both megacryst and groundmass labradorite crystals were fractionated from melts with similar composition (Welch et al., 2019). According to Stewart et al. (1966), highly porphyritic basalt hosting sunstones within the Rabbit Basin (southern sunstone locations) are not only petrographically similar but also temporally and spatially correlative with plagioclase-rich flows of the Steens Basalt of CRBG. The elemental composition of the basalts of 'Harney County' (the northernmost sunstone location) hosting the sunstones is similar to the Picture Gorge basalts of the CRB suite (E. Cahoon, pers. comm., 2020), but this may only indicate that they formed from similar sources. According to Badur (2020), results of $^{40}Ar/^{39}Ar$ ages show that the basalt matrix ages of the 'Rabbit Basin' hosting sunstones seem comparable to lavas of the High Lava Plain Trend but are much younger than the Steens Basalt.

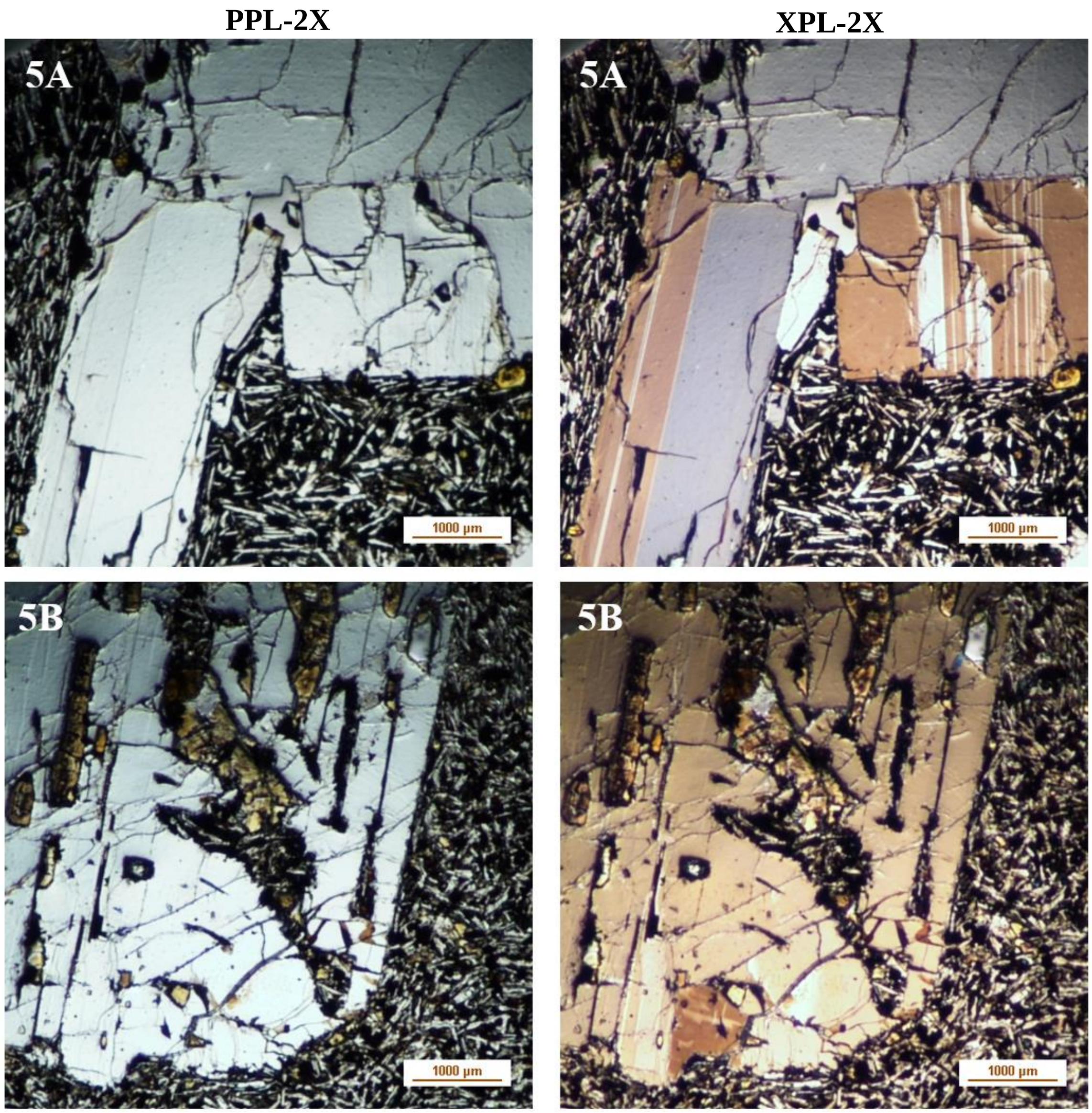

Figure 5. Microscope images of altered basalt and groundmass labradorite crystals. 5A. LEB-003 - Little Eagle Butte (the southern Plush area) - Whole-rock sample. 5B. DE16-001 - Double Eagle (the southern Plush area) - Whole-rock sample.

Oregon Sunstones

The Oregon legislature named sunstone as the state gem in 1985 (Hofmeister and Rossman, 1985). The reason for this is that the native copper inclusions in plagioclase are found almost exclusively in the sunstones of Oregon. The Oregon Sunstone (Fig. 6) was first characterized by Andersen (1917) and by Hofmeister and Rossman (1985), who discovered that the copper plates had a minimum of 90% purity. The rarest and valuable sunstone group is the colored sunstone especially colored intense red or having a green rim or combination of these two colors ("watermelon"). Copper concentration decreases from schiller to red to pale yellow which is similar to the observed sequence in zones (Fig. 6A) and finally, uncolored sunstones have very low copper levels. While copper can be seen as a visible copper plate, it cannot be seen when it gets exsolved in sub-microscopic size. Due to the uneven distribution of very thin copper inclusions in the core of the sunstones, determining an overall precise copper concentration is challenging. However, copper has been estimated as up to 300 ppm in high gem-quality sunstones (Welch et al., 2019). Also, the occurrence of native copper in crystal cores lead to the suggestion that the amount of copper in the host magmas differed over time (Hofmeister and Rossman, 1985b; Johnston et al., 1991).

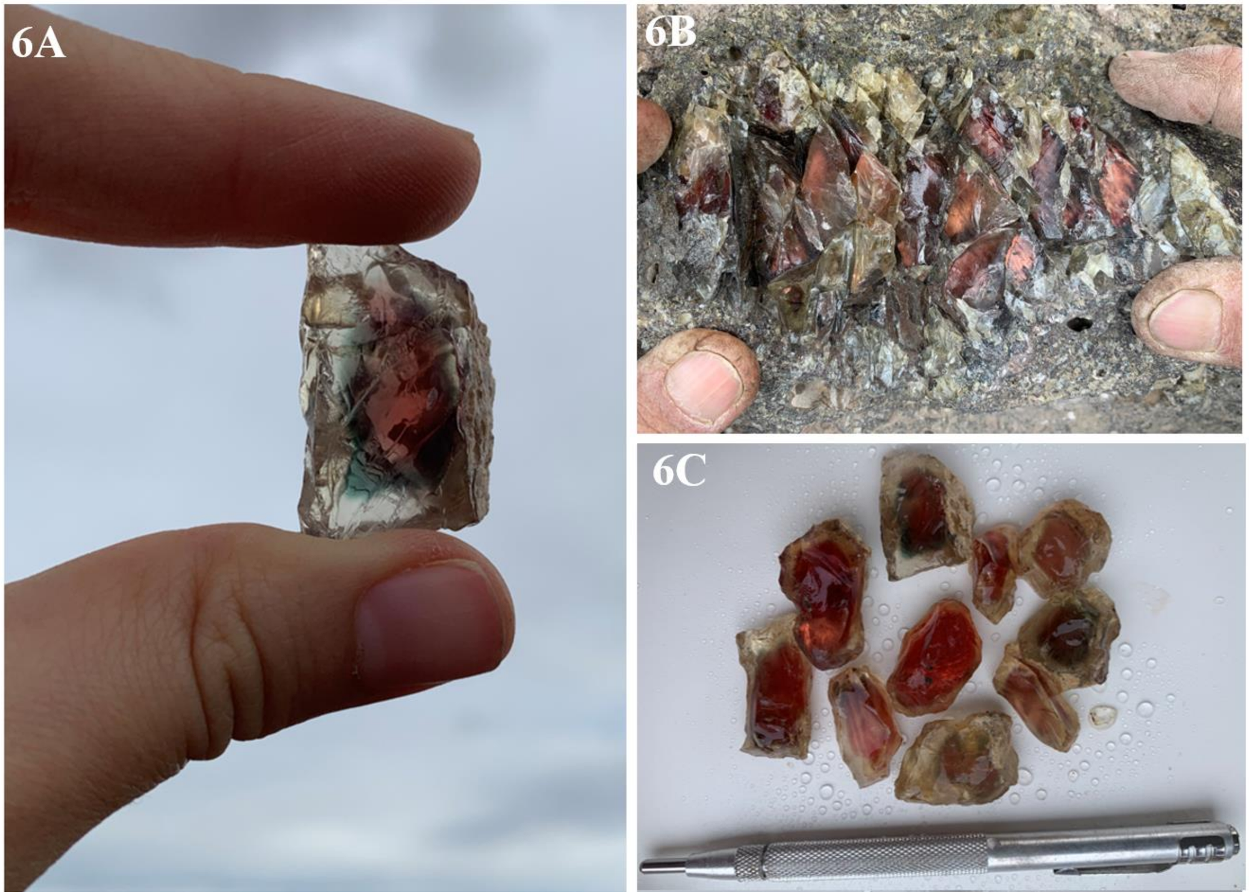

Figure 6. Gem-quality Oregon Sunstones collected from Double Eagle #16 Mine. 6A: The reddish copper core is surrounded by the green color of protoenstatite. 6B: Blocky labradorite feldspar crystal within the host basalt. 6C: Some of the highest quality Oregon Sunstones have differed in the color pink (champagne), red, green.

The highest quality gemstones differ in color (pink, red, green) and may also contain flakes of native copper (Hofmeister and Rossman, 1985b) (Fig. 7). Some of the sunstones have copper inclusions in them surrounded by an unusual dichroic red to green-colored rim. This distinctive green coloring of these sunstones is interpreted to result from crystallographically oriented nanocrystals of protoenstatite in combination with copper nanocrystals (Xu et al., 2017). Protoenstatite is the magnesium endmember of the pyroxene mineral group and is reported to be a high-temperature form. It is observed that the copper platelets preferentially grew within the phenocrysts along crystallographic boundaries, and, where present, the micron-scale inclusions of protoenstatite (green rim, Fig. 7) are also distributed in consistent zones around copper platelets (Xu et al., 2017).

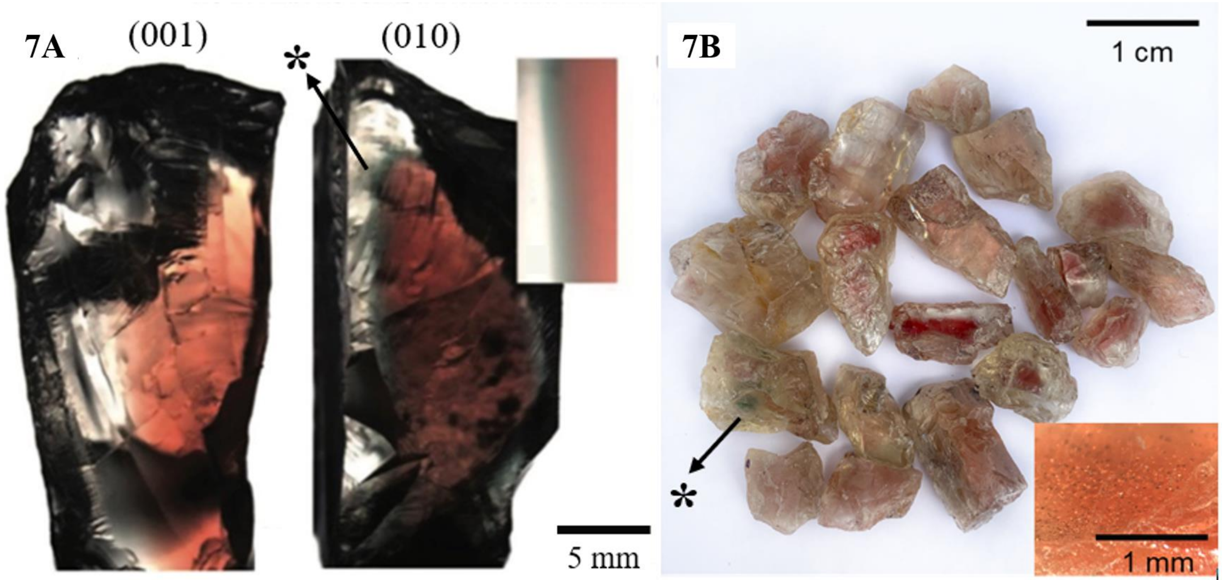

Figure 7. Gem-quality Oregon Sunstone looking down along the normal of (001), and along b-axis [010]. Notice the extremely clear rim in image 7A along with the color zoning. In some crystals, a green border becomes brownish-red when looking down along the normal of (001). The inset in 7A illustrates the specifics of the red to green transition (~4 mm thick) (Modified from (Xu et al., 2017). 7B: Labradoritic 'sunstone' samples from the Dust Devil Mine (samples of this study). (*****) Some crystals contain a green rim (protoenstatite) or a cloudy zone around the copper core.

These metal copper inclusions as preferentially oriented mineral platelets are responsible for the aventurescence or "schiller effect". In gemology, aventurescence is an observed optical phenomenon when inclusions form a pattern of brilliant flashes and color spots within certain gems. The term "schiller effect" is generally used for these special gems and types of aventurescence (Hofmeister and Rossman, 1985). While aventurescence can be seen in many kinds of labradorite feldspar, the effects are usually created by hematite or goethite inclusions. However, the Oregon Sunstones (labradorite) have copper inclusions, which are formed by the exsolution process. The schiller in Oregon Sunstones is oriented to (001) and (010) in a transparent matrix because of its thin, round, and highly reflective platelets (Fig. 7A).

Pleochroism is the ability of a mineral to absorb different wavelengths of transmitted light depending upon its crystallographic orientations. Although pleochroism is absent in other feldspars, Oregon Sunstones with green rims exhibit pleochroism which increases their unique and valuable nature. The green part of the sunstone might seem red from another distinct direction. Pleochroism is much more apparent in intensely colored sunstones samples. Clear parts of the sunstone crystal do not exhibit pleochroism. Other optical properties and physical properties of Oregon Sunstones are also shown in Table 1.

The rarest and thus the most valuable sunstone pieces are the colored ones including intense red, green, and a combination of two-color, as well as the transparent sunstone with visible copper inclusion. Most miners try to establish their own grading system. While colorless or pale-yellow sunstones without copper inclusion cost approximately $20 per carat; pink, red, green, or bicolored sunstones range from between $50 and $300 per carat. Large sunstone gemstones over 3 carats and having intense red color can cost up to $1,700 per carat ("Oregon Sunstone Value, Price, and Jewelry Information - Gem Society"). However, according to the International Gem Society, seven distinct factors must be considered when pricing sunstones: Schiller, clear hues, mid-deep tones, constellation/aventurescence, two-tone/dichroic, classic sunstone, and mystique.

Table 1. Physical Properties of Oregon Sunstones ("Oregon Sunstone Value, Price, and Jewelry Information - Gem Society").

Name	Oregon Sunstone
Is a Variety of	Feldspar
Crystallography	Triclinic
Refractive Index	1.539-1.573
Colors	Red, green, yellow, and and clear as well as multi-colors
Hardness	6-6.5
Wearability	Poor
Fracture	Uneven
Specific Gravity	2.71-2.73
Birefringence	0.008
Cleavage	Perfect two directions
Heat Sensitivity	No
Special Care Instructions	Avoid rough handling
Transparency	Transparent to opaque
Phenomena	Aventurescence or schiller effect
Formula	Oregon sunstone is a variety of labradorite, a mineral in the plagioclase feldspar solid-solution series, with a composition of 68% anorthite (CaAl2Si2O8)
Pleochroism	Usually absent in feldspar but notable in Oregon sunstone
Optics	a = 1.559-1.563; γ = 1.569-1.573. Biaxial (+)
Optic Sign	Biaxial +
Etymology	After the state and the "sun-like" golden red schiller effect found in some of these stones
Occurrence	Basalt flows
Inclusions	Copper inclusions

Figure 8 and figure 9 show two sunstone mines sampled in the course of this study; Double Eagle #16 Mine and Ponderosa Mine, respectively. The Double Eagle #16 Mine produces some of the highest quality Oregon Sunstone ever discovered. In the Lake County at the Double Eagle and Dust Devil #16 Mines, the plagioclase megacryst in basalt flows 1-2 meters thick with lobate margins and irregular, hummocky surfaces. Ponderosa Mine, unlike the other mines that are located in Plush, is located in Harney County. The Ponderosa Mine is the largest producer by volume (Johnston et al., 1991). The Ponderosa Mine occurrence is within a volcanic breccia that could represent a debris flour or eruptive volcanic vent (Dr. Emily Cahoon, personal communication, 2021). The lithology exposed in walls to the open pit of Ponderosa contains angular plagioclase crystal fragments and "bombs" of plagioclase-rich basalt that formed in association with explosive volcanism.

Figure 8. Double Eagle #16 Mine. 8A: Some of the top-quality schiller Oregon Sunstones. 8B: Digging area with Mr. Aldrich who is the owner of the Double Eagle Mine.

Figure 9. Ponderosa Mine. 9A: The mine operations. 9B: Digging area with Dr. Emily Cahoon (flow is outlined). 9C: Note that it contains angular plagioclase crystal fragments and "bombs" of basalt (black). Vertical gouges and scour marks are from mining equipment. 9D: The close image of basaltic rock fragment that contains Oregon Sunstone (white arrow).

Concerning Native Copper and Ionic Copper in Minerals

Copper has a reddish color and bright metallic luster and is among the few metals that exist as a native metal in nature. Copper has a boiling point and melting point of 2567°C and 1083.4±0.2°C respectively, and a specific gravity of 8.96 kg/dm^3 at 20°C. It is a transition metal and has two different valence states. Cu^{+1} has one valence electron, Cu^{+2} has two valence electrons. In this study, single plagioclase megacrysts that have the copper schiller effect (Fig. 10) were cut in various orientations (including parallel to (010) and perpendicular to (010), etc.) in order to show the unusual abundance of native copper lamellae.

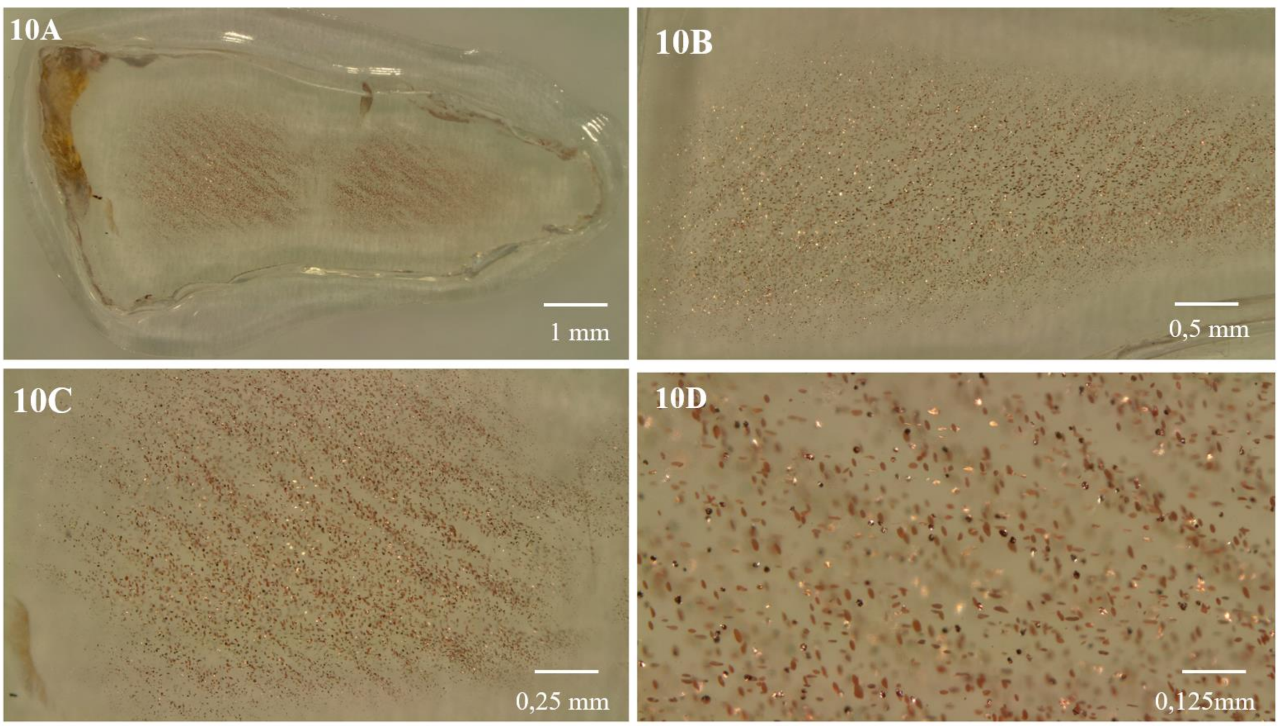

Figure 10. Native copper inclusions in Oregon Sunstone crystal (PMC-2) taken from Ponderosa Mine. Magnification level increases from 10A to 10D.This section is cut parallel to (010).

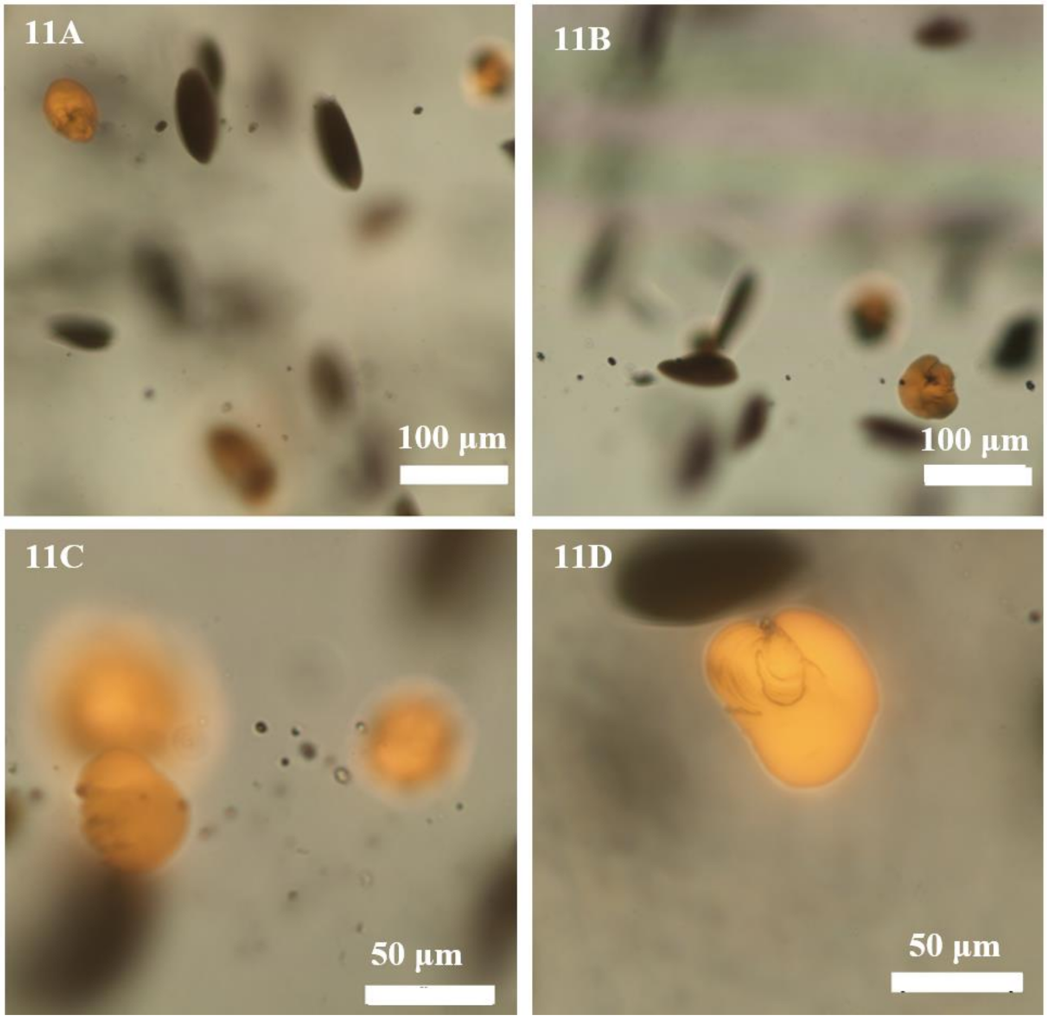

Figure 11. Higher magnification images of plagioclase megacrysts (PMC-2). 11A & 11B have different local planes of the same area, as do 11C & 11D.

Partition coefficients (D) are measures of how an element is distributed with respect to another phase and whether they are compatible or incompatible. According to Berzelius–Goldschmidt classification, chalcophile elements preferentially bond with sulfur to form sulfides, and have low affinity for oxygen. Copper is a chalcophile element and it is moderately incompatible with plagioclase in basalt. Thus, the concentration of copper rises in a silicate melt during the magma differentiation (Liu et al., 2014; Wierman, 2018). Liu et al. (2014) noted that copper is moderately incompatible ($D_{Cu} < 0.2$) with all the silicate minerals in the upper mantle.

Thus, during partial melting of mantle and magmatic differentiation, if sulfide is absent, copper should be enriched in any remaining melts. The D_{Cu} values are important to identify the copper behavior during mantle melting. The copper contents of mantle-derived primitive basaltic magmas include MORBs (mid-ocean ridge basalts), arc basalts, and OIBs (ocean island basalts), with ranges of 60–80, 50–100, and 80–120 ppm, respectively, while the copper contents of the primitive upper mantle range approximately 20–30 ppm (Lee et al., 2012; Liu et al., 2014). Jensen (1982) suggested that copper could substitute into an intermediate plagioclase structure as Cu^{1+} (in place of Na) or as Cu^{2+} (in place of Ca).

Concerning Plagioclase, and Huttenlocher Exsolution

The most common minerals in Earth's crust are feldspars of which plagioclase is the most abundant. Plagioclase can form under a wide range of pressure and temperature conditions depending on magma composition, temperature, and water content. These properties make it an incredibly beneficial mineral for identifying the source, chemistry, and evolution of parental magma. Plagioclase feldspars are a continuous series of solid solutions, ranging from pure albite, $NaAlSi_3O_8$, to pure anorthite, $CaAl_2Si_2O_8$, which is accomplished at high temperatures (1,200°C to 1,500°C) by coupled substitutions. This means that Ca^{2+} substitutes Na^{+}, having similar ionic radii, while the balance of charge is controlled by the substitution of Al^{3+} with Si^{4+}. For the compositional ranges of An_5-An_{25}, An_{40}-An_{60}, and An_{65}-An_{85}, three chemical exsolution gaps with resuling exsolution are identified, which are respectively called Peristerite exsolution, Boggild exsolution, and Huttenlocher exsolution. In non-volcanic plagioclases, with bulk compositions of $An_{67–90}$, Huttenlocher intergrowths are common (Willaime,1985). The plagioclase in the present study is ~ An_{67} and can be classified as labradorite (Hofmeister and Rossman, 1985a). Stewart et al. (1966) also observed the plagioclase in Lake County, stating that the phenocrysts developed in a magma chamber with a crystallizing temperature of ~ 1,100°C and cooled rapidly in lava flows, typically not forming exsolution.

Previous Research Relevant to Copper Diffusion, and Al-Si Ordering in Lake County and Harney County Plagioclase

Copper is known to rapidly diffuse within labradorite feldspar (Jin et al., 2021), which is surprising in view of its ionic radius and mass. Diffusion experiments show that Cu diffusion in plagioclase (log D = -13.0 to -11.5 m^2 s^{-1} at 1000°C) is exceptionally rapid (Audétat et al., 2018). Copper diffusion coefficients are 2–3 orders of magnitude lower in olivine, clinopyroxene, apatite, and orthopyroxene than plagioclase, but remain high in comparison to most other elements. As noted by Audétat et al. (2018), re-equilibration experiments on melt inclusions and quantitative modeling show that at 1000°C, plagioclase-hosted melt inclusions may re-equilibrate their copper content with that of the surrounding magma in a few hours to a few weeks, but similar scales of diffusion in apatite-, clinopyroxene-, orthopyroxene-, and olivine-hosted melt inclusions would require tens of years to hundreds of years. Figures 12A and 12B show experimentally induced copper diffusion profiles in plagioclase. To model these diffusion profiles (Fig. 12C), Audétat et al. (2018) assumed diffusion via two mechanisms that varied in rate.

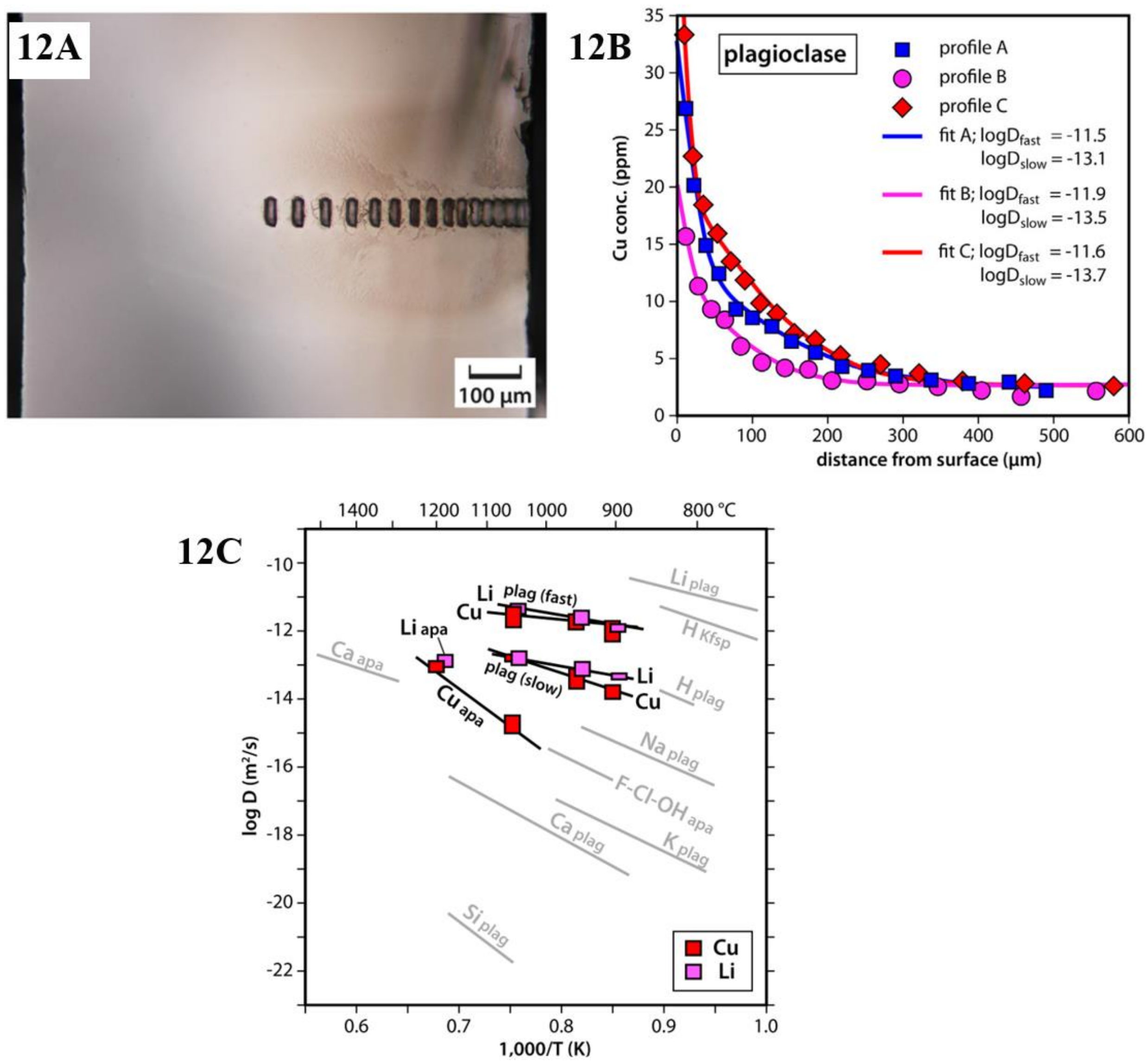

Figure 12. 12A: Transmitted-light photomicrographs of polished single-crystals of plagioclase. 12B: Corresponding Cu diffusion profiles were determined along with three perpendicular directions. 12C: Measured Cu diffusion coefficients in plagioclase compared to published diffusion coefficients of other elements (Audétat et al., 2018).

Heating experiments by Jin et al. (2019) demonstrate structural changes in portions of the Lake County Sunstone before and after heating (Fig. 13). The tetrahedra in the framework are shaded blue and yellow to represent Al- and Si-dominated T-sites, respectively. Note that the distribution of Al tetrahedra (blue) is more homogeneous after heat treatment (Fig. 13B).

The experiments by Jin et al. (2019) show that structural reorganization of Lake County Plagioclase can occur for two weeks at ~1100°C.

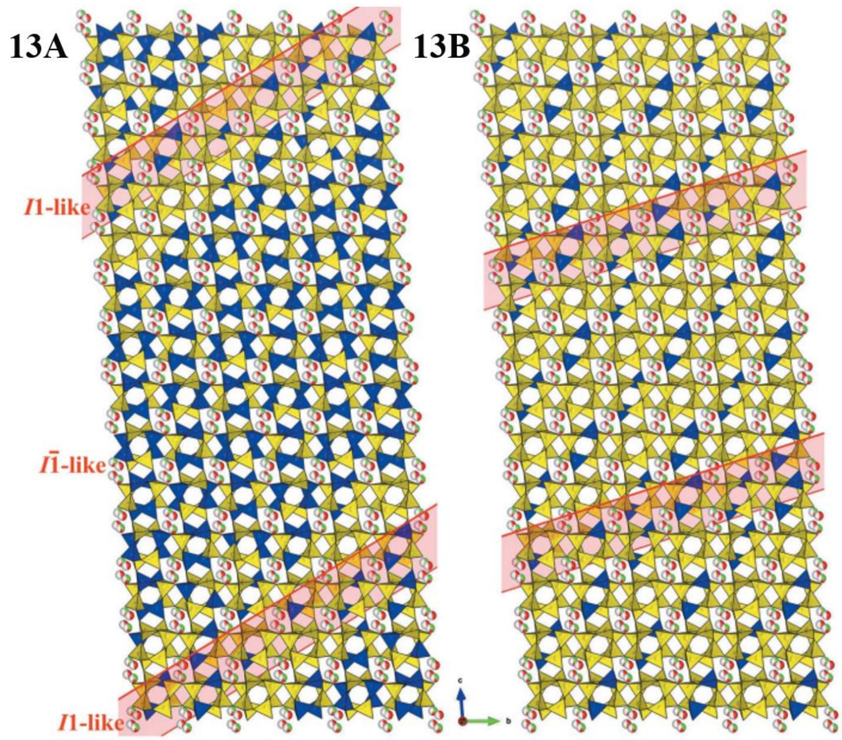

Figure 13. Lake County sunstone structures before (13A) and after (13B) heating treatment. The center of the I1-like domain is shown by the red planes (Jin et al., 2019).

Hofmeister and Rossman (1985b) interpreted that because concentrations of copper increase with differentiation of a host magma, higher concentrations of copper may have been incorporated followed by exsolution of native copper in plagioclase. Jensen (1982) suggested that pressure and temperature changes affect coppers relative compatibility, allowing a small amount of copper to be incorporated into plagioclase. Jensen (1982) also suggested that Cu^{1+} can substitute for Na^{1+} while Cu^{2+} can substitute for Ca^{2+} in plagioclase.

Xu et al. (2017) show that copper is incorporated into the feldspar crystal associated with formation of protoenstatite at high pressure and temperature conditions during early crystal formation before exsolving. In gem-quality labradorite, this structure of the protoenstatite with the copper nanocrystals inside it is called a ‘watermelon crystal’. They infer that in these “watermelon” crystals (Fig. 7), the cores are formed at the early phases of magma chamber formation at high-pressure and temperature conditions, and native copper crystallizes during the last phases of the magma chamber but prior to eruption. Also, it is suggested that clear rims are formed at a later stage and under different temperature and pressure conditions.

As reported by Johnston et al. (1991), the inclusions are quite thin and it is remarkably difficult to isolate and investigate distinct plates for microprobe analysis. Johnston also proposed that sunstones of the Ponderosa Mine formed in a magma chamber that was chemically stable and uniform for a long period of time. The melt contained an elevated amount of copper that was integrated into the feldspar lattice. When the pressure and temperature lowered, the feldspar lattice could not sustain the high copper levels. As a result, copper then precipitated via exsolution.

Objectives of this Study

The timing of extrusion of the basalts hosting the sunstones has not been dated previously in the literature. Providing temporal constraints and determining the ages of the sunstone-bearing lavas is one of the main objectives of this research. In this research, results of $^{40}Ar/^{39}Ar$ ages of basalt hosting sunstones will be compared with the age of the Steens Basalt (~16.7 Ma; Jarboe et al., 2008), and the age of the HLP basalts (ranging from 2 to 10 Ma) (Jordan et al., 2004). Aspects of the petrologic and geochemical character of the sunstones will also be documented and discussed to give some context for comparing them to plagioclase in other, regional basalts.

MATERIALS AND METHODS

Methods of this research include mineral chemistry (electron microprobe analyzer, major element, inductively coupled plasma mass spectrometry, trace element), and $^{40}Ar/^{39}Ar$ geochronology. Samples studied in this research were obtained from the Dust Devil Mine (provided by Don Buford), the Double Eagle #16 Mine (provided by Debbie and John Aldrich), the Ponderosa Mine (provided John Woodmark), from the collection of Dr. George Kamenov, from collection from these mines by Dr. Willis Hames and Dr. Emily Cahoon, and from samples personally collected by Cisil Bengisu Badur from these mines in 2021. One sunstone sample, GK-DD-1, mounted in epoxy (Fig. 14A) comes from Dust Devil Mine (the southern Plush area) and was provided by Dr. George Kamenov of the University of Florida, and used for the Electron microprobe WDS map (Fig. 14B), $^{87}Sr/^{86}Sr$ variation diagram (Fig. 21), and REE/trace element data (Fig. 22). Four samples of basaltic groundmasses (LEB-001, LEB-003, DE16-001 and SW19-DD01) containing sunstones, and three samples of megacryst (LEBC-1, DE16-CY, and PMC-2) provided by Dr. Emily Cahoon were commercially prepared for EMPA (electron microprobe analysis) (in Figures 17-20) at Spectrum Petrographics. While all samples came from the southern Plush area, just PMC-2 was collected from Harney County, 120 miles further south. Whole-rock and plagioclase samples used for analysis are shown in Table 2. Except for GK-DD-1 and CB-PLJ-1, all samples of phenocrysts and matrix were prepared for separate laser $^{40}Ar/^{39}Ar$ age studies (in Figures 23-26), and analyzed in the Auburn Noble Isotope Mass Analysis Lab (ANIMAL) of Auburn University. EMPA and mass spectrometry methods and data are detailed in the appendices.

Table 2. Whole-rock and plagioclase samples used for the analyses.

Sample ID	Mine Name	Material	Analytical Method
LEB-001	Little Eagle Butte	Whole-rock	EMPA, $^{40}Ar/^{39}Ar$
LEB-003	Little Eagle Butte	Whole-rock	EMPA, $^{40}Ar/^{39}Ar$
DE16-001	Double Eagle	Whole-rock	EMPA, $^{40}Ar/^{39}Ar$
SW19-DD01	Dust Devil	Whole-rock	EMPA, $^{40}Ar/^{39}Ar$
LEBC-1	Little Eagle Butte	Plagioclase	$^{40}Ar/^{39}Ar$
DE16-CY	Double Eagle	Plagioclase	$^{40}Ar/^{39}Ar$
CB-PLJ-1	Dust Devil	Plagioclase	$^{40}Ar/^{39}Ar$
GK-DD1	Dust Devil	Plagioclase	EMPA, $^{87}Sr/^{86}Sr$ variation diagram, and REE/trace element data
PMC-2	Ponderosa	Plagioclase	EMPA, $^{40}Ar/^{39}Ar$

RESULTS

Results of this research will be presented in three different sections; petrology (electron microprobe data), geochemistry ($^{87}Sr/^{86}Sr$ data, Rare Earth Element (REE) data/trace element data), and geochronology ($^{40}Ar/^{39}Ar$ data).

Petrology

Electron Microprobe Data

The image of a single plagioclase megacryst (GK-DD-1) mounted in epoxy (Fig. 14A, provided by Dr. George Kamenov) shows the copper schiller effect created by the thin lamellae of exsolved metallic copper. The copper lamellae can be seen at higher magnification with an electron microprobe wavelength-dispersive spectrometry (WDS) map (Fig. 14B) where ‘warmer’ colors indicate higher copper content and an inclusion ~0.5 microns thick and 65 microns long. The white dots indicate positions for electron microprobe analyses presented in Figure 15.

The first result of this research is to investigate possible correlations between Huttenlocher exsolution and the observed copper lamellae by obtaining the electron microprobe analysis in Figure 15. Copper occurs as thin platelets (copper schiller) with crystallographically-controlled orientations. Subtle Ca-Na changes of about 0.2 - 0.3 atoms per formula unit are consistent with Huttenlocher exsolution in zones that appear to parallel the exsolved copper lamellae.

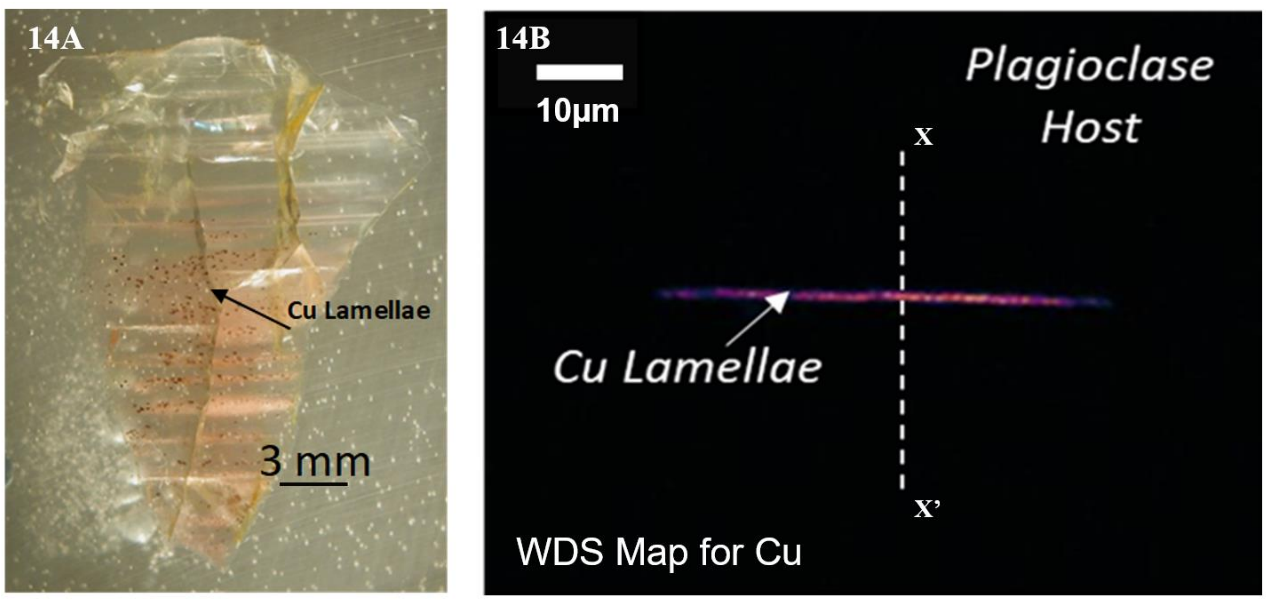

Figure 14. 14A: Photograph of a plagioclase crystal (from Dust Devil Mine (GK-DD-1), the southern Plush area) mounted in epoxy, showing the copper 'schiller' effect created by thin lamellae of copper. The approximate area for 'Cu Lamellae' is shown (exaggerated). This study sample was provided by Dr. George Kamenov of the University of Florida. 14B: Electron microprobe WDS map for the distribution of copper, in and around a single copper lamellae.

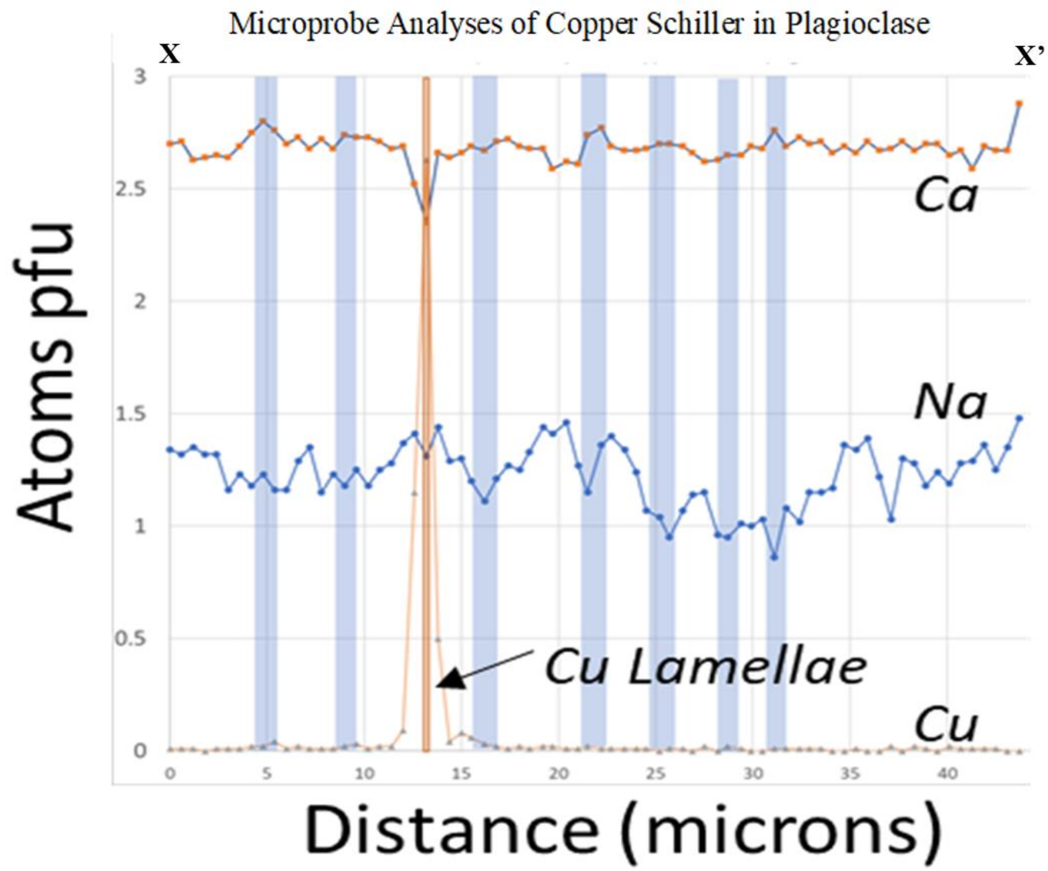

Figure 15. Electron microprobe analyses of plagioclase and copper, with atoms per formula unit (pfu) indicated along section x-x' of figure 14. Electron microprobe data were obtained by using the AU Geosciences Department EMPA.

Basaltic groundmasses (LEB-001, LEB-003, DE16-001 and SW19-DD01) containing sunstones, and three samples of megacryst (LEBC-1, DE16-CY, and PMC-2) prepared for electron microprobe analysis. These samples were studied using the Auburn University Electron Microprobe Analyzer (AU-EMPA) (Fig. 16), and several points and line analyses were carried out on the samples for plagioclase megacryst, fine matrix plagioclase, and fine pyroxene. The electron microprobe analyses (raw data presented in Appendix 1) were calibrated using various silicate mineral standards (anorthite, amelia, microcline).

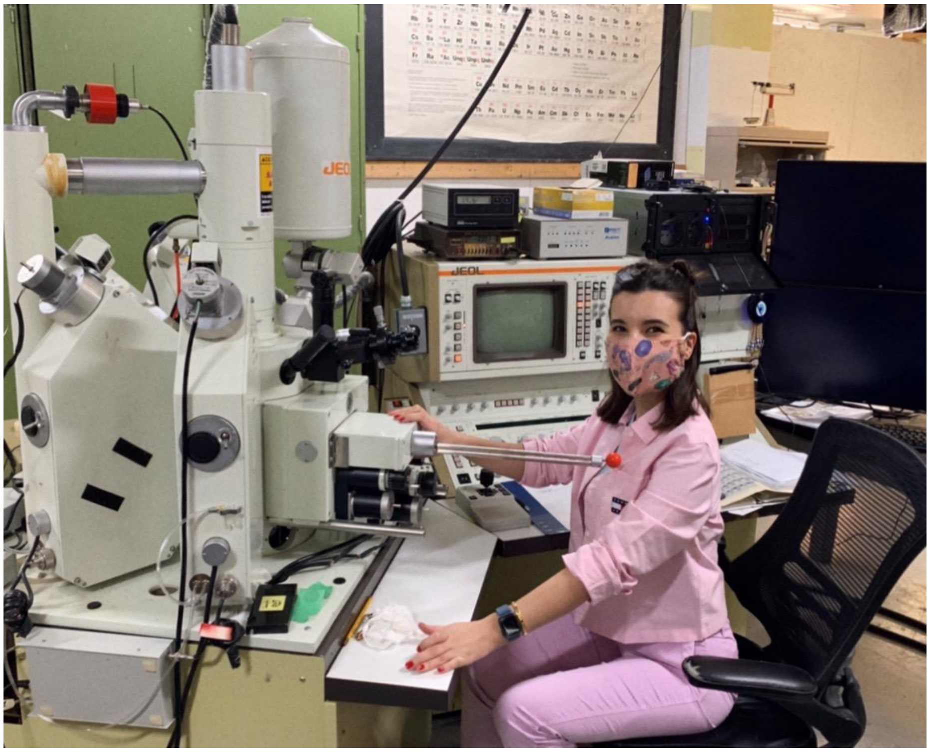

Figure 16. Auburn University Electron Microprobe Analyzer (AU-EMPA).

Data obtained from the AU-EMPA confirm that plagioclase megacrysts (Fig. 17) are labradorite. Spot analyses of megacrysts were completed for both rim and core. These data from plagioclase megacrysts show no distinct chemical variability or zonation between core and rim for these four samples (Fig. 17). Line traverse analyses were also conducted for each matrix plagioclase from rim to rim. These analyses of fine matrix plagioclase show a general trend from labradorite to andesine (Fig. 18). WDS (wavelength-dispersive spectroscopy) and BSE (back-scattered electron) images for fine matrix plagioclases show that potassium is enriched in the rims of fine matrix plagioclase relative to their cores (Fig. 19).

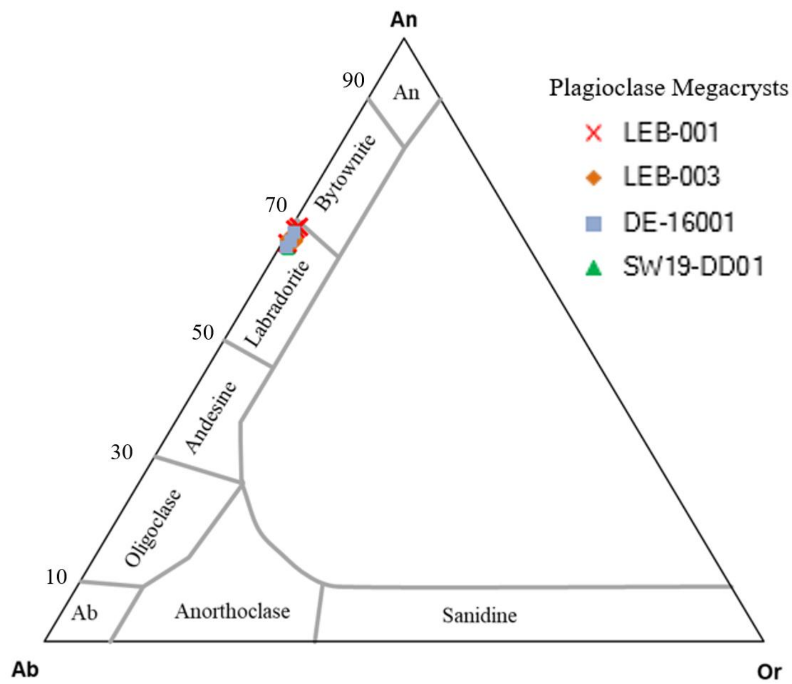

Figure 17. A feldspar ternary diagram of EMPA analyses for plagioclase megacrysts (n=11). The data were obtained by analyses of core and rim show no distinct differences in composition.

These measurements show that the more finely grained crystals of matrix plagioclase with a typical tholeiitic magma series show an expected enrichment of potassium and sodium from their cores to their rims. Microprobe results also show fine-grained phases in the mesostasis of the basalts that are very rich in potassium and silica that appear to be sanidine and quartz. These petrographic observations and mineral chemistry are consistent with the growth of a late generation of plagioclase and matrix phases during fractional crystallization and eruption of the basaltic lavas.

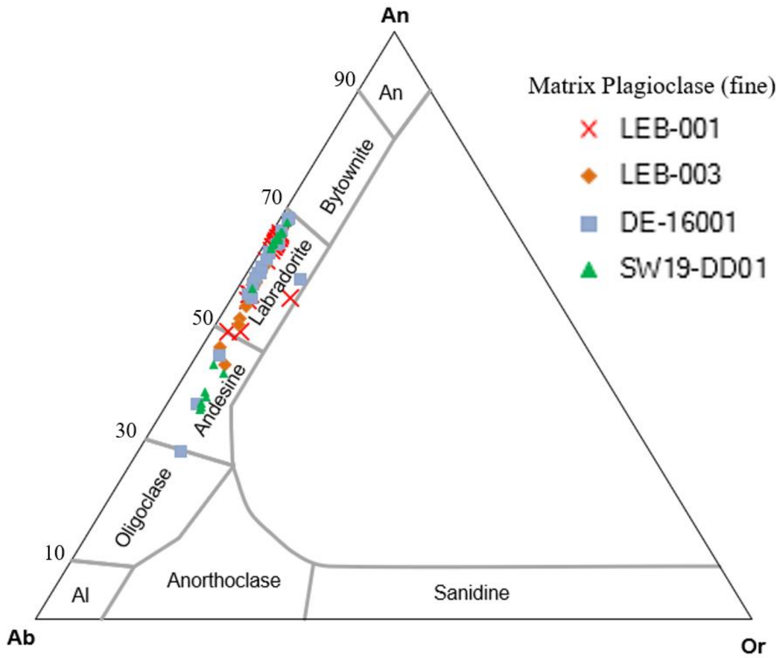

Figure 18. A feldspar ternary diagram of EMPA analyses for fine matrix plagioclase (n=160). Note that the matrix plagioclase composition varies from labradorite to andesine/oligoclase in the same samples.

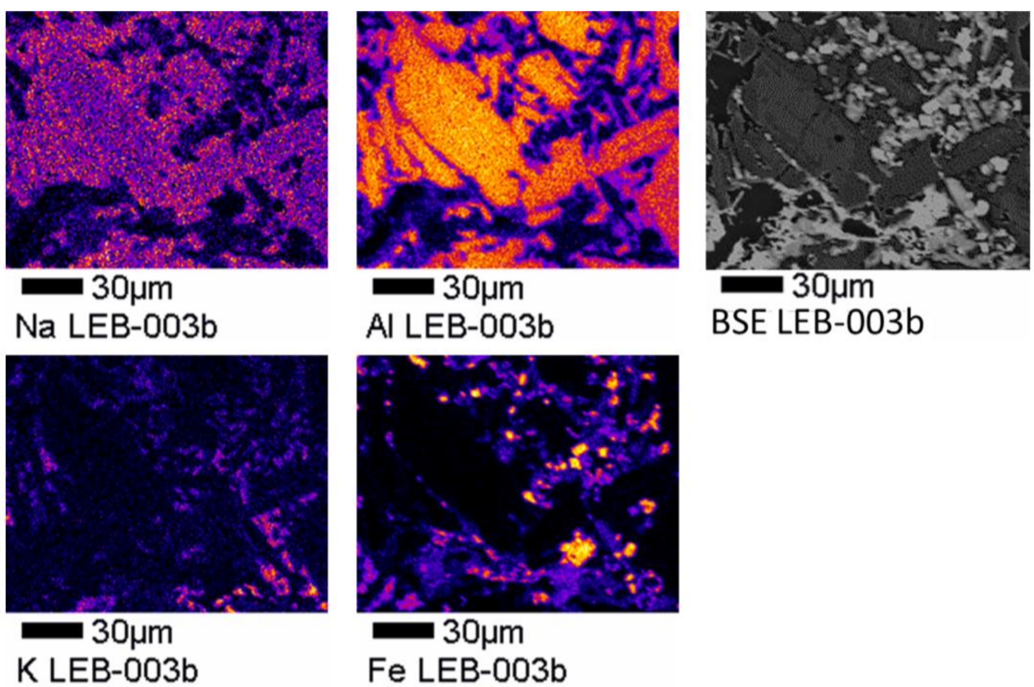

Figure 19. Backscattered Electron (BSE) images of sample of LEB-003. 'Image-J' was used in order to assign false color. Note that increasing Na and decreasing Al contents of matrix plagioclase from core to rim. These variations are responsible for the variations shown in Figure 18.

Fine-grained pyroxene crystals of the matrix were also selected for EMPA spot analyses of each sample (Fig. 20). These pyroxene crystals occur sporadically in the basalt as subhedral crystals 0.1 - 0.3 mm in maximum dimension. The analyses show that the pyroxene is augite, with Wo (wollastonite) value for four samples ranging between 40.96 and 45.55, and the En (enstatite) value ranging between 32.04 and 43.99, and the Fs (ferrosillite) values as high as 23.97. Thus, the pyroxene trend is closer to the range of diopside, and there are small ranges of Mg-Fe for each sample.

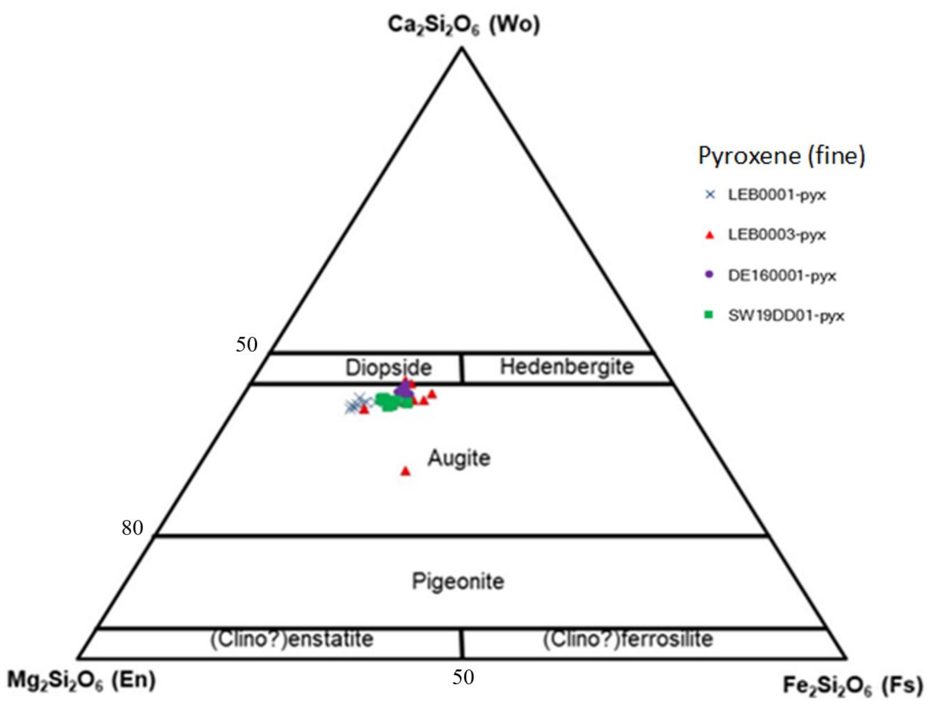

Figure 20. Pyroxene ternary diagram of 39 pyroxene analyses from the microprobe data. Wo: wollastonite, En: enstatite, Fs: ferrosillite.

Geochemistry

$^{87}Sr/^{86}Sr$ Data

Apart from the copper platelets in crystal cores, sunstones appear to have remarkably homogeneous distributions of major and trace elements as reported by (Badur et al., 2020). $^{87}Sr/^{86}Sr$ data from high-precision thermal ionization mass spectrometry (TIMS) analyses for Oregon Sunstones have been provided by Dr. George Kamenov at the University of Florida and used to produce the $^{87}Sr/^{86}Sr$ variation diagram in figure 21. Plagioclase crystals also exhibit internally homogeneous $^{87}Sr/^{86}Sr$ ratios of ~ 0.70365 (Fig. 21), comparable to plagioclase in Steens Basalt of the Columbia River Basalt Group (Ramos et al., 2005). In agreement with homogeneous $^{87}Sr/^{86}Sr$ and major element data, Laser Ablation Inductively Coupled Plasma Mass Spectrometry (LA-ICP-MS) data also show that the trace element concentrations are not zoned from the core to rim. The homogeneous nature of $^{87}Sr/^{86}Sr$ and the major (as discussed on pages 35-38) and trace element data indicate that the crystals have not undergone any late-stage of chemical transformation (as could occur through alteration or weathering).

21A

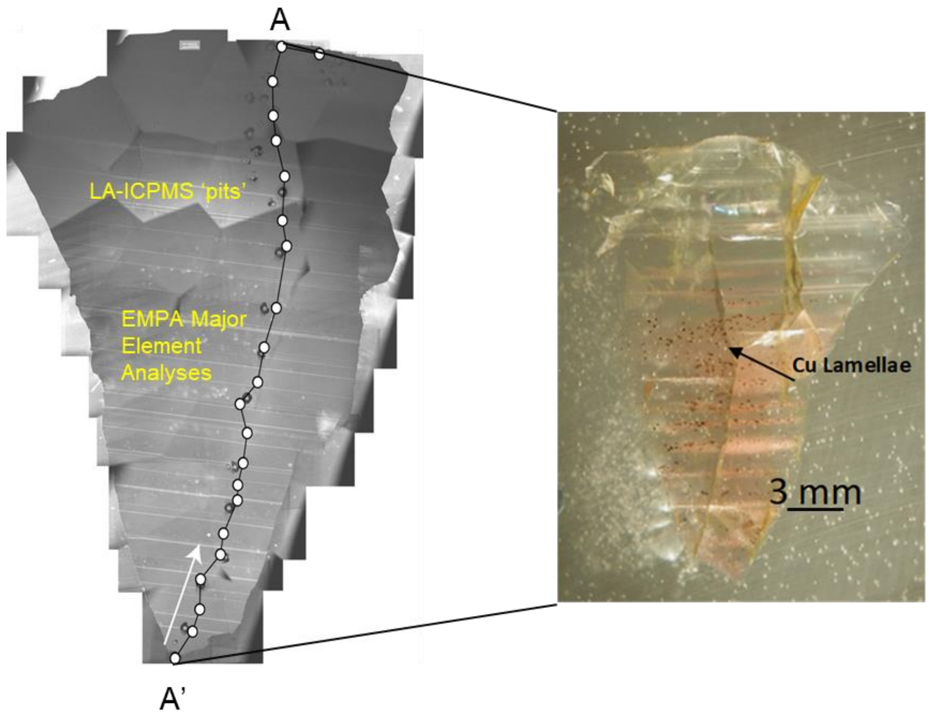

21B

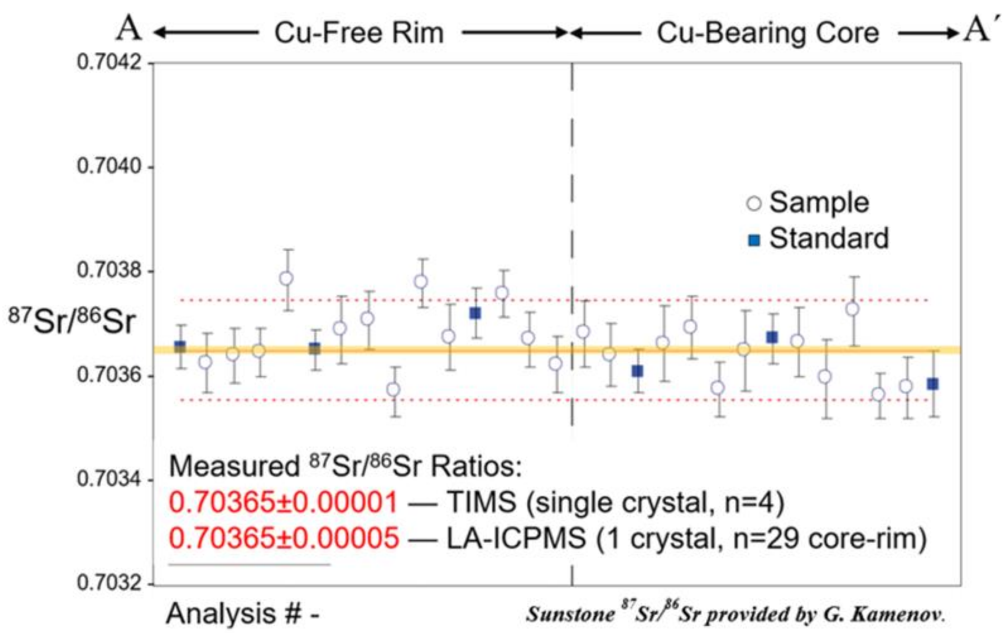

Figure 21. Measurement locations for the $^{87}Sr/^{86}Sr$ variation diagram in figure 21B (from A to A´) that was obtained at the University of Florida with the plagioclase crystal sample provided by Dr. George Kamenov. 21B: $^{87}Sr/^{86}Sr$ variation diagram obtained by TIMS and LA-ICP-MS analysis of a sunstone from its Cu-free rim to Cu-bearing core. This is the same crystal that microprobe data is presented for in Figure 15.

REE/Trace Element Data

In addition to $^{87}Sr/^{86}Sr$ data, Chondrite-normalized Rare Earth Element (REE) data were provided by Dr. George Kamenov. The pattern of average Steens Mountain Basalts and Oregon Sunstones (10 sunstone crystals from the Dust Devil Mine) have an Ocean Island Basalt-like trend on the REE diagram (Fig. 22) (Sun and McDonough, 1989; Moore et al., 2018). The sunstones have very primitive REE compositions, and REE for several sunstone crystals with or without copper are similar. In addition, for the sunstone crystals, there is a prominent positive anomaly for Eu, which is typical of plagioclase fractionation (Winter, 2010).

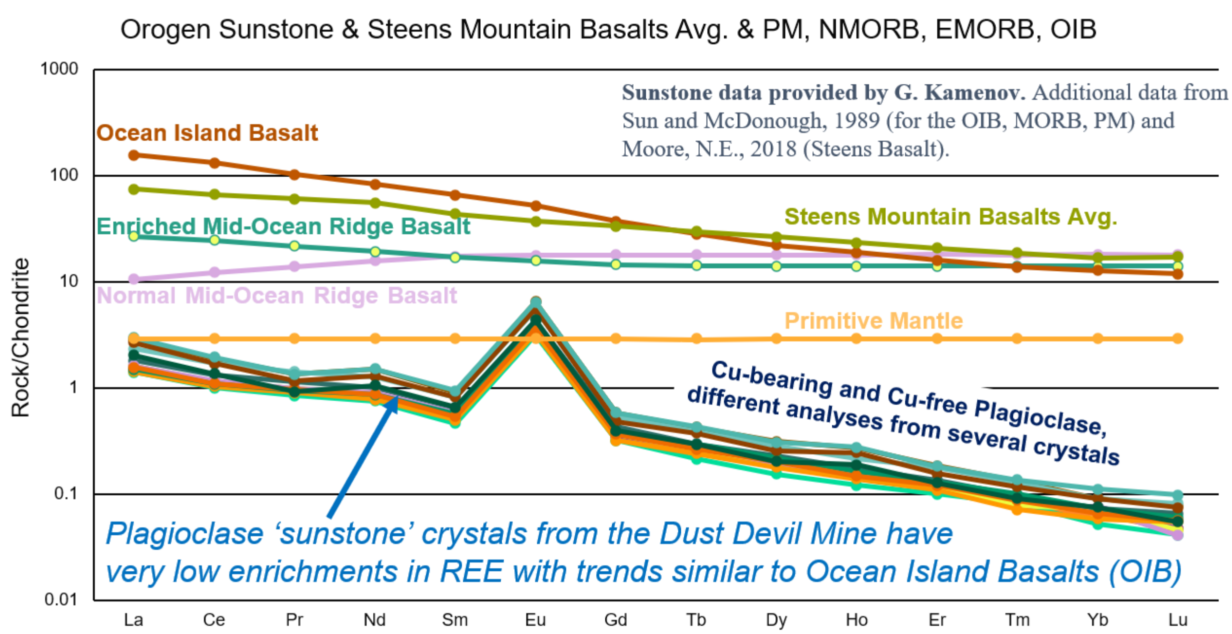

Figure 22. Chondrite-normalized REE diagram.

Age Determinations

^{40}Ar/ ^{39}Ar Data

^{40}Ar/^{39}Ar geochronology is among the most essential techniques for constraining the date of basalt eruption. Plagioclase seems to be the most notable crystal to date in otherwise low potassium basalt because it is abundant and can usually be separated easily. However, phenocrysts of plagioclase can contain magmatic 'excess' ^{40}Ar and be unsuitable for dating. The final crystallization products of basalts - the 'groundmass'- can contain more potassic feldspars including K-rich sanidine. Thus, many studies focus ^{40}Ar/^{39}Ar dating efforts on the groundmass and this is typical of studies to date young basalts (<50 Ma or so). ^{40}Ar/^{39}Ar age results in this research (data presented in Appendix 2) were collected with three strategies: analysis of basaltic groundmasses, analysis of relatively large broken plagioclase pieces (1-2 mm in size), analysis of plagioclase megacrysts (up to 2 cm in maximum dimension). These samples were crushed, sieved, and picked for irradiation. The samples were subsequently analyzed in the ANIMAL facility (see also Appendix 2).

Aliquots of approximately 10 mg from each sample were incrementally heated using a CO_2 laser to generate the ^{40}Ar/^{39}Ar data (see Appendix 2). Although three different phases (plagioclase megacrysts, smaller fragments, and matrix) were typically analyzed for each basalt sample and all of the ^{40}Ar/^{39}Ar data are in Appendix 2, only the results for the matrix samples are shown (in Figures 23-26) as these are most useful for evaluating age for reasons as discussed below. Inverse isochron plots are shown for the resulting data in part 'A' of Figures 23-26 as these are useful to identify radiogenic and extraneous sources of ^{40}Ar. Overall, the results for each sample define a mixing line between a single radiogenic component (shown by the X-axis intercept) and an extraneous component that is similar to the argon isotopic composition of modern air (the Y-axis intercepts). Thus, the isochron plots show the data to be suitable for ‘model age’ calculations (where the measured ^{40}Ar is corrected for contaminating air). In addition, part B of each figure shows the percentage of radiogenic yield (the percentage of radiogenic ^{40}Ar relative to contaminating air) and the apparent Ca/K ratio defined by argon isotopes for each incremental heating analysis. The results show that radiogenic yields of initial, lower temperature heating steps reach ~60-90% $^{40}Ar^{*}$ by the middle of the heating experiment and then decrease to ~20% with high-temperature steps. The apparent calcium to potassium ratios begins relatively low and then tend to increase through the analysis. These data can be interpreted to indicate initial degassing of a phases with more potassium (presumably finely grained feldspars) followed by derivation of measured argon from high-calcium phases (likely the centers of plagioclase crystals and pyroxenes).

In contrast to the complexities of argon derived from atmosphere and Ca-K sources in these plagioclase samples, the ages defined by the groundmass material are simple and straightforward. Plateau ages are defined for each sample, ranging from 9.40±0.18 Ma (for a sample from the Double Eagle Mine, Figure 25) to 9.16±0.13 Ma (for a sample from the Dust Devil Mine, Figure 26). Three of these plateau ages are essentially the same as ‘total gas’ ages with ~100% of the $^{39}Ar_K$ released. The mean of all four matrix plateau ages is 9.16±0.12 Ma (95% c.l., MSWD=1.13). This mean age is interpreted to represent the timing of crystallization for finely grained phases of the groundmass (feldspars, pyroxenes) during the eruption and quenching of the basaltic lavas as sampled from the Lake County sunstone mines.

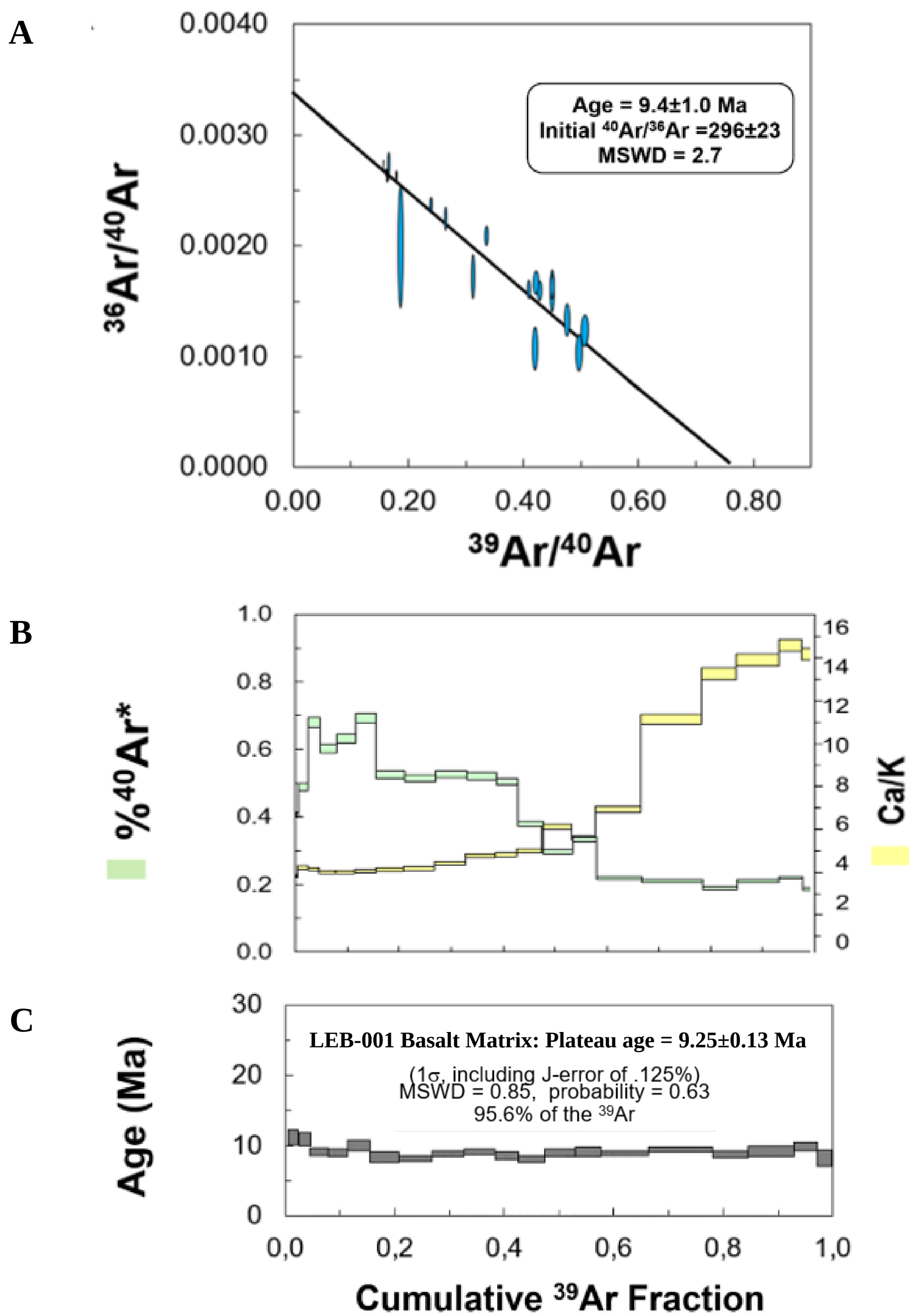

Figure 23. $^{40}Ar/^{39}Ar$ data from LEB-001. A: Data are shown on an inverse isochron plot. B: Apparent $^{40}Ar^{*}$ - Ca/K plot. C: $^{40}Ar/^{39}Ar$ incremental heating age spectrum for about 20 plagioclase crystal fragments from matrix. Results of individual age spectra are quoted at the 1-sigma confidence level.

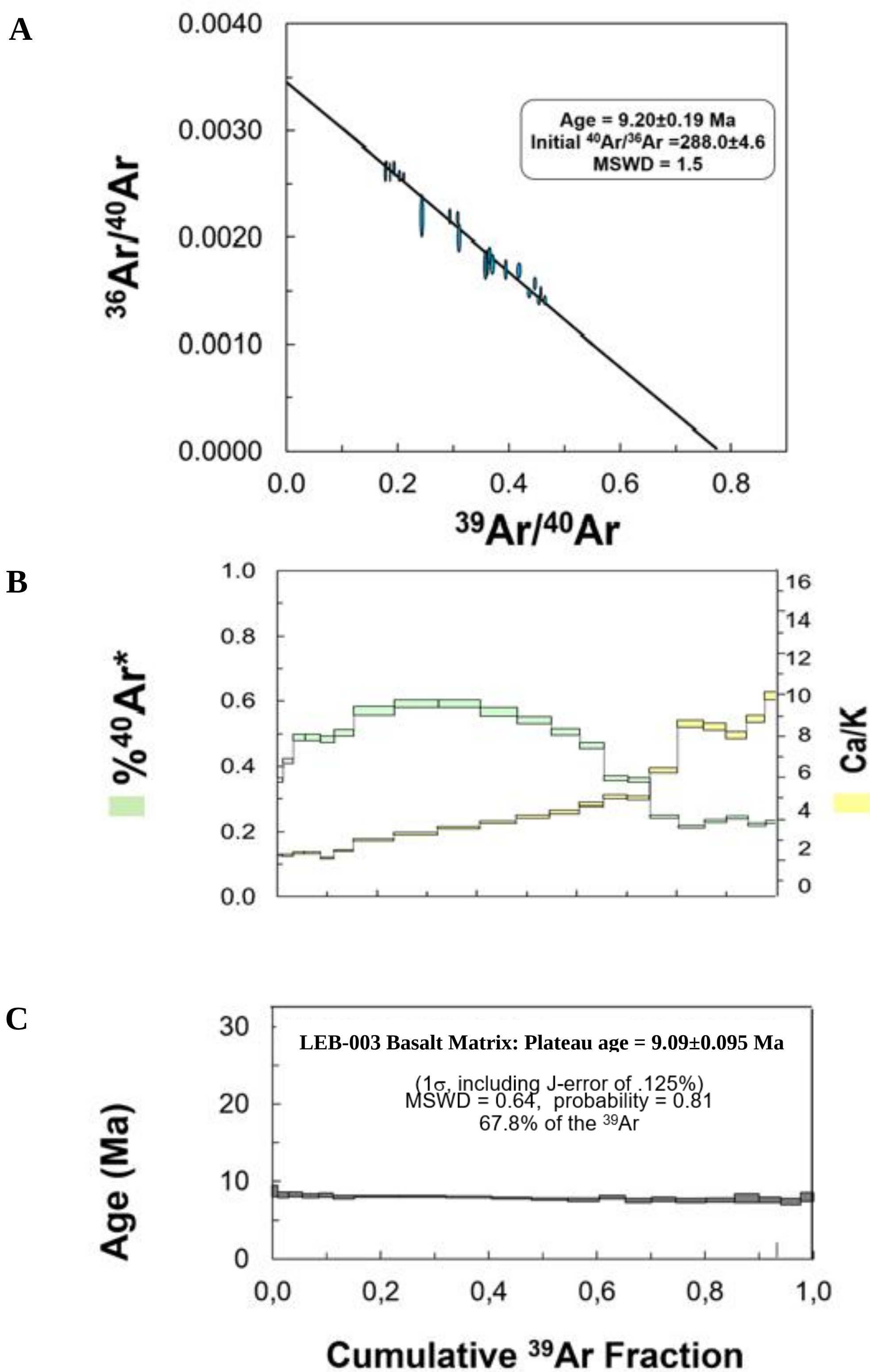

Figure 24. $^{40}Ar/^{39}Ar$ data from LEB-003. A: Data are shown on an inverse isochron plot. B: Apparent $^{40}Ar^{*}$ - Ca/K plot, C: $^{40}Ar/^{39}Ar$ incremental heating age spectrum for about 20 plagioclase crystal fragments from matrix.

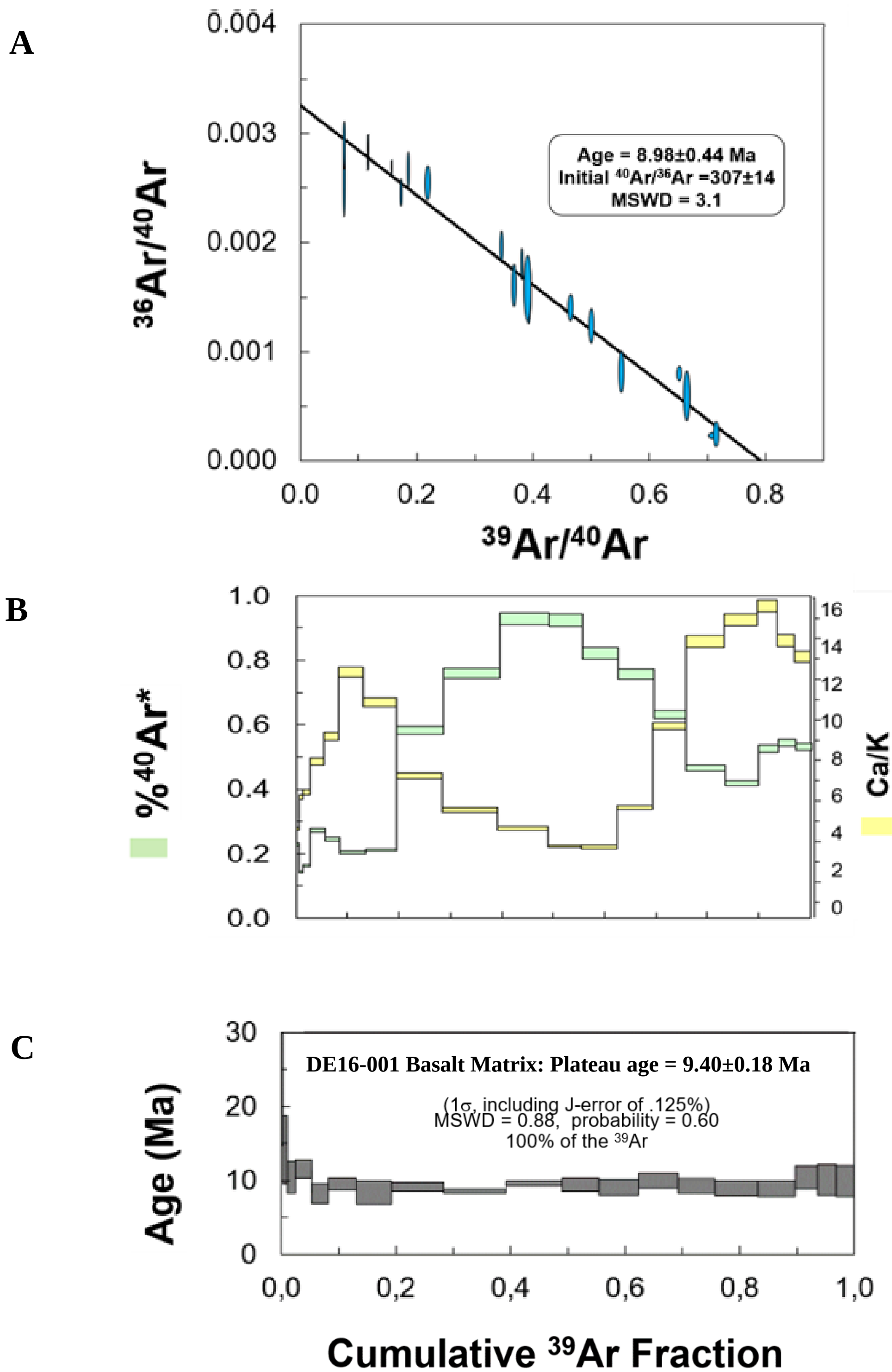

Figure 25. $^{40}Ar/^{39}Ar$ data from DE16-001. A: Data are shown on an inverse isochron plot. B: Apparent $^{40}Ar^{*}$ - Ca/K plot. C: $^{40}Ar/^{39}Ar$ incremental heating age spectrum for about 20 plagioclase crystal fragments from matrix.

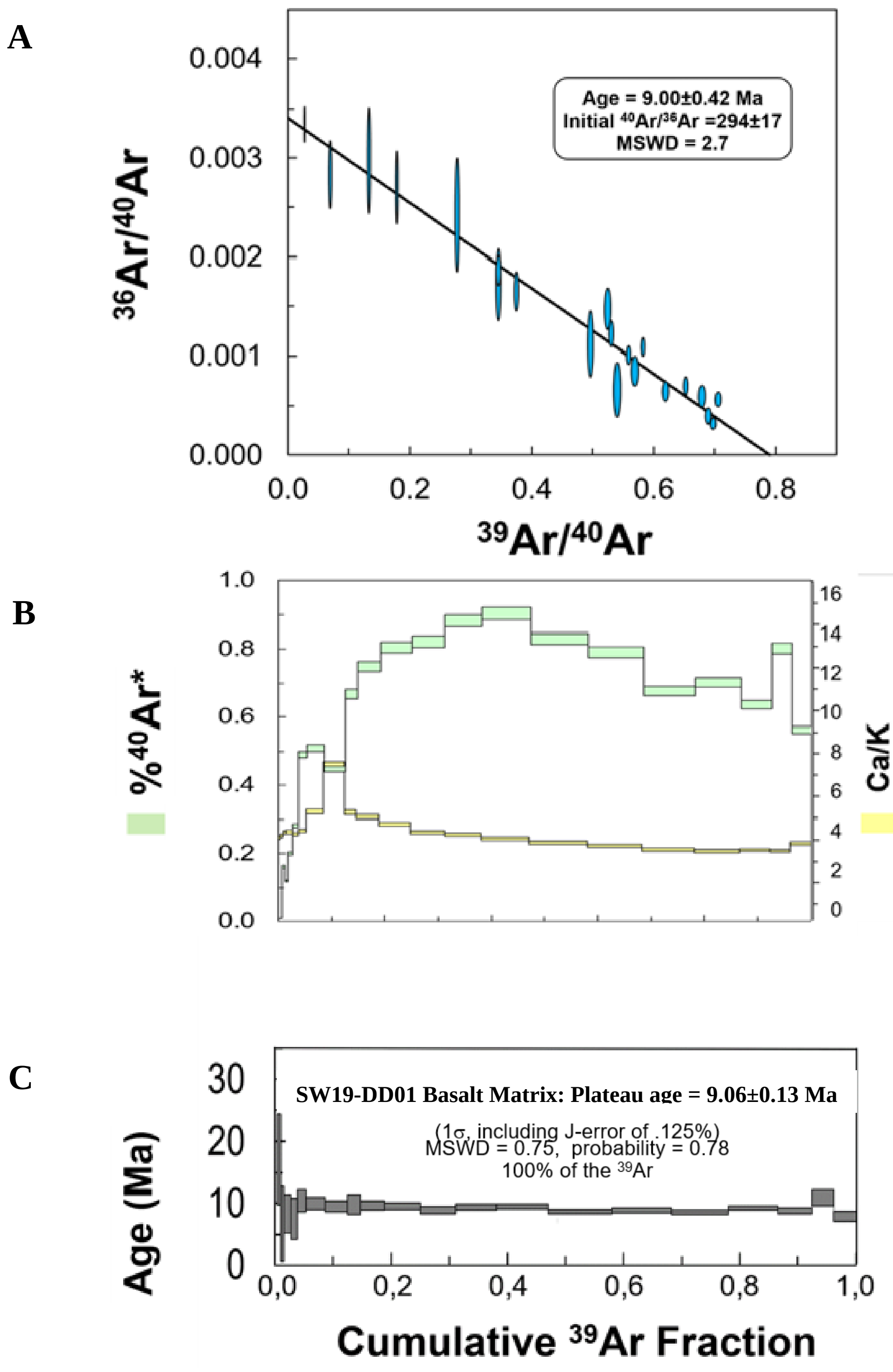

Figure 26. $^{40}Ar/^{39}Ar$ data from SW19-DD01. A: Data are shown on an inverse isochron plot. B: Apparent $^{40}Ar^{*}$ - Ca/K plot. C: $^{40}Ar/^{39}Ar$ incremental heating age spectrum for about 20 plagioclase crystal fragments from matrix.

DISCUSSION

Although there are many observations as summarized, a few areas of incomplete understanding exist regarding the nature and origin of sunstones in Oregon. For example, there was no definitive conclusion on which temperatures and pressure conditions copper substitution in plagioclase occurs and also how fast copper exsolves. One possibility is that if copper substitution in plagioclase is possible at high temperature and pressure, the copper might exsolve very rapidly (perhaps on a scale of a year or less) with decreases in pressure and temperature (Ramos et al., 2005). Such exsolution would occur along favored crystallographic lattice planes in the plagioclase. This process of grain-scale Cu-diffusion could be consistent with the Sr zoning profiles measured by (Ramos et al., 2005) in the Steens Basalts. Their observations are compatible with volume diffusion at the total crystal scale, and formation with durations of high-temperature exchange with the host magma from 5 to 1500 years intervals at constant temperatures of 1100°C (as modeled by Ramos et al., 2005). The observations of homogeneous distributions of major, trace and REE elements, along with the homogeneous distribution of strontium isotopes in a crystal with a copper-rich core may indicate that mass transport of copper by diffusion occurred during cooling and decompression, in a time scale that was too brief to form obvious (micron-scale) redistribution of Sr isotopes and most elements.

The second discussion topic to be addressed is how copper substitution was governed. The copper in these plagioclase (labradorite, ~ An_{67}) could occur by substitution of Cu^{+2} for Ca or Cu^{+1} for Na in the distorted 9-coordinated site of the plagioclase. Thus, the initial copper substitution may have been governed by the same, well-known coupled exchange mechanism that governs the balance of Ca and Na in plagioclase. Copper has the valences of 0, +1 and +2 and could occur in tetrahedral (IV) octahedral (VI) or 8-fold (VIII) coordination. The ionic radius is 0.74 A for +2

Cu^{IV} and 0.91 A for +2 Cu^{VI}. Extrapolating those values leads to a predicted radius of ~1.05 A for a hypothetical Cu^{VIII}. Taking that value, the cation-anion radius ratio (R_c/R_a) for Cu^{VIII} would be ~0.82 A. The range of radius (R_c/R_a) suitable for 8-coordination is 0.732-1.00 A (similar trends occur for Cu^{+1}). Thus, substitution of copper in an 8-coordinated site seems permissible. The distorted 9-coordinated site might favor a larger cation, but this is not as straightforward as consideration of the ideal sites. Also, higher temperatures and increased vibrational energy may favor substitution of a smaller cation (Cu) into a larger site, as compressibility of the site at high pressure may also favor smaller cations.

The last discussion topic is whether the sunstones formed along with the eruption of Steens-type lavas. The age of the sunstone host basalts is not previously determined in the literature. In this research, the mean of the basalt matrix age of the 'Plush area' of 9.16±0.12 Ma (n=4, 95% c.l.) is distinctly younger than the Steens Basalt at Steens Mountain (~16.7 Ma). This observation means lava flows of the 'Plush area' are not directly part of the 'Steens-type' flows as exposed in the Steens Mountain section. The age of 9.16 Ma is entirely consistent with the trend of ages of the High Plains Lavas (as reported by Jordan et al. (2004); Fig. 2 and 3).

Geochronological data of plagioclase megacrysts from the Ponderosa Mine (raw data is presented in Appendix 2) give complex age spectra with individual ages ranging from 14 to 20 Ma, results that are similar to those obtained from the megacrysts from the 'Plush area' in this study. However, due to the lack of basalt matrix samples from the Ponderosa Mine, the basalt matrix age and a suitably precise estimate for the timing of eruption at the Ponderosa Mine is not constrained by this study.

PROPOSED ADDITIONAL RESEARCH

The first proposed additional research has to do with diffusion modeling. There are diffusion data that can be used for modeling diffusion of major elements in plagioclase (Ramos et al., 2005), along with copper and lithium (Audétat et al., 2018). This type of modeling could also extend to comparisons of copper colloids to the exsolved platelets (Hofmeister and Rossman, 1985b). By using existing diffusion data, a series of cooling paths could be modeled. The plausible cooling paths could be sufficiently rapid to prevent diffusion of most elements (Ca, Sr, etc.), but that would permit copper to diffuse and form exsolved platelets of copper as observed in this study.

Another line of additional research would be to determine statistically the orientation of the exsolved copper schiller. If widespread and consistent among the sunstones, the (010) orientation of the exsolved copper schiller differs from the plane favored for Huttenlocher exsolution, where lamellae commonly have an angle of 16° ~ to 20° ~ against (010) that are most clearly apparent along (100). This intergrowth pattern reflects across albite twin planes (Vernon, 1965). A similar direction near ($\bar{1}41$) for an e-plagioclase (i.e. plagioclase with type e diffractions separated by disordered boundaries) in a Huttenlocher intergrowth (Willaime, 1985). A systematic and non-destructive study of the crystallographic orientation of schiller in a large number of indexed (oriented) sunstones (>100) might be undertaken even with a simple two-circle goniometer.

In this work, it is hypothesized that the copper in plagioclase was incorporated during crystal growth at high temperatures deep within Earth's lithosphere. Subsequently, as the copper-bearing plagioclase ascended and cooled, the incompatibility of Cu, Ca, and Na led to the formation of the copper 'schiller' along with incipient Huttenlocher-style exsolution planes via diffusion. If this is true, and if the original Cu-Na-Ca concentrations can be reconstructed and are provided with data bearing on the diffusivity for these elements, then more information about the original temperature of formation and rate of cooling and ascent for the sunstones can be determined. Also, the orientation of thin copper schiller platelets should be investigated and modelled crystographically. If platelets are usually oriented near to (010), they would be close to the ideal orientation expected for Huttenlocher exsolution in labradorite.

Hypothesis of Sunstone Development

In figure 27, a simple sunstone development hypothesis is illustrated. It is proposed that an early magma chamber (wherein the phenocrysts were grown) was chemically stable and uniform for a long period of time. Plagioclase crystals floated in a denser magma and accumulated near the top (Fig. 27). The activity of copper in this early magma was sufficient to permit Cu^{1+} and/or Cu^{2+} to substitute into plagioclase phenocryst where it distributed uniformly. At a high temperature (a), labradorite with copper had a uniform distribution of major and trace elements. Subsequently, cooling permitted copper exsolution but without significant mobility of major and trace elements (b). It is obvious that the copper platelets are physically placed within the phenocrysts along crystallographic boundaries that seems mostly along (010) as reported previously. After the formation of labradorite with exsolved copper platelets, the phenocryst basalt quenched, erupted, and reached final matrix crystallization (c) with the copper-free rim and with uniform major, trace, REE data, and uniform $^{87}Sr/^{86}Sr$ at the low temperature.

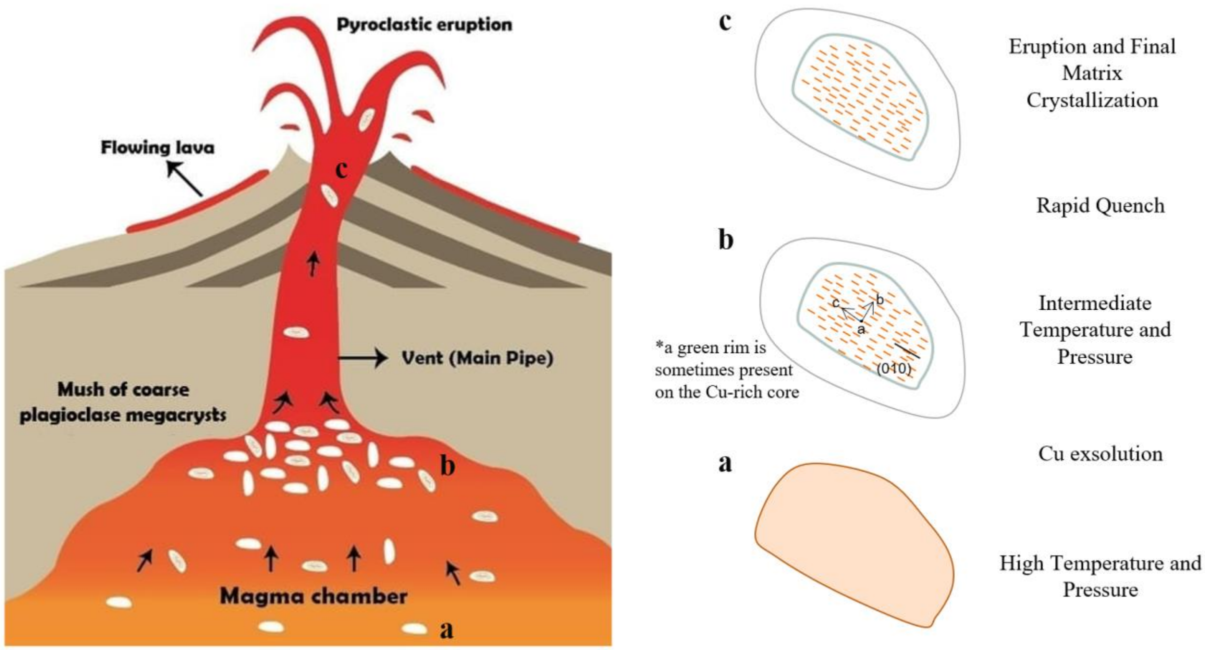

Figure 27. Magma chamber wherein the phenocrysts were grown and hypothesis of sunstone development.

CONCLUSION

The observed homogeneous distribution of major and trace elements and strontium isotopes with cores rich in copper platelets is perplexing. In combination with previous work, our new data indicate rapid exsolution of copper with initial cooling, but those temperatures remained sufficiently high to prevent diffusion of almost all other elements. The age of eruption for basalts hosting sunstones at Plush, Oregon was determined at 9.16±0.12 Ma (as 95% c.l.). The age obtained for the sunstones at the Plush area is comparable to the lavas of the High Lava Plain Trend. Thus, the eruptive ages for basalts at the mines of the Plush area are almost 8 million years younger than the Steen Mountain basalt flow which has been estimated to be ~16.7 Ma. This observation means the sunstone-bearing lava flows of the 'Plush area' were not directly part of earlier eruptions that formed the 'Steens-type' flows of the CRBG and, instead, are part of the High Plains Lavas.

REFERENCES

Andersen, O., 1917, Aventurine labradorite from California: American Mineralogist, v. 2, p. 91.

Audétat, A., Zhang, L., and Ni, H., 2018, Copper and Li diffusion in plagioclase, pyroxenes, olivine and apatite, and consequences for the composition of melt inclusions: Geochimica et Cosmochimica Acta, v. 243, p. 99–115, doi:10.1016/j.gca.2018.09.016.

Badur, Ç.B., 2020, IMPLICATIONS FOR THE HISTORY OF SUNSTONES FROM SOUTHWESTERN OREGON FROM NEW CHEMICAL, ISOTOPIC AND GEOCHRONOLOGIC DATA, *in* GSA, https://gsa.confex.com/gsa/2020AM/webprogram/Paper354204.html (accessed November 2021).

Brueseke, M.E., Heizler, M.T., Hart, W.K., and Mertzman, S.A., 2007, Distribution and geochronology of Oregon Plateau (U.S.A.) flood basalt volcanism: The Steens Basalt revisited: Journal of Volcanology and Geothermal Research, v. 161, p. 187–214, doi:10.1016/j.jvolgeores.2006.12.004.

Camp, V.E., Ross, M.E., Duncan, R.A., Jarboe, N.A., Coe, R.S., Hanan, B.B., and Johnson, J.A., 2013, The Steens Basalt: Earliest lavas of the Columbia River Basalt Group, *in* Reidel, S.P., Camp, V.E., Ross, M.E., Wolff, J.A., Martin, B.S., Tolan, T.L., and Wells, R.E. eds., The Columbia River Flood Basalt Province, Geological Society of America, v. 497, p. 0, doi:10.1130/2013.2497(04).

Hames, W. Early Yellowstone hotspot magmatism and gold metallogeny:, https://www.academia.edu/31906367/Early_Yellowstone_hotspot_magmatism_and_gold_metallogeny (accessed March 2020).

Hames, W., Unger, D., Saunders, J., and Kamenov, G., 2009, Early Yellowstone hotspot magmatism and gold metallogeny: Journal of Volcanology and Geothermal Research, v. 188, p. 214–224, doi:10.1016/j.jvolgeores.2009.07.020.

Hofmeister, A.M., and Rossman, G.R., 1985a, Exsolution of metallic copper from Lake County labradorite: Geology, v. 13, p. 644–647, doi:10.1130/0091-7613(1985)13<644:EOMCFL>2.0.CO;2.

Hofmeister, A.M., and Rossman, G.R., 1985b, Exsolution of metallic copper from Lake County labradorite: Geology, v. 13, p. 644–647, doi:10.1130/0091-7613(1985)13<644:EOMCFL>2.0.CO;2.

Jarboe, N.A., Coe, R.S., Renne, P.R., Glen, J.M.G., and Mankinen, E.A., 2008a, Quickly erupted volcanic sections of the Steens Basalt, Columbia River Basalt Group: Secular variation, tectonic rotation, and the Steens Mountain reversal: Geochemistry, Geophysics, Geosystems, v. 9, p. n/a-n/a, doi:10.1029/2008gc002067.

Jensen, A., 1982, The distribution of Cu across three basaltic lava flows from the Faeroe Islands: undefined, /paper/The-distribution-of-Cu-across-three-basaltic-lava-Jensen/34f0e3ff55a7a84b047755ee3cc2814348181cd7 (accessed March 2021).

Jin, S., Ma, L., Sun, Z., and Palke, A., 2021, DIFFUSION MECHANISM OF CU IN THE GEM-QUALITY LABRADORITE FELDSPAR:, doi:10.1130/abs/2021AM-364265.

Jin, S., Xu, H., Wang, X., Zhang, D., Jacobs, R., and Morgan, D., 2019, The incommensurately modulated structures of volcanic plagioclase: displacement, ordering and phase transition: Acta crystallographica Section B, Structural science, crystal engineering and materials, v. 75, p. 643–656, doi:10.1107/S2052520619006243.

Johnston, C.L., Gunter, M.E., and Knowles, C.R., 1991, Sunstone Labradorite from the Ponderosa Mine, Oregon: Gems & Gemology, v. 27, p. 220–233, doi:10.5741/GEMS.27.4.220.

Jordan, B., Grunder, A., Duncan, R., and Deino, A., 2004, Geochronology of age-progressive volcanism of the Oregon High Lava Plains: Implications for the plume interpretation of Yellowstone: Journal of Geophysical Research B: Solid Earth, v. 109, doi:10.1029/2003JB002776.

Lee, C.-T.A., Luffi, P., Chin, E.J., Bouchet, R., Dasgupta, R., Morton, D.M., Roux, V.L., Yin, Q., and Jin, D., 2012, Copper Systematics in Arc Magmas and Implications for Crust-Mantle Differentiation: Science, v. 336, p. 64–68, doi:10.1126/science.1217313.

Liu, X., Xiong, X., Audétat, A., Li, Y., Song, M., Li, L., Sun, W., and Ding, X., 2014, Partitioning of copper between olivine, orthopyroxene, clinopyroxene, spinel, garnet and silicate melts at upper mantle conditions: Geochimica et Cosmochimica Acta, v. 125, p. 1–22, doi:10.1016/j.gca.2013.09.039.

Moore, N.E., Grunder, A.L., and Bohrson, W.A., 2018, The three-stage petrochemical evolution of the Steens Basalt (southeast Oregon, USA) compared to large igneous provinces and layered mafic intrusions: Geosphere, v. 14, p. 2505–2532, doi:10.1130/GES01665.1.

Oregon Sunstone Value, Price, and Jewelry Information - Gem Society International Gem Society, https://www.gemsociety.org/article/oregon-sunstone-jewelry-and-gemstone-information/ (accessed October 2021).

Ramos, F.C., Wolff, J.A., and Tollstrup, D.L., 2005, Sr isotope disequilibrium in Columbia River flood basalts: Evidence for rapid shallow-level open-system processes: Geology, v. 33, p. 457–460, doi:10.1130/G21512.1.

Stewart, D.B., Walker, G.W., Wright, T.L., and Fahey, J.J., 1966, Physical properties of calcic labradorite from Lake County, Oregon: American Mineralogist, v. 51, p. 177–197.

Sun, S., and McDonough, W., 1989, Chemical and isotopic systematics of ocean basalts: Implications for mantle composition and processes, in Magmatism in the Ocean Basins: Geol. Soc. Spec. Publ., v. 423, p. 13–345.

Three Occurrences of Oregon Sunstone | Gems & Gemology, http://www.gia.edu/sites/Satellite?c=Page&cid=1495237975666&childpagename=GIA/Page/GGArticleDetail&pagename=GIA/Wrapper&WRAPPERPAGE=GIA/Wrapper (accessed February 2021).

Vernon, R.H., 1965, Plagioclase twins in some mafic gneisses from Broken Hill, Australia: Mineralogical Magazine and Journal of the Mineralogical Society, v. 35, p. 488–507, doi:10.1180/minmag.1965.035.271.04.

Welch, S., Cahoon, E., and Steiner, A., 2019, Oregon Sunstones: major element and copper variability between copper-bearing labradorite and basaltic groundmass. AGU Fall Meeting Abstract.

Wierman, C.T. Copper partitioning in mid-Miocene flood basalts from the Northern Great Basin (U.S.A): implications for Cu behavior in flood basalt provinces: , p. 147.

Willaime, C., 1985, Feldspars and feldspathoids -Structures, properties and occurrences. Ed. W.L. Brown, 1984: Bulletin de Minéralogie, v. 108, p. 733–733.

Winter, J.D., 2010, Principles of igneous and metamorphic petrology: New York, Prentice Hall.

Xu, H., Hill, T.R., Konishi, H., and Farfan, G., 2017, Protoenstatite: A new mineral in Oregon sunstones with “watermelon” colors: American Mineralogist, v. 102, p. 2146–2149, doi:10.2138/am-2017-6186.

APPENDIX 1

The Auburn University Electron Microprobe Analysis Lab (AU-EMPA) hosts a JEOL JXA-8600 EMPA equipped with 4 wavelength-dispersive spectrometers (WDS) and detectors for the backscattered electron (BSE) and scanning electron microscopy (SEM) study. The following table shows synthetic and natural standards used routinely for the analysis of feldspars and other silicates. Beam conditions of 15 kV and 20 nA with beam sizes of 1-5 nm and 20 second counting times were used for measurement of standards and unknown phases.

EMPA Methods for Feldspar and Pyroxene

Elements	1(TAP)	2(TAP)	3(PET)	4(LIF)	Mineral standards
Na	x				Amelia
Mg	x				Oliv-2566
Al_3		x			Anorthite
Si_5	x				Amelia
K			x		Microcline
Ca_5			x		Anorthite
Fe_2				x	Fayalite
Ba_3				x	Barite

Elements	1(TAP)	2(TAP)	3(PET)	4(LIF)	Mineral standards
Na	x				Amelia
Mg	x				Oliv-2566
Al_3		x			Anorthite
Si_{11}	x				Woll-2
K			x		Microcline
Ca_2			x		Woll-2
Fe_2				x	Fayalite
Ti_3			x		Ilmenite
Mn				x	P-130
Cr_5				x	Choromite

*Crystals; TAP: Thallium acid phthalate, PET: Pentanerythritol, LIF: Lithium fluoride

Oxide Weight Percent Values for Wollastonite and Diopside Standards Used for the Preceding Analyses

Pt#	SiO_2	TiO_2	Al_2O_3	Cr_2O_3	FeO	MnO	MgO	CaO	Na_2O	K_2O	Total
Wol 1	51,14	0	0	0	0	0,0113	0,1376	48,81	0,0733	0,013	100,19
Wol 2	52,56	0,0111	0	0,0193	0,0777	0,0225	0,1916	49,09	0,0261	0,0144	102,01
Wol 3	51,1	0,0112	0	0,0162	0,0251	0,017	0,1006	48,97	0,0053	0,0101	100,25
Wol 4	52,43	0	0,1105	0,0161	0,0194	0,0028	0,1522	48,72	0,0573	0	101,51
Wol 5	51,91	0	0	0	0	0,0927	0,1404	49,19	0,0156	0	101,35
Wol 6	51,66	0	0	0	0	0	0,1319	49,15	0,0208	0,0115	100,97
Wol 7	51,93	0,0389	0,0697	0,0257	0	0,0394	0,1591	49,03	0	0	101,29
Wol 8	51,17	0	0	0,0032	0,0248	0	0,0809	48,69	0,0052	0	99,98

Pt#	SiO_2	TiO_2	Al_2O_3	Cr_2O_3	FeO	MnO	MgO	CaO	Na_2O	K_2O	Total
Diopside 1	54,12	0,1435	0,5398	0,0129	0,8291	0,0397	19,64	25,58	0,3797	0	101,29
Diopside 2	53,72	0,0446	0,4708	0	0,842	0,1459	19,71	25,74	0,4325	0,0031	101,1
Diopside 3	53,1	0,022	0,5589	0,0289	0,7895	0,0593	19,41	25,8	0,3882	0	100,16
Diopside 4	53,88	0,033	0,4988	0,0289	0,9066	0,1271	19,7	25,45	0,3881	0	101,01
Diopside 5	53,53	0	0,5042	0	0,8546	0,0339	19,5	25,21	0,3493	0,0168	100
Diopside 6	54,17	0,0387	0,4798	0,0129	0,9059	0,0568	19,5	25,76	0,3953	0,0292	101,35
Diopside 7	54,03	0,0165	0,5303	0	0,721	0,0113	19,37	25,54	0,3093	0	100,52
Diopside 8	52,61	0,0713	0,5924	0	0,8182	0,062	19,59	25,24	0,3723	0,0152	99,37

EMPA Data from Plagioclase Megacrysts

Label	LEB-001$m_{c,r}$ (megacryst)		
Date	12/24/2020		
X(mm)	62.4315	62.2893	61.4492
Y(mm)	43.7365	42.6674	43.9385
Oxide Weight Percent: LEB-001$m_{c,r}$ (megacryst)			
Pt#	1	2	3
SiO2	49.71	49.26	49.70
Al2O3	31.02	31.63	31.69
FeO	0.39	0.59	0.50
MgO	0.16	0.11	0.07
MnO	0.12	0.07	0.00
CaO	13.59	13.78	13.84
Na2O	3.77	3.35	3.47
K2O	0.13	0.16	0.13
Total	98.89	98.94	99.41
Cations in Formula (based on 32 oxygen)			
Si	9.18	9.10	9.13
Al	6.75	6.89	6.86
Fe	0.06	0.09	0.08
Mg	0.04	0.03	0.02
Mn	0.02	0.01	0.00
Ca	2.69	2.73	2.72
Na	1.35	1.20	1.24
K	0.03	0.04	0.03
Sum IV:	15.94	15.98	15.99
Sum Alk.	4.07	3.96	3.99
Ca	66.05%	68.78%	68.25%
Na	33.17%	30.27%	30.97%
K	0.78%	0.96%	0.78%

Label	LEB-003$m_{c,r}$ (megacryst)		
Date	12/24/2020		
X(mm)	31.5713	31.2849	
Y(mm)	44.9717	45.9552	
Oxide Weight Percent: LEB-003$m_{c,r}$ (megacryst)			
Pt#	1	2	
SiO2	49.62	50.30	
Al2O3	31.17	30.94	
FeO	0.37	0.56	
MgO	0.11	0.10	
MnO	0.02	0.07	
CaO	13.66	13.38	
Na2O	3.70	3.57	
K2O	0.16	0.19	
Total	98.82	99.12	
Cations in Formula (based on 32 oxygen)			
Si	9.17	9.26	
Al	6.79	6.71	
Fe	0.06	0.09	
Mg	0.03	0.03	
Mn	0.00	0.01	
Ca	2.70	2.64	
Na	1.33	1.27	
K	0.04	0.05	
Sum IV:	15.96	15.97	
Sum Alk.	4.07	3.96	
Ca	66.47%	66.66%	
Na	32.59%	32.20%	
K	0.93%	1.15%	

Label	DE16001m$_{c,r}$ (megacryst)		
Date	12/24/2020		
X(mm)	60.0603	58.9073	59.4518
Y(mm)	70.4541	71.0748	71.1833
Oxide Weight Percent: DE16001mc,r (megacryst)			
Pt#	1	2	3
SiO2	50.27	50.05	51.60
Al2O3	30.28	29.91	29.64
FeO	0.37	0.25	0.42
MgO	0.14	0.10	0.13
MnO	0.00	0.14	0.00
CaO	14.07	13.45	13.27
Na2O	3.59	3.66	3.78
K2O	0.12	0.15	0.13
Total	98.83	97.71	98.97
Cations in Formula (based on 32 oxygen)			
Si	11.64	11.72	11.80
Al	8.27	8.25	7.99
Fe	0.07	0.05	0.08
Mg	0.05	0.03	0.05
Mn	0.00	0.03	0.00
Ca	3.49	3.37	3.25
Na	1.61	1.66	1.68
K	0.03	0.05	0.04
Sum IV:	19.91	19.97	19.80
Sum Alk.	5.14	5.08	4.97
Ca	67.94%	66.40%	65.47%
Na	31.38%	32.71%	33.76%
K	0.67%	0.89%	0.78%

Label	SW19-DD01m$_{c,r}$ (megacryst)		
Date	12/23/2020		
X(mm)	31.7055	31.7055	31.6032
Y(mm)	69.9246	70.5424	69.783
Oxide Weight Percent: SW19-DD01mc,r (megacryst)			
Pt#	1	2	3
SiO2	50.73	50.62	51.71
Al2O3	31.22	30.98	30.72
FeO	0.59	0.58	0.97
MgO	0.08	0.10	0.09
MnO	0.00	0.07	0.00
CaO	13.91	13.89	13.16
Na2O	3.47	3.51	3.71
K2O	0.12	0.12	0.19
Total	100.13	99.88	100.56
Cations in Formula (based on 32 oxygen)			
Si	9.24	9.25	9.37
Al	6.71	6.67	6.56
Fe	0.09	0.09	0.15
Mg	0.02	0.03	0.03
Mn	0.00	0.01	0.00
Ca	2.72	2.72	2.56
Na	1.23	1.24	1.30
K	0.03	0.03	0.04
Sum IV:	15.95	15.93	15.94
Sum Alk.	3.97	3.99	3.91
Ca	68.40%	68.14%	65.45%
Na	30.89%	31.17%	33.40%
K	0.71%	0.69%	1.14%

EMPA Data from Fine Matrix Plagioclase

Label	LEB-001mp2 (matrix plag)									
Date	12/25/2020									
X(mm)	60.1045	60.1044	60.1043	60.1042	60.104	60.1039	60.1038	60.1037	60.1035	60.1034
Y(mm)	39.8714	39.8707	39.87	39.8693	39.8686	39.8679	39.8671	39.8665	39.8658	39.865
Oxide Weight Percent: LEB-001mp2 (matrix plag)										
Pt#	1	2	3	4	5	6	7	8	9	10
SiO2	50.76	51.15	51.74	51.45	50.44	50.20	50.71	50.13	50.43	50.80
Al2O3	30.39	30.88	30.53	31.14	31.91	30.97	31.05	31.03	31.43	31.06
FeO	0.95	1.03	0.96	1.03	1.02	0.98	1.04	1.02	1.01	0.97
MgO	0.00	0.01	0.07	0.00	0.00	0.03	0.03	0.00	0.00	0.01
MnO	0.03	0.01	0.10	0.00	0.00	0.07	0.08	0.00	0.00	0.00
CaO	12.96	12.95	13.05	13.17	13.08	13.24	13.03	12.87	12.78	12.77
Na2O	3.71	3.71	3.83	3.76	3.83	3.67	3.89	3.80	3.58	3.91
K2O	0.22	0.26	0.25	0.24	0.23	0.22	0.24	0.24	0.24	0.26
Total	99.02	100.00	100.54	100.80	100.50	99.38	100.07	99.08	99.47	99.78
Cations in Formula (based on 32 oxygen)										
Si	9.35	9.33	9.39	9.32	9.17	9.23	9.26	9.24	9.24	9.29
Al	6.60	6.64	6.53	6.65	6.84	6.71	6.69	6.74	6.79	6.69
Fe	0.15	0.16	0.15	0.16	0.15	0.15	0.16	0.16	0.16	0.15
Mg	0.00	0.00	0.02	0.00	0.00	0.01	0.01	0.00	0.00	0.00
Mn	0.00	0.00	0.02	0.00	0.00	0.01	0.01	0.00	0.00	0.00
Ca	2.56	2.53	2.54	2.56	2.55	2.61	2.55	2.54	2.51	2.50
Na	1.33	1.31	1.35	1.32	1.35	1.31	1.38	1.36	1.27	1.39
K	0.05	0.06	0.06	0.06	0.05	0.05	0.06	0.06	0.06	0.06
Sum IV:	15.95	15.97	15.92	15.96	16.01	15.95	15.95	15.98	16.03	15.98
Sum Alk.	3.94	3.90	3.94	3.93	3.95	3.97	3.98	3.96	3.84	3.95
Mole Percent										
Ab	64.99%	64.84%	64.37%	64.98%	64.48%	65.71%	64.02%	64.24%	65.39%	63.35%
An	33.68%	33.63%	34.20%	33.58%	34.18%	32.97%	34.60%	34.34%	33.16%	35.11%
Or	1.33%	1.53%	1.44%	1.44%	1.34%	1.32%	1.39%	1.42%	1.46%	1.54%

Label	LEB-001mp2 (matrix plag)									
Date	12/25/2020									
X(mm)	60.1033	60.1032	60.103	60.103	60.1028	60.1027	60.1026	60.1025	60.1023	60.1022
Y(mm)	39.8643	39.8636	39.863	39.8622	39.8615	39.8608	39.8601	39.8594	39.8587	39.858
Oxide Weight Percent: LEB-001mp2 (matrix plag)										
Pt#	11	12	13	14	15	16	17	18	19	20
SiO2	51.61	51.34	50.91	52.22	53.41	53.15	53.73	55.67	57.48	60.22
Al2O3	31.03	30.48	30.41	30.00	28.87	28.07	28.39	27.55	26.99	26.06
FeO	1.00	0.97	1.16	1.52	1.74	1.76	1.44	1.17	1.11	0.96
MgO	0.04	0.08	0.00	0.04	0.06	0.03	0.01	0.00	0.00	0.07
MnO	0.02	0.00	0.11	0.05	0.00	0.07	0.01	0.01	0.08	0.04
CaO	12.92	12.78	12.90	12.31	11.27	11.02	10.81	9.93	8.91	7.48
Na2O	4.05	3.91	3.88	4.15	4.78	4.64	4.75	5.46	4.72	2.79
K2O	0.27	0.22	0.25	0.30	0.33	0.37	0.40	0.40	0.60	0.93
Total	100.94	99.78	99.62	100.60	100.46	99.11	99.55	100.19	99.91	98.55
Cations in Formula (based on 32 oxygen)										
Si	9.33	9.38	9.34	9.48	9.69	9.77	9.81	10.05	10.32	10.78
Al	6.61	6.56	6.58	6.42	6.18	6.08	6.11	5.86	5.71	5.50
Fe	0.15	0.15	0.18	0.23	0.26	0.27	0.22	0.18	0.17	0.14
Mg	0.01	0.02	0.00	0.01	0.02	0.01	0.00	0.00	0.00	0.02
Mn	0.00	0.00	0.02	0.01	0.00	0.01	0.00	0.00	0.01	0.01
Ca	2.50	2.50	2.54	2.39	2.19	2.17	2.11	1.92	1.71	1.43
Na	1.42	1.39	1.38	1.46	1.68	1.65	1.68	1.91	1.64	0.97
K	0.06	0.05	0.06	0.07	0.08	0.09	0.09	0.09	0.14	0.21
Sum IV:	15.95	15.95	15.92	15.90	15.87	15.86	15.91	15.92	16.04	16.28
Sum Alk.	3.99	3.94	3.98	3.93	3.95	3.91	3.89	3.93	3.50	2.62
Mole Percent										
Ab	62.82%	63.51%	63.79%	61.00%	55.46%	55.47%	54.36%	48.94%	49.03%	54.79%
An	35.65%	35.17%	34.73%	37.23%	42.58%	42.28%	43.24%	48.71%	47.02%	37.05%
Or	1.54%	1.32%	1.49%	1.77%	1.96%	2.24%	2.40%	2.36%	3.95%	8.15%

Label	LEB-003mp (matrix plag)									
Date	12/24/2020									
X(mm)	21.7355	21.7368	21.7381	21.7393	21.7407	21.742	21.7432	21.7445	21.7458	21.7471
Y(mm)	43.435	43.435	43.435	43.435	43.435	43.435	43.435	43.435	43.435	43.435
Oxide Weight Percent: LEB-003mp (matrix plag)										
Pt#	1	2	3	4	5	6	7	8	9	10
SiO2	53.82	52.09	51.21	51.86	51.56	50.82	50.80	51.59	51.74	51.10
Al2O3	25.19	28.25	28.78	27.89	27.59	28.43	27.70	27.57	27.49	27.74
FeO	1.35	0.89	0.92	1.01	1.07	0.97	0.89	1.01	0.93	0.86
MgO	0.23	0.13	0.07	0.07	0.06	0.05	0.07	0.13	0.22	0.13
MnO	0.00	0.02	0.13	0.08	0.00	0.00	0.03	0.08	0.07	0.00
CaO	9.37	11.86	12.30	12.27	12.06	12.22	12.07	11.73	11.86	11.71
Na2O	5.70	4.42	4.69	4.47	4.22	4.21	4.40	4.58	4.78	4.58
K2O	0.43	0.31	0.26	0.29	0.29	0.28	0.31	0.35	0.35	0.34
Total	96.09	97.96	98.36	97.96	96.84	96.98	96.26	97.03	97.44	96.45
Cations in Formula (based on 32 oxygen)										
Si	10.16	9.68	9.52	9.66	9.70	9.56	9.63	9.70	9.69	9.65
Al	5.61	6.19	6.30	6.13	6.12	6.30	6.19	6.11	6.07	6.18
Fe	0.21	0.14	0.14	0.16	0.17	0.15	0.14	0.16	0.15	0.14
Mg	0.06	0.04	0.02	0.02	0.02	0.01	0.02	0.04	0.06	0.04
Mn	0.00	0.00	0.02	0.01	0.00	0.00	0.00	0.01	0.01	0.00
Ca	1.90	2.36	2.45	2.45	2.43	2.46	2.45	2.36	2.38	2.37
Na	2.09	1.59	1.69	1.62	1.54	1.54	1.62	1.67	1.74	1.68
K	0.10	0.07	0.06	0.07	0.07	0.07	0.07	0.08	0.08	0.08
Sum IV:	15.77	15.86	15.82	15.79	15.82	15.86	15.82	15.80	15.76	15.83
Sum Alk.	4.09	4.03	4.20	4.14	4.04	4.06	4.14	4.12	4.20	4.13
Mole Percent										
Ab	46.39%	58.64%	58.30%	59.24%	60.17%	60.58%	59.16%	57.39%	56.65%	57.40%
An	51.09%	39.56%	40.24%	39.07%	38.11%	37.78%	39.04%	40.56%	41.33%	40.64%
Or	2.52%	1.80%	1.46%	1.69%	1.72%	1.64%	1.81%	2.04%	2.02%	1.96%

Label	LEB-003mp (matrix plag)									
Date										
X(mm)	21.7484	21.7497	21.751	21.7523	21.7535	21.7548	21.7562	21.7574	21.7587	21.76
Y(mm)	43.435	43.435	43.435	43.435	43.435	43.435	43.435	43.435	43.435	43.435
Oxide Weight Percent: LEB-003mp (matrix plag)										
Pt#	11	12	13	14	15	16	17	18	19	20
SiO2	50.91	51.84	51.61	51.18	52.57	54.10	55.40	53.54	56.82	64.71
Al2O3	27.88	27.50	27.78	27.62	27.70	25.64	25.39	26.25	23.81	19.99
FeO	0.89	1.03	0.96	1.01	0.87	1.20	1.37	1.28	1.37	1.12
MgO	0.08	0.12	0.07	0.21	0.10	0.11	0.20	0.08	0.00	0.07
MnO	0.01	0.00	0.15	0.07	0.12	0.00	0.05	0.04	0.04	0.07
CaO	11.69	11.89	11.72	11.93	11.74	10.17	9.69	10.17	8.41	4.94
Na2O	4.70	4.61	4.39	4.16	4.72	5.02	4.97	4.64	5.56	3.66
K2O	0.34	0.32	0.28	0.30	0.30	0.47	0.51	0.43	0.74	1.87
Total	96.49	97.30	96.95	96.48	98.11	96.72	97.57	96.43	96.74	96.42
Cations in Formula (based on 32 oxygen)										
Si	9.62	9.71	9.69	9.67	9.76	10.14	10.27	10.06	10.58	11.77
Al	6.21	6.07	6.15	6.15	6.06	5.66	5.55	5.81	5.23	4.29
Fe	0.14	0.16	0.15	0.16	0.13	0.19	0.21	0.20	0.21	0.17
Mg	0.02	0.03	0.02	0.06	0.03	0.03	0.05	0.02	0.00	0.02
Mn	0.00	0.00	0.02	0.01	0.02	0.00	0.01	0.01	0.01	0.01
Ca	2.37	2.39	2.36	2.41	2.33	2.04	1.92	2.05	1.68	0.96
Na	1.72	1.68	1.60	1.52	1.70	1.82	1.79	1.69	2.01	1.29
K	0.08	0.08	0.07	0.07	0.07	0.11	0.12	0.10	0.18	0.43
Sum IV:	15.84	15.79	15.84	15.82	15.82	15.80	15.81	15.87	15.81	16.06
Sum Alk.	4.17	4.14	4.03	4.01	4.10	3.98	3.83	3.84	3.86	2.69
Mole Percent										
Ab	56.75%	57.66%	58.59%	60.20%	56.87%	51.32%	50.24%	53.31%	43.44%	35.83%
An	41.30%	40.47%	39.73%	38.00%	41.39%	45.86%	46.64%	44.03%	51.99%	48.05%
Or	1.95%	1.87%	1.69%	1.80%	1.74%	2.82%	3.12%	2.66%	4.57%	16.13%

Label	DE16-001mp1 (matrix plag)									
Date	12/23/2020									
X(mm)	61.6799	61.6792	61.6784	61.6777	61.677	61.6762	61.6755	61.6748	61.674	61.6733
Y(mm)	66.2963	66.2949	66.2935	66.292	66.2906	66.2891	66.2876	66.2862	66.2848	66.2833
Oxide Weight Percent: DE16001mp1 (matrix plag)										
Pt#	1	2	3	4	5	6	7	8	9	10
SiO2	64.48	62.79	56.99	52.25	51.90	53.15	53.35	52.47	52.04	51.90
Al2O3	23.28	24.52	26.59	28.85	29.17	27.76	28.04	28.11	28.38	29.91
FeO	1.09	0.85	1.06	0.98	2.24	2.50	1.24	1.12	1.50	1.00
MgO	0.11	0.12	0.09	0.04	0.17	0.22	0.09	0.04	0.55	0.16
MnO	0.14	0.05	0.14	0.00	0.01	0.04	0.00	0.01	0.11	0.04
CaO	4.35	6.31	9.52	11.96	12.25	11.08	11.43	11.57	12.40	13.03
Na2O	2.35	2.07	4.08	4.45	3.90	4.41	4.20	4.44	3.64	3.55
K2O	1.84	0.74	0.42	0.28	0.22	0.32	0.32	0.27	0.32	0.23
Total	97.63	97.45	98.88	98.81	99.88	99.48	98.66	98.05	98.94	99.83
Cations in Formula (based on 32 oxygen)										
Si	11.50	11.22	10.33	9.63	9.51	9.76	9.81	9.73	9.60	9.47
Al	4.89	5.16	5.68	6.26	6.30	6.01	6.08	6.15	6.17	6.43
Fe	0.16	0.13	0.16	0.15	0.34	0.38	0.19	0.17	0.23	0.15
Mg	0.03	0.03	0.02	0.01	0.05	0.06	0.02	0.01	0.15	0.04
Mn	0.02	0.01	0.02	0.00	0.00	0.01	0.00	0.00	0.02	0.01
Ca	0.83	1.21	1.85	2.36	2.41	2.18	2.25	2.30	2.45	2.55
Na	0.81	0.72	1.43	1.59	1.39	1.57	1.50	1.60	1.30	1.26
K	0.42	0.17	0.10	0.07	0.05	0.07	0.07	0.06	0.07	0.05
Sum IV:	16.39	16.38	16.01	15.89	15.82	15.78	15.89	15.88	15.77	15.91
Sum Alk.	2.06	2.09	3.38	4.02	3.85	3.83	3.83	3.96	3.83	3.86
Mole Percent										
Ab	40.33%	57.71%	54.70%	58.78%	62.57%	57.00%	58.88%	58.04%	64.02%	66.04%
An	39.37%	34.23%	42.44%	39.59%	36.06%	41.07%	39.16%	40.32%	34.02%	32.57%
Or	20.30%	8.05%	2.86%	1.64%	1.37%	1.94%	1.96%	1.64%	1.95%	1.39%

Label	DE16-001mp1 (matrix plag)									
Date										
X(mm)	61.6726	61.6718	61.6711	61.6704	61.6697	61.6689	61.6682	61.6675	61.6667	61.666
Y(mm)	66.2818	66.2804	66.279	66.2775	66.276	66.2746	66.2731	66.2717	66.2703	66.2688
Oxide Weight Percent: DE16001mp1 (matrix plag)										
Pt#	11	12	13	14	15	16	17	18	19	20
SiO2	51.58	51.20	52.82	51.71	51.59	52.99	53.74	56.88	59.38	61.49
Al2O3	30.65	30.69	28.74	29.76	29.11	29.19	27.81	26.79	25.28	23.68
FeO	0.81	0.90	1.40	1.21	1.66	1.00	0.93	0.95	0.70	0.67
MgO	0.07	0.06	0.09	0.15	0.44	0.19	0.05	0.09	0.02	0.00
MnO	0.02	0.10	0.00	0.00	0.04	0.00	0.00	0.11	0.15	0.00
CaO	13.62	13.47	11.72	12.39	12.34	12.15	10.68	8.97	7.19	5.66
Na2O	3.41	3.33	4.16	3.99	3.69	4.07	4.54	5.73	6.43	7.14
K2O	0.21	0.22	0.26	0.25	0.28	0.27	0.33	0.53	0.72	0.99
Total	100.38	99.98	99.19	99.47	99.15	99.85	98.08	100.05	99.88	99.63
Cations in Formula (based on 32 oxygen)										
Si	9.37	9.34	9.69	9.48	9.50	9.64	9.91	10.25	10.64	10.99
Al	6.56	6.60	6.21	6.43	6.32	6.26	6.04	5.69	5.34	4.99
Fe	0.12	0.14	0.21	0.19	0.26	0.15	0.14	0.14	0.11	0.10
Mg	0.02	0.02	0.03	0.04	0.12	0.05	0.01	0.02	0.00	0.00
Mn	0.00	0.02	0.00	0.00	0.01	0.00	0.00	0.02	0.02	0.00
Ca	2.65	2.63	2.30	2.43	2.44	2.37	2.11	1.73	1.38	1.08
Na	1.20	1.18	1.48	1.42	1.32	1.44	1.62	2.00	2.23	2.48
K	0.05	0.05	0.06	0.06	0.07	0.06	0.08	0.12	0.17	0.23
Sum IV:	15.93	15.94	15.90	15.91	15.83	15.90	15.95	15.93	15.98	15.98
Sum Alk.	3.90	3.86	3.84	3.91	3.82	3.87	3.81	3.86	3.78	3.79
Mole Percent										
Ab	67.94%	68.15%	59.92%	62.25%	63.76%	61.26%	55.37%	44.90%	36.52%	28.63%
An	30.79%	30.50%	38.50%	36.29%	34.51%	37.15%	42.61%	51.92%	59.11%	65.39%
Or	1.26%	1.35%	1.57%	1.47%	1.73%	1.59%	2.03%	3.18%	4.37%	5.98%

Label	SW19-DD01mp (matrix plag)									
Date	12/22/2020									
X(mm)	19.4398	19.4398	19.4398	19.4398	19.4398	19.4398	19.4398	19.4398	19.4398	19.4398
Y(mm)	68.7488	68.7474	68.746	68.7446	68.7432	68.7418	68.7404	68.739	68.7376	68.7362
Oxide Weight Percent: SW19-DD01mp(matrix plag)										
Pt#	1	2	3	4	5	6	7	8	9	10
SiO2	60.35	61.58	61.88	60.46	59.7	60.01	57.74	55.13	53.83	52.36
Al2O3	23.55	23.7	24.93	24.74	24.2	25.08	26.42	29.04	30	30.57
FeO	1.112	1.1229	0.9557	1.0373	0.9147	1.0279	1.067	0.8	0.8448	0.6846
MgO	0.2213	0.2134	0.0799	0	0.0766	0.0184	0.0821	0.1075	0.114	0.1719
MnO	0.1203	0.1018	0.1139	0.1019	0.066	0.0301	0.0121	0.1221	0.0241	0.0483
CaO	7.19	7.2	6.98	7.05	7.09	7.58	8.79	11.31	12.93	13.01
Na2O	6.32	5.01	6.28	6.45	5.95	6.15	5.99	4.61	3.89	3.96
K2O	0.7591	0.7401	0.8271	0.8163	0.7662	0.6965	0.5342	0.3301	0.213	0.2033
Total	99.64	99.67	102.04	100.66	98.76	100.6	100.64	101.45	101.85	101.01
Cations in Formula (based on 32 oxygen)										
Si	10.85	10.98	10.82	10.75	10.79	10.68	10.33	9.84	9.60	9.44
Al	4.99	4.98	5.14	5.19	5.16	5.26	5.57	6.11	6.31	6.49
Fe	0.17	0.17	0.14	0.15	0.14	0.15	0.16	0.12	0.13	0.10
Mg	0.06	0.06	0.02	0.00	0.02	0.00	0.02	0.03	0.03	0.05
Mn	0.02	0.02	0.02	0.02	0.01	0.00	0.00	0.02	0.00	0.01
Ca	1.38	1.38	1.31	1.34	1.37	1.45	1.69	2.16	2.47	2.51
Na	2.20	1.73	2.13	2.22	2.09	2.12	2.08	1.60	1.35	1.38
K	0.17	0.17	0.18	0.19	0.18	0.16	0.12	0.08	0.05	0.05
Sum IV:	15.84	15.96	15.96	15.94	15.95	15.94	15.91	15.94	15.91	15.93
Sum Alk.	3.76	3.28	3.62	3.75	3.64	3.73	3.89	3.83	3.87	3.94
Mole Percent										
Ab	36.81%	41.98%	36.10%	35.79%	37.77%	38.79%	43.37%	56.41%	63.93%	63.71%
An	58.57%	52.88%	58.80%	59.27%	57.37%	56.97%	53.50%	41.62%	34.82%	35.10%
Or	4.63%	5.14%	5.09%	4.94%	4.86%	4.24%	3.14%	1.96%	1.25%	1.19%

Label	SW19-DD01mp (matrix plag)									
Date										
X(mm)	19.4398	19.4398	19.4398	19.4398	19.4398	19.4398	19.4398	19.4398	19.4398	19.4398
Y(mm)	68.7348	68.7334	68.732	68.7306	68.7292	68.7278	68.7264	68.725	68.7236	68.7222
Oxide Weight Percent: SW19-DD01mp(matrix plag)										
Pt#	11	12	13	14	15	16	17	18	19	20
SiO2	53.86	52.81	51.91	53.58	53.84	53.36	53	53.35	52.95	53.78
Al2O3	30.39	30.46	30.66	30.61	30.41	29.89	29.6	30.34	29.94	29.67
FeO	0.755	0.745	0.7491	0.7346	0.5596	0.7165	0.7123	0.7998	0.673	1.1388
MgO	0.1522	0.1408	0.1377	0.1066	0.1037	0.0365	0.121	0.1364	0.0548	0.08
MnO	0	0.0363	0	0.079	0.0611	0.0061	0	0	0.1093	0.1214
CaO	13.16	13.23	13.19	13.24	13.26	13.06	13.3	13.06	13.16	13
Na2O	3.75	3.66	3.62	3.95	4.14	3.71	3.38	3.97	3.63	3.75
K2O	0.1827	0.2384	0.2229	0.1862	0.2334	0.2298	0.2176	0.2001	0.2019	0.2533
Total	102.25	101.32	100.49	102.48	102.61	101.01	100.33	101.86	100.71	101.8
Cations in Formula (based on 32 oxygen)										
Si	9.57	9.48	9.40	9.51	9.55	9.59	9.59	9.53	9.56	9.62
Al	6.36	6.45	6.55	6.41	6.35	6.33	6.32	6.39	6.37	6.25
Fe	0.11	0.11	0.11	0.11	0.08	0.11	0.11	0.12	0.10	0.17
Mg	0.04	0.04	0.04	0.03	0.03	0.01	0.03	0.04	0.01	0.02
Mn	0.00	0.01	0.00	0.01	0.01	0.00	0.00	0.00	0.02	0.02
Ca	2.50	2.55	2.56	2.52	2.52	2.52	2.58	2.50	2.54	2.49
Na	1.29	1.27	1.27	1.36	1.42	1.29	1.19	1.38	1.27	1.30
K	0.04	0.05	0.05	0.04	0.05	0.05	0.05	0.05	0.05	0.06
Sum IV:	15.93	15.93	15.95	15.92	15.90	15.93	15.91	15.91	15.92	15.87
Sum Alk.	3.84	3.87	3.88	3.92	4.00	3.86	3.82	3.92	3.86	3.85
Mole Percent										
Ab	65.26%	65.69%	65.92%	64.23%	63.05%	65.14%	67.59%	63.75%	65.89%	64.71%
An	33.66%	32.90%	32.75%	34.69%	35.63%	33.50%	31.09%	35.08%	32.90%	33.79%
Or	1.08%	1.41%	1.33%	1.08%	1.32%	1.36%	1.32%	1.16%	1.20%	1.50%

EMPA Data from Finely Grained Pyroxene Crystals of Matrix

Label	**LEB001pyx1**							
Date	1/15/2021							
X(mm)	70.8885	70.5806	70.616	70.6322	70.5328	70.6817	70.4918	69.5975
Y(mm)	40.8301	40.7885	40.8186	40.8422	40.6968	40.5101	40.5143	40.308
Oxide Weight Percent: LEB-001pyx								
Pt#	22	24	25	26	27	28	29	30
SiO2	49.41	52.7	50.22	52.8	51.15	51.82	52.09	53.58
TiO2	1.15	0.84	1.04	0.88	1.14	1.27	1.02	0.79
Al2O3	2.81	1.73	3.19	1.9	2.49	3.06	3.01	1.75
Cr2O3	0.04	0.03	0	0	0.04	0	0	0.07
FeO	10.63	9.23	9.42	9.19	10.24	9.79	9.65	9.6
MnO	0.33	0.39	0.22	0.26	0.36	0.31	0.2	0.32
MgO	13.39	15.11	14.39	15.07	14.19	14.02	14.79	14.96
CaO	19.43	20.01	20.38	19.52	20.09	19.54	20.03	19.67
Na2O	0.49	0.62	0.31	0.37	0.47	1.6	0.58	0.33
K2O	0.02	0	0.01	0.06	0	0.01	0.01	0.03
Total	97.7	100.66	99.2	100.05	100.18	101.41	101.38	101.11
Cations in Formula (based on 6 oxygen)								
Si	1.9	1.95	1.89	1.96	1.91	1.91	1.91	1.97
Ti	0.03	0.02	0.03	0.02	0.03	0.04	0.03	0.02
Al	0.13	0.08	0.14	0.08	0.11	0.13	0.13	0.08
Cr	0	0	0	0	0	0	0	0
Fe	0.34	0.29	0.3	0.28	0.32	0.3	0.3	0.29
Mn	0.01	0.01	0.01	0.01	0.01	0.01	0.01	0.01
Mg	0.77	0.83	0.81	0.83	0.79	0.77	0.81	0.82
Ca	0.8	0.79	0.82	0.77	0.8	0.77	0.79	0.77
Na	0.04	0.04	0.02	0.03	0.03	0.11	0.04	0.02
K	0	0	0	0	0	0	0	0
Sum IV:	2.03	2.02	2.03	2.04	2.02	2.04	2.04	2.04
Sum	1.91	1.91	1.93	1.89	1.92	1.84	1.89	1.89
Wo	41.92%	41.48%	42.68%	40.96%	42.01%	41.85%	41.61%	41.00%
En	40.19%	43.58%	41.92%	43.99%	41.28%	41.78%	42.74%	43.38%
Fs	17.90%	14.94%	15.40%	15.05%	16.71%	16.37%	15.65%	15.62%

Label	**LEB003pyx**								
Date	1/19/2021								
X(mm)	17.3951	17.8176	17.8529	17.9916	18.8261	18.9067	19.0218	19.3153	19.2955	19.6559
Y(mm)	39.586	39.8655	39.8697	39.8455	39.8711	39.8649	39.869	39.8527	39.8074	39.8046
Oxide Weight Percent: LEB-003pyx									
Pt#	44	46	47	48	49	50	51	52	53	54
SiO2	48.76	48.06	50.26	49.34	50.63	50.07	49.78	51.26	52.70	48.14
TiO2	2.98	1.76	1.48	1.87	2.17	2.47	2.76	1.96	1.19	3.16
Al2O3	3.03	3.60	2.61	2.36	2.26	2.77	2.93	2.52	2.04	4.89
Cr2O3	0.07	0.00	0.00	0.03	0.00	0.00	0.04	0.01	0.03	0.00
FeO	14.06	11.66	16.36	13.04	11.89	14.41	12.38	13.40	10.58	12.75
MnO	0.45	0.41	0.51	0.42	0.32	0.41	0.38	0.45	0.38	0.26
MgO	11.07	11.35	14.05	12.37	13.27	10.57	11.26	11.61	14.76	11.68
CaO	19.41	20.82	14.38	19.85	20.23	19.94	20.73	19.57	19.91	18.93
Na2O	0.53	0.81	0.35	0.72	0.52	0.66	0.65	0.60	0.56	0.47
K2O	0.05	0.17	0.73	0.06	0.02	0.06	0.03	0.03	0.02	0.10
Total	100.42	98.65	100.71	100.06	101.30	101.36	100.94	101.41	102.18	100.38
Cations in Formula (based on 6 oxygen)									
Si	1.86	1.86	1.90	1.88	1.89	1.89	1.88	1.92	1.93	1.82
Ti	0.09	0.05	0.04	0.05	0.06	0.07	0.08	0.06	0.03	0.09
Al	0.14	0.16	0.12	0.11	0.10	0.12	0.13	0.11	0.09	0.22
Cr	0.00	0.00	0.00	0.00	0.00	0.00	0.00	0.00	0.00	0.00
Fe	0.45	0.38	0.52	0.42	0.37	0.45	0.39	0.42	0.32	0.40
Mn	0.01	0.01	0.02	0.01	0.01	0.01	0.01	0.01	0.01	0.01
Mg	0.63	0.65	0.79	0.70	0.74	0.59	0.63	0.65	0.81	0.66
Ca	0.79	0.86	0.58	0.81	0.81	0.81	0.84	0.78	0.78	0.77
Na	0.04	0.06	0.03	0.05	0.04	0.05	0.05	0.04	0.04	0.03
K	0.00	0.01	0.04	0.00	0.00	0.00	0.00	0.00	0.00	0.00
Sum IV:	1.99	2.02	2.02	1.99	1.99	2.01	2.01	2.03	2.02	2.04
Sum	1.87	1.89	1.89	1.93	1.92	1.86	1.86	1.85	1.91	1.83
Wo	42.39%	45.55%	30.80%	42.02%	42.17%	43.45%	45.01%	42.38%	40.88%	41.94%
En	33.64%	34.54%	41.86%	36.43%	38.48%	32.04%	34.01%	34.98%	42.16%	36.01%
Fs	23.97%	19.91%	27.35%	21.55%	19.35%	24.51%	20.98%	22.65%	16.96%	22.05%

Label	DE16001pyx									
Date	1/19/2021									
X(mm)	61.0552	61.6024	61.806	61.9118	62.6089	63.2148	63.3965	63.4865	63.1182	61.5659
Y(mm)	64.5205	64.4079	64.4278	64.3703	64.2682	64.1205	63.8405	63.6952	71.3957	71.279
Oxide Weight Percent: DE16001pyx										
Pt#	56	57	58	59	60	61	62	63	64	65
SiO2	45.87	48.51	47.50	47.83	48.92	47.94	47.35	47.39	47.20	49.75
TiO2	2.69	1.93	2.82	2.73	2.78	2.87	2.89	2.96	2.56	2.06
Al2O3	4.46	2.72	3.82	4.12	4.38	4.02	4.74	5.12	4.13	3.59
Cr2O3	0.06	0.00	0.05	0.03	0.00	0.02	0.00	0.01	0.00	0.03
FeO	12.36	12.66	12.46	12.19	12.77	13.05	12.42	12.10	12.76	12.05
MnO	0.26	0.35	0.32	0.29	0.24	0.32	0.16	0.29	0.25	0.28
MgO	11.73	13.09	12.16	12.33	12.07	11.79	11.84	12.02	12.03	12.93
CaO	21.10	20.06	20.76	20.61	20.24	20.25	20.91	20.68	20.72	19.96
Na2O	0.48	0.50	0.52	0.57	0.59	0.41	0.67	0.40	0.48	0.56
K2O	0.00	0.00	0.01	0.00	0.02	0.01	0.01	0.00	0.00	0.02
Total	99.02	99.82	100.42	100.70	102.02	100.67	100.99	100.96	100.13	101.23
Cations in Formula (based on 6 oxygen)										
Si	1.78	1.85	1.81	1.81	1.82	1.82	1.79	1.79	1.80	1.86
Ti	0.08	0.06	0.08	0.08	0.08	0.08	0.08	0.08	0.07	0.06
Al	0.20	0.12	0.17	0.18	0.19	0.18	0.21	0.23	0.19	0.16
Cr	0.00	0.00	0.00	0.00	0.00	0.00	0.00	0.00	0.00	0.00
Fe	0.40	0.40	0.40	0.39	0.40	0.41	0.39	0.38	0.41	0.38
Mn	0.01	0.01	0.01	0.01	0.01	0.01	0.01	0.01	0.01	0.01
Mg	0.68	0.75	0.69	0.70	0.67	0.67	0.67	0.68	0.69	0.72
Ca	0.88	0.82	0.85	0.84	0.81	0.82	0.85	0.84	0.85	0.80
Na	0.04	0.04	0.04	0.04	0.04	0.03	0.05	0.03	0.04	0.04
K	0.00	0.00	0.00	0.00	0.00	0.00	0.00	0.00	0.00	0.00
Sum IV:	1.98	1.97	1.98	1.99	2.02	2.00	2.00	2.01	1.99	2.02
Sum	1.95	1.97	1.93	1.92	1.88	1.90	1.91	1.89	1.94	1.90
Wo	44.83%	41.66%	43.80%	43.59%	43.06%	43.23%	44.42%	44.14%	43.70%	42.15%
En	34.67%	37.82%	35.69%	36.28%	35.73%	35.02%	34.99%	35.70%	35.30%	37.99%
Fs	20.50%	20.52%	20.52%	20.12%	21.21%	21.75%	20.59%	20.16%	21.00%	19.86%

Label	SW19DD01pyx										
Date	1/19/2021										
X(mm)	20.8782	20.5589	20.5999	20.5014	18.3017	17.8044	17.6696	20.3883	19.6484	19.0006	17.8929
Y(mm)	65.786	65.3562	65.0805	63.4802	63.4388	63.4291	63.059	62.8011	63.994	63.5313	63.3888
Oxide Weight Percent: SW19DD01pyx											
Pt#	66	67	68	69	70	71	72	73	74	75	76
SiO2	47.40	48.30	48.07	48.01	47.08	46.98	45.88	47.68	47.90	47.68	48.46
TiO2	1.94	2.15	2.21	2.17	2.14	2.16	2.74	2.05	2.27	2.16	2.30
Al2O3	3.99	3.97	3.33	4.31	3.21	3.29	3.37	3.39	4.48	3.55	4.14
Cr2O3	0.00	0.02	0.03	0.02	0.01	0.00	0.07	0.00	0.02	0.02	0.02
FeO	11.22	11.37	12.02	11.23	12.23	12.07	12.95	12.18	11.17	11.53	12.13
MnO	0.21	0.31	0.24	0.30	0.28	0.38	0.39	0.26	0.19	0.24	0.24
MgO	13.41	13.21	13.29	13.35	13.14	12.97	11.94	12.62	13.27	13.20	12.94
CaO	20.14	20.28	19.61	20.13	19.82	19.73	19.31	19.77	20.13	20.03	19.72
Na2O	0.46	0.33	0.43	0.44	0.57	0.38	0.67	0.45	0.63	0.30	0.62
K2O	0.00	0.01	0.00	0.03	0.00	0.02	0.00	0.00	0.02	0.01	0.04
Total	98.77	99.95	99.22	99.99	98.46	98.00	97.32	98.40	100.08	98.72	100.61
Cations in Formula (based on 6 oxygen)											
Si	1.82	1.83	1.84	1.82	1.82	1.83	1.81	1.84	1.81	1.83	1.83
Ti	0.06	0.06	0.06	0.06	0.06	0.06	0.08	0.06	0.06	0.06	0.07
Al	0.18	0.18	0.15	0.19	0.15	0.15	0.16	0.15	0.20	0.16	0.18
Cr	0.00	0.00	0.00	0.00	0.00	0.00	0.00	0.00	0.00	0.00	0.00
Fe	0.36	0.36	0.38	0.36	0.40	0.39	0.43	0.39	0.35	0.37	0.38
Mn	0.01	0.01	0.01	0.01	0.01	0.01	0.01	0.01	0.01	0.01	0.01
Mg	0.77	0.75	0.76	0.75	0.76	0.75	0.70	0.73	0.75	0.76	0.73
Ca	0.83	0.82	0.80	0.82	0.82	0.82	0.82	0.82	0.82	0.82	0.80
Na	0.03	0.02	0.03	0.03	0.04	0.03	0.05	0.03	0.05	0.02	0.05
K	0.00	0.00	0.00	0.00	0.00	0.00	0.00	0.00	0.00	0.00	0.00
Sum IV:	2.00	2.01	1.99	2.01	1.97	1.98	1.96	2.00	2.01	1.99	2.01
Sum	1.96	1.93	1.95	1.93	1.98	1.97	1.94	1.94	1.92	1.95	1.91
Wo	42.35%	42.67%	41.30%	42.41%	41.60%	41.81%	41.95%	42.21%	42.55%	42.26%	41.79%
En	39.23%	38.66%	38.94%	39.13%	38.37%	38.23%	36.09%	37.49%	39.02%	38.75%	38.15%
Fs	18.42%	18.67%	19.76%	18.47%	20.03%	19.96%	21.96%	20.30%	18.43%	18.99%	20.06%

APPENDIX 2

Laboratory Description and Monitors

Irradiation Package: AU-37
Median Date of Irradiation: 7/2/21
Monitors, Ages
(as summarized in Schaen et al., 2021):
GA1550 Biotite Age (Ma): 9.944E+07
FC Sanidine Age (Ma): 2.820E+07
Dates of Analyses: 9/17/2021 through 9/29/2021
Measured 40/36 of Air during analyses: 291.6±1.5
Assumed $^{40}Ar/^{36}Ar$ of Air (Nier, 1950): 295.5
Irradiation Production Factors:
$^{(36/37)}$Ca: 0.0003046±0.0000084
$^{(39/37)}$Ca: 0.0007380±0.0000370
$^{(40/39)}$K: 0±0.0044
$^{(38/39)}$Cl: 0.01±0.01

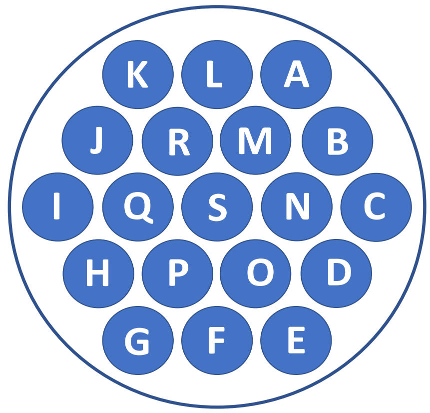

These analyses were determined in the Auburn Noble Isotope Mass Analysis Lab (ANIMAL). The GLM-110 mass spectrometer was used for analysis, that is a 10-cm radius 90° sector instrument with double focusing geometry, a Nier-type source, and a single detector (an ATP discrete dynode-style electron multiplier, see Hames, 2020 for additional description). Samples were fused for gas extraction with a CO_2 laser. Operation of the laser, extraction line and mass spectrometer were fully automated. The time required for one complete analysis cycle is 20 minutes (4 minutes gettering, followed by generally 10 measurements per peak and baseline, 30 measurements of m/e=36). Sample inlet and equilibration time is 5 s for a half-split of a sample and 20 s for an entire sample. Blanks were measured following every 5th analysis. Blank corrections to ^{36}Ar measurements are based on an average or regression of several blanks measured for a given day of analysis. Air aliquots are typically analyzed 3 times per day (generally at the beginning of the day). Data were reduced using an Excel spreadsheet and Isoplot (Ludwig, 2012, Sp. Pub. BGC, 75 p.). Samples were irradiated for 16 hours with Cd shielding in the US Geological Survey TRIGA research reactor in Denver, CO.

Unless indicated otherwise, the data for individual measurements are in volts and errors are the standard deviation of measurement and do not include the error in estimating the J-Value (0.15% at the 95% confidence level). P = Laser Power Level (10 = 100%), t = laser heating time (s). Data are corrected for blank, mass discrimination, and interfering nuclear reactions. The rubric for irradiation filenames is: “AU + package” + “layer, radial position” + “phase” + “planchet hole # and sequence”, saved as a text file. All samples for this study were within layers 2 and 3 of AU37, with positions labeled as in sketch to the right, and the monitor data for these layers are included in the dataset below.

			m/e=40	39	38	37	36	moles 40
A representative anlaysis of a procedural 'blank' during the course of this analytical work.								
blank.9.27.21.d.txt			0.00750 ± 0.000091	0.00023 ± 0.000016	0.00003 ± 0.000011	0.00011 ± 0.000021	0.000055 ± 0.000008	4.60E-17
A representative analysis of air from a pipette during the course of this analysis.								
air.9.27.21.a.txt			11.89496 ± 0.006118	-0.00043 ± 0.000077	0.00773 ± 0.000066	0.00008 ± 0.000036	0.0408516 ± 0.000119	8.09E-14

40Ar/36Ar	40Ar/38Ar
291.17 ± 0.86387	**1539.0 ± 13.25**

Sample	P	t	40Ar (*+atm)	39 ArK	38 (atm+Cl)	37 (Ca)	36 (atm)	Moles 40Ar*	%Rad	R	J-Value	%-sd
Measurements of argon isotopes and the J-value for single crystals of GA-1550 biotite (Layers 2 and 3 of AU37).												
au37.2c.bio.25a.txt	2.5	10	4.98326 ± 0.003577	0.35134 ± 0.000723	0.00234 ± 0.000022	0.01441 ± 0.000115	0.000470 ± 0.000008	3.39E-14	97%	13.78814	0.004049 ± 0.000009	0.2%
au37.2c.bio.26a.txt	2.5	10	3.58179 ± 0.002525	0.24022 ± 0.000412	0.00168 ± 0.000012	0.00206 ± 0.000040	0.000918 ± 0.000011	2.44E-14	92%	13.78174	0.004051 ± 0.000009	0.2%
au37.2c.bio.28a.txt	2.5	10	0.80087 ± 0.000453	0.05620 ± 0.000267	0.00039 ± 0.000009	0.00039 ± 0.000022	0.000098 ± 0.000005	5.45E-15	96%	13.73328	0.004065 ± 0.000022	0.5%
au37.2g.bio.30a.txt	2.5	10	4.24082 ± 0.002888	0.30270 ± 0.000547	0.00191 ± 0.000013	0.00039 ± 0.000013	0.000190 ± 0.000006	2.89E-14	99%	13.82505	0.004038 ± 0.000008	0.2%
au37.2g.bio.31a.txt	2.5	10	0.84599 ± 0.001168	0.05594 ± 0.000262	0.00041 ± 0.000006	0.00008 ± 0.000012	0.000255 ± 0.000005	5.76E-15	91%	13.77505	0.004053 ± 0.000023	0.6%
au37.2g.bio.32a.txt	2.5	10	1.74497 ± 0.000980	0.12661 ± 0.000329	0.00083 ± 0.000008	0.00039 ± 0.000014	0.000031 ± 0.000008	1.19E-14	99%	13.71075	0.004072 ± 0.000012	0.3%
au37.2g.bio.33a.txt	2.5	10	0.88232 ± 0.001082	0.06142 ± 0.000310	0.00036 ± 0.000007	0.00027 ± 0.000012	0.000117 ± 0.000005	6.00E-15	96%	13.80324	0.004044 ± 0.000023	0.6%
au37.2g.bio.34a.txt	2.5	10	1.91402 ± 0.001178	0.13409 ± 0.000309	0.00092 ± 0.000007	0.00078 ± 0.000023	0.000224 ± 0.000006	1.30E-14	97%	13.78089	0.004051 ± 0.000011	0.3%
au37.2k.bio.35a.txt	2.5	10	4.95095 ± 0.003033	0.33044 ± 0.000348	0.00245 ± 0.000019	0.00165 ± 0.000027	0.001346 ± 0.000011	3.37E-14	92%	13.77900	0.004052 ± 0.000006	0.2%
au37.2k.bio.36a.txt	2.5	10	0.80822 ± 0.001015	0.05601 ± 0.000251	0.00042 ± 0.000007	0.00918 ± 0.000067	0.000116 ± 0.000006	5.50E-15	96%	13.81826	0.004040 ± 0.000022	0.5%
au37.2k.bio.37a.txt	2.5	10	1.44811 ± 0.000992	0.09596 ± 0.000280	0.00105 ± 0.000019	0.07989 ± 0.000395	0.000419 ± 0.000008	9.85E-15	91%	13.80239	0.004045 ± 0.000016	0.4%
au37.2k.bio.38a.txt	2.5	10	1.63418 ± 0.001651	0.11676 ± 0.000287	0.00088 ± 0.000011	0.00076 ± 0.000023	0.000078 ± 0.000005	1.11E-14	99%	13.79931	0.004046 ± 0.000012	0.3%
au37.2k.bio.39a.txt	2.5	10	0.53383 ± 0.000633	0.03809 ± 0.000186	0.00026 ± 0.000006	0.00011 ± 0.000011	0.000028 ± 0.000005	3.63E-15	98%	13.79736	0.004046 ± 0.000023	0.6%
au37.2s.bio.40a.txt	2.5	10	4.05207 ± 0.002102	0.28827 ± 0.000720	0.00197 ± 0.000021	0.00118 ± 0.000038	0.000261 ± 0.000010	2.76E-14	98%	13.78856	0.004049 ± 0.000011	0.3%
au37.2s.bio.41a.txt	2.5	10	7.65283 ± 0.006288	0.53261 ± 0.000633	0.00395 ± 0.000031	0.00781 ± 0.000059	0.001033 ± 0.000010	5.21E-14	96%	13.79563	0.004047 ± 0.000006	0.2%
au37.2s.bio.42a.txt	2.5	10	0.44020 ± 0.000619	0.03081 ± 0.000089	0.00021 ± 0.000005	0.00008 ± 0.000019	0.000040 ± 0.000005	2.99E-15	97%	13.90594	0.004015 ± 0.000019	0.5%
au37.2s.bio.43a.txt	2.5	10	0.98463 ± 0.001130	0.06718 ± 0.000202	0.00048 ± 0.000008	0.00009 ± 0.000013	0.000170 ± 0.000006	6.70E-15	95%	13.90705	0.004014 ± 0.000016	0.4%
au37.3a.bio.45a.txt	2.5	10	3.44289 ± 0.002285	0.23913 ± 0.000241	0.00175 ± 0.000022	0.00054 ± 0.000020	0.000372 ± 0.000007	2.34E-14	97%	13.93742	0.004006 ± 0.000006	0.1%
au37.3a.bio.46a.txt	2.5	10	3.91163 ± 0.003621	0.25584 ± 0.000768	0.00189 ± 0.000019	0.00099 ± 0.000032	0.001217 ± 0.000013	2.66E-14	91%	13.88303	0.004021 ± 0.000015	0.4%
au37.3a.bio.47a.txt	2.5	10	2.75687 ± 0.003188	0.19747 ± 0.000402	0.00129 ± 0.000016	0.01085 ± 0.000133	0.000069 ± 0.000005	1.88E-14	99%	13.85812	0.004028 ± 0.000010	0.2%
au37.3a.bio.48a.txt	2.5	10	2.02760 ± 0.001831	0.13853 ± 0.000375	0.00105 ± 0.000023	0.00017 ± 0.000012	0.000384 ± 0.000007	1.38E-14	94%	13.81706	0.004040 ± 0.000013	0.3%
au37.3a.bio.49a.txt	2.5	10	0.88219 ± 0.000955	0.06055 ± 0.000273	0.00039 ± 0.000008	0.00012 ± 0.000014	0.000139 ± 0.000006	6.00E-15	95%	13.88974	0.004019 ± 0.000021	0.5%
au37.3e.bio.50a.txt	2.5	10	5.25516 ± 0.002557	0.36762 ± 0.000815	0.00263 ± 0.000027	0.00174 ± 0.000030	0.000539 ± 0.000011	3.58E-14	97%	13.86197	0.004027 ± 0.000010	0.2%
au37.3e.bio.51a.txt	2.5	10	2.23677 ± 0.001155	0.15593 ± 0.000380	0.00104 ± 0.000011	0.00043 ± 0.000020	0.000247 ± 0.000006	1.52E-14	97%	13.87783	0.004023 ± 0.000011	0.3%
au37.3e.bio.52a.txt	2.5	10	1.47645 ± 0.001176	0.10506 ± 0.000274	0.00071 ± 0.000011	0.00007 ± 0.000014	0.000037 ± 0.000009	1.00E-14	99%	13.94823	0.004002 ± 0.000013	0.3%
au37.3e.bio.53a.txt	2.5	10	2.66973 ± 0.002373	0.18863 ± 0.000303	0.00123 ± 0.000008	0.00054 ± 0.000019	0.000191 ± 0.000007	1.82E-14	98%	13.85414	0.004030 ± 0.000008	0.2%
au37.3e.bio.54a.txt	2.5	10	1.07531 ± 0.001727	0.07639 ± 0.000226	0.00047 ± 0.000007	0.00033 ± 0.000030	0.000040 ± 0.000011	7.32E-15	99%	13.92336	0.004010 ± 0.000019	0.5%
au37.3i.bio.55a.txt	2.5	10	0.47404 ± 0.000533	0.02857 ± 0.000178	0.00024 ± 0.000005	0.00003 ± 0.000011	0.000245 ± 0.000007	3.22E-15	85%	14.05980	0.003971 ± 0.000036	0.9%
au37.3i.bio.56a.txt	2.5	10	2.82708 ± 0.001681	0.18663 ± 0.000388	0.00137 ± 0.000015	0.00032 ± 0.000016	0.000812 ± 0.000009	1.92E-14	92%	13.86192	0.004027 ± 0.000010	0.3%
au37.3i.bio.57a.txt	2.5	10	2.77552 ± 0.001383	0.19791 ± 0.000589	0.00127 ± 0.000017	0.00042 ± 0.000017	0.000125 ± 0.000007	1.89E-14	99%	13.83807	0.004034 ± 0.000013	0.3%
au37.3i.bio.58a.txt	2.5	10	2.55237 ± 0.001647	0.16292 ± 0.000417	0.00121 ± 0.000011	0.00077 ± 0.000022	0.000965 ± 0.000012	1.74E-14	89%	13.91673	0.004011 ± 0.000013	0.3%
au37.3i.bio.59a.txt	2.5	10	1.60070 ± 0.001201	0.10794 ± 0.000274	0.00075 ± 0.000005	0.00044 ± 0.000023	0.000371 ± 0.000009	1.09E-14	93%	13.81436	0.004041 ± 0.000014	0.3%
au37.3s.bio.60a.txt	2.5	10	1.84798 ± 0.001494	0.12605 ± 0.000297	0.00085 ± 0.000008	0.00024 ± 0.000015	0.000347 ± 0.000009	1.26E-14	94%	13.84610	0.004032 ± 0.000012	0.3%
au37.3s.bio.61a.txt	2.5	10	1.14946 ± 0.001215	0.07689 ± 0.000264	0.00058 ± 0.000012	0.00296 ± 0.000033	0.000294 ± 0.000007	7.82E-15	92%	13.81972	0.004040 ± 0.000018	0.4%
au37.3s.bio.62a.txt	2.5	10	0.48656 ± 0.000630	0.03243 ± 0.000173	0.00023 ± 0.000007	0.00008 ± 0.000018	0.000113 ± 0.000006	3.31E-15	93%	13.97738	0.003994 ± 0.000028	0.7%
au37.3s.bio.63a.txt	2.5	10	0.97274 ± 0.001824	0.06961 ± 0.000335	0.00047 ± 0.000006	0.00012 ± 0.000010	0.000048 ± 0.000005	6.62E-15	99%	13.77077	0.004054 ± 0.000022	0.5%
au37.3s.bio.64a.txt	2.5	10	2.07141 ± 0.001670	0.14244 ± 0.000269	0.00096 ± 0.000014	0.00022 ± 0.000020	0.000339 ± 0.000013	1.41E-14	95%	13.83894	0.004034 ± 0.000012	0.3%

Sample	P	t	40Ar (*+atm)	39 ArK	38 (atm+Cl)	37 (Ca)	36 (atm)	Moles 40Ar*	%Rad	R	J-Value	%-sd
Measuremnt of argon isotopes and J-values for the monitor FCS (layers 2 and 3 of AU37).												
au37.2c.san.13a.txt	2.5	10	6.15738 ± 0.006217	1.60349 ± 0.001495	0.00478 ± 0.000024	0.01004 ± 0.000086	0.000022 ± 0.000005	4.19E-14	100%	3.83596	0.0040474 ± 0.0000057	0.14%
au37.2c.san.14a.txt	2.5	10	6.56780 ± 0.007998	1.70332 ± 0.001535	0.00414 ± 0.000033	0.01162 ± 0.000106	0.000115 ± 0.000007	4.47E-14	99%	3.83588	0.0040474 ± 0.0000063	0.16%
au37.2c.san.15a.txt	2.5	10	5.19879 ± 0.005835	1.35437 ± 0.001518	0.00395 ± 0.000025	0.00902 ± 0.000070	0.000006 ± 0.000006	3.54E-14	100%	3.83728	0.0040460 ± 0.0000067	0.17%
au37.2c.san.16a.txt	2.5	10	5.24117 ± 0.002772	1.36169 ± 0.001198	0.00374 ± 0.000013	0.00978 ± 0.000048	0.000085 ± 0.000006	3.57E-14	100%	3.83066	0.0040530 ± 0.0000044	0.11%
au37.2c.san.17a.txt	2.4	10	4.84163 ± 0.006920	1.25313 ± 0.001979	0.00390 ± 0.000026	0.00902 ± 0.000076	0.000036 ± 0.000005	3.29E-14	100%	3.85511	0.0040273 ± 0.0000087	0.22%
au37.2s.san.18a.txt	2.4	10	7.69460 ± 0.010692	1.96932 ± 0.002869	0.00515 ± 0.000031	0.02288 ± 0.000104	0.000299 ± 0.000008	5.23E-14	99%	3.86233	0.0040197 ± 0.0000083	0.21%
au37.2s.san.19a.txt	2.4	10	7.66317 ± 0.009728	1.98697 ± 0.002686	0.00550 ± 0.000026	0.01528 ± 0.000111	0.000133 ± 0.000011	5.21E-14	99%	3.83698	0.0040463 ± 0.0000078	0.19%
au37.2s.san.20a.txt	2.4	10	4.18581 ± 0.005366	1.08604 ± 0.001581	0.00279 ± 0.000022	0.00764 ± 0.000073	0.000001 ± 0.000003	2.85E-14	100%	3.85391	0.0040285 ± 0.0000082	0.20%
au37.2s.san.21a.txt	2.4	10	7.76086 ± 0.009193	2.00331 ± 0.001240	0.00543 ± 0.000023	0.01510 ± 0.000112	0.000237 ± 0.000013	5.28E-14	99%	3.83904	0.0040441 ± 0.0000058	0.14%
au37.2s.san.22a.txt	2.4	10	7.04751 ± 0.010251	1.82007 ± 0.002749	0.00561 ± 0.000033	0.01115 ± 0.000115	0.000212 ± 0.000007	4.79E-14	99%	3.83765	0.0040456 ± 0.0000087	0.21%
au37.3i.san.33a.txt	2.4	10	6.25399 ± 0.004028	1.62306 ± 0.001375	0.00457 ± 0.000030	0.01296 ± 0.000104	0.000028 ± 0.000008	4.25E-14	100%	3.84803	0.0040347 ± 0.0000046	0.12%
au37.3i.san.34a.txt	2.4	10	6.13209 ± 0.004137	1.58807 ± 0.001658	0.00447 ± 0.000019	0.00962 ± 0.000111	-0.000002 -± 0.000017	4.17E-14	100%	3.86172	0.0040204 ± 0.0000052	0.13%
au37.3i.san.35a.txt	2.4	10	8.48256 ± 0.007995	2.19216 ± 0.002199	0.00724 ± 0.000028	0.01411 ± 0.000104	0.000076 ± 0.000009	5.77E-14	100%	3.85920	0.0040230 ± 0.0000057	0.14%
au37.3i.san.36a.txt	2.5	10	9.45375 ± 0.004568	2.44706 ± 0.001288	0.00744 ± 0.000038	0.01679 ± 0.000049	0.000119 ± 0.000010	6.43E-14	100%	3.84897	0.0040337 ± 0.0000032	0.08%
au37.3i.san.37a.txt	2.5	10	5.00117 ± 0.002681	1.28959 ± 0.001236	0.00355 ± 0.000029	0.00929 ± 0.000111	0.000053 ± 0.000008	3.40E-14	100%	3.86585	0.0040161 ± 0.0000048	0.12%
au37.3s.san.38a.txt	2.5	10	8.87477 ± 0.009499	2.30286 ± 0.002066	0.00664 ± 0.000044	0.01687 ± 0.000188	0.000063 ± 0.000010	6.04E-14	100%	3.84578	0.0040370 ± 0.0000058	0.14%
au37.3s.san.39a.txt	2.5	10	6.64066 ± 0.005027	1.71576 ± 0.002557	0.00511 ± 0.000037	0.01258 ± 0.000134	0.000004 ± 0.000004	4.52E-14	100%	3.86977	0.0040120 ± 0.0000069	0.17%
au37.3s.san.40a.txt	2.5	10	8.31488 ± 0.010280	2.15494 ± 0.002186	0.00622 ± 0.000017	0.01431 ± 0.000095	0.000051 ± 0.000008	5.66E-14	100%	3.85156	0.0040310 ± 0.0000066	0.16%
au37.3s.san.41a.txt	2.5	10	5.13946 ± 0.006242	1.33119 ± 0.000929	0.00402 ± 0.000027	0.01003 ± 0.000091	0.000057 ± 0.000008	3.50E-14	100%	3.84826	0.0040344 ± 0.0000060	0.15%
au37.3s.san.42a.txt	2.5	10	6.36338 ± 0.008361	1.56403 ± 0.001413	0.00433 ± 0.000018	0.01622 ± 0.000140	0.001079 ± 0.000010	4.33E-14	95%	3.86465	0.0040173 ± 0.0000070	0.18%

J-Values used for layers 2 and 3 on the basis of GA-1550 and FCS analyses

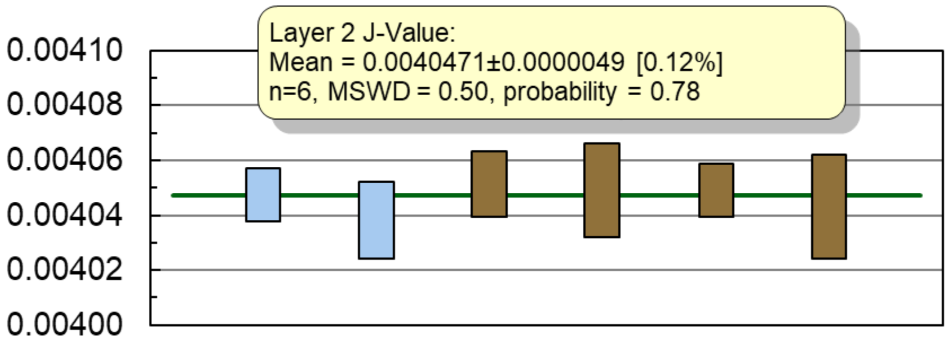

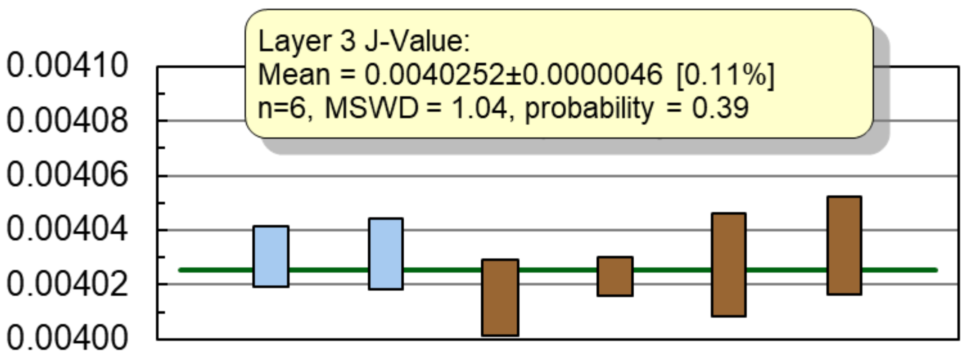

Analysis of Air During This Project

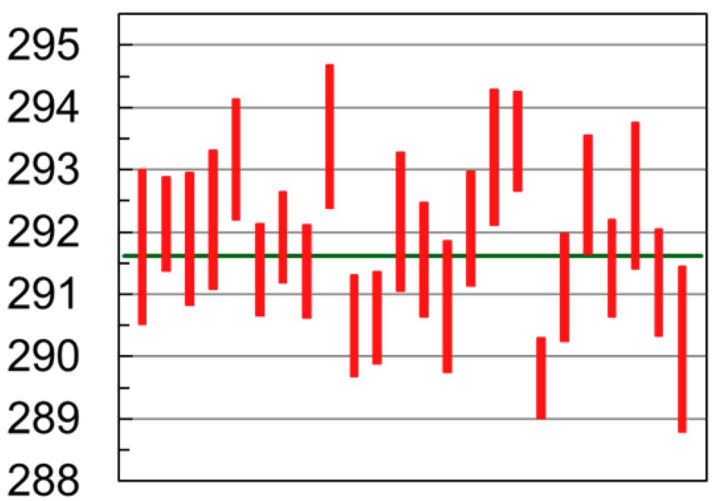

Result of Matrix $^{40}Ar/^{39}Ar$ Dating

Sample	P	t	40Ar (*+atm)	39 ArK	38 (atm+Cl)	37 (Ca)	36 (atm)	Moles 40Ar*	%Rad	R	Age (Ma)	%-sd
Label: LEB-001												
au37.2j.bas.4a.txt	0.6	30	0.01880 ± 0.000194	0.00348 ± 0.000039	0.00002 ± 0.000005	0.01268 ± 0.000090	0.000038 ± 0.000007	1.28E-16	40.8%	2.19926	16.22 ± 4.80	30%
au37.2j.bas.4b.txt	0.7	30	0.04285 ± 0.000180	0.01331 ± 0.000054	0.00005 ± 0.000004	0.05369 ± 0.000573	0.000074 ± 0.000006	2.92E-16	49.0%	1.57717	11.65 ± 1.13	10%
au37.2j.bas.4c.txt	0.7	30	0.04036 ± 0.000190	0.01691 ± 0.000073	0.00007 ± 0.000003	0.06671 ± 0.000355	0.000043 ± 0.000005	2.75E-16	68.2%	1.62765	12.02 ± 0.98	8%
au37.2j.bas.4d.txt	0.8	30	0.05321 ± 0.000177	0.02520 ± 0.000134	0.00006 ± 0.000003	0.09600 ± 0.000490	0.000071 ± 0.000005	3.62E-16	60.4%	1.27623	9.43 ± 0.63	7%
au37.2j.bas.4e.txt	0.8	30	0.05422 ± 0.000369	0.02730 ± 0.000134	0.00018 ± 0.000006	0.10436 ± 0.000646	0.000067 ± 0.000005	3.69E-16	63.4%	1.25903	9.30 ± 0.60	6%
au37.2j.bas.4f.txt	0.9	30	0.06193 ± 0.000349	0.03060 ± 0.000160	0.00147 ± 0.000023	0.11874 ± 0.001003	0.000064 ± 0.000007	4.21E-16	69.3%	1.40227	10.36 ± 0.75	7%
au37.2j.bas.4g.txt	1	30	0.09280 ± 0.000353	0.04152 ± 0.000174	0.00205 ± 0.000041	0.16325 ± 0.000593	0.000149 ± 0.000012	6.31E-16	52.7%	1.17747	8.70 ± 0.82	9%
au37.2j.bas.4h.txt	1.1	30	0.09969 ± 0.000364	0.04459 ± 0.000194	0.00098 ± 0.000016	0.17741 ± 0.001015	0.000163 ± 0.000007	6.78E-16	51.6%	1.15306	8.52 ± 0.45	5%
au37.2j.bas.4i.txt	1.2	30	0.10386 ± 0.000451	0.04428 ± 0.000100	0.00041 ± 0.000008	0.18793 ± 0.000908	0.000166 ± 0.000006	7.07E-16	52.7%	1.23719	9.14 ± 0.41	4%
au37.2j.bas.4j.txt	1.3	30	0.10651 ± 0.000230	0.04338 ± 0.000128	0.00023 ± 0.000008	0.19967 ± 0.001559	0.000172 ± 0.000006	7.25E-16	52.2%	1.28210	9.47 ± 0.40	4%
au37.2j.bas.4k.txt	1.4	30	0.07673 ± 0.000316	0.03222 ± 0.000170	0.00021 ± 0.000009	0.14930 ± 0.000487	0.000128 ± 0.000005	5.22E-16	50.6%	1.20510	8.91 ± 0.50	6%
au37.2j.bas.4l.txt	1.5	30	0.11048 ± 0.000371	0.03681 ± 0.000181	0.00018 ± 0.000005	0.17719 ± 0.001013	0.000231 ± 0.000007	7.52E-16	38.1%	1.14412	8.46 ± 0.50	6%
au37.2j.bas.4m.txt	1.7	30	0.17654 ± 0.000401	0.04193 ± 0.000160	0.00032 ± 0.000005	0.24963 ± 0.001111	0.000419 ± 0.000008	1.20E-15	29.9%	1.25761	9.29 ± 0.53	6%
au37.2j.bas.4n.txt	1.8	30	0.13519 ± 0.000330	0.03540 ± 0.000181	0.00022 ± 0.000005	0.19207 ± 0.001228	0.000305 ± 0.000010	9.20E-16	33.4%	1.27626	9.43 ± 0.73	8%
au37.2j.bas.4o.txt	2	30	0.37042 ± 0.000571	0.06546 ± 0.000184	0.00053 ± 0.000009	0.44503 ± 0.001515	0.000977 ± 0.000010	2.52E-15	22.1%	1.24790	9.22 ± 0.43	5%
au37.2j.bas.4p.txt	2.2	30	0.56008 ± 0.000410	0.08946 ± 0.000267	0.00079 ± 0.000010	0.98900 ± 0.002732	0.001494 ± 0.000012	3.81E-15	21.2%	1.32687	9.80 ± 0.39	4%
au37.2j.bas.4q.txt	2.3	20	0.32385 ± 0.000415	0.05042 ± 0.000137	0.00047 ± 0.000012	0.66534 ± 0.001643	0.000885 ± 0.000008	2.20E-15	19.2%	1.23469	9.12 ± 0.45	5%
au37.2j.bas.4r.txt	2.4	20	0.37865 ± 0.000718	0.06189 ± 0.000198	0.00052 ± 0.000007	0.85809 ± 0.001468	0.001011 ± 0.000017	2.58E-15	21.1%	1.29330	9.56 ± 0.77	8%
au37.2j.bas.4s.txt	2.5	20	0.20561 ± 0.000153	0.03299 ± 0.000140	0.00027 ± 0.000010	0.48017 ± 0.001419	0.000541 ± 0.000007	1.40E-15	22.2%	1.38537	10.23 ± 0.67	7%
au37.2j.bas.4t.txt	2.6	20	0.12522 ± 0.000485	0.02049 ± 0.000120	0.00018 ± 0.000007	0.28954 ± 0.001395	0.000344 ± 0.000008	8.52E-16	18.8%	1.14967	8.50 ± 1.17	14%

Age = 9.25±0.13 Ma
(1σ, including J-error of .125%)
MSWD = 0.85, probability = 0.63
95.6% of the 39Ar, steps 4 through 20

Sample	P	t	40Ar (*+atm)	39 ArK	38 (atm+Cl)	37 (Ca)	36 (atm)	Moles 40Ar*	%Rad	R	Age (Ma)	%-sd
Label: LEB-003												
au37.2q.bas.3a.txt	0.6	30	0.05569 ± 0.000238	0.01360 ± 0.000052	0.00004 ± 0.000003	0.02805 ± 0.000219	0.000121 ± 0.000007	3.79E-16	35.7%	1.46155	10.80 ± 1.27	12%
au37.2q.bas.3b.txt	0.7	30	0.07542 ± 0.000345	0.02346 ± 0.000116	0.00004 ± 0.000003	0.04790 ± 0.000509	0.000149 ± 0.000006	5.13E-16	41.7%	1.34215	9.92 ± 0.66	7%
au37.2q.bas.3c.txt	0.7	30	0.07806 ± 0.000201	0.02801 ± 0.000144	0.00007 ± 0.000004	0.06101 ± 0.000612	0.000134 ± 0.000007	5.31E-16	49.2%	1.36949	10.12 ± 0.64	6%
au37.2q.bas.3d.txt	0.8	30	0.09989 ± 0.000534	0.03714 ± 0.000179	0.00007 ± 0.000001	0.08035 ± 0.000827	0.000172 ± 0.000006	6.80E-16	49.0%	1.31749	9.73 ± 0.44	5%
au37.2q.bas.3e.txt	0.8	30	0.09003 ± 0.000235	0.03263 ± 0.000119	0.00009 ± 0.000004	0.06260 ± 0.000472	0.000157 ± 0.000007	6.12E-16	48.5%	1.33810	9.89 ± 0.54	5%
au37.2q.bas.3f.txt	0.8	30	0.11752 ± 0.000229	0.04648 ± 0.000208	0.00015 ± 0.000005	0.10623 ± 0.000721	0.000197 ± 0.000007	8.00E-16	50.4%	1.27523	9.42 ± 0.41	4%
au37.2q.bas.3g.txt	0.9	30	0.22211 ± 0.000306	0.09718 ± 0.000345	0.00032 ± 0.000006	0.27238 ± 0.001128	0.000323 ± 0.000007	1.51E-15	57.0%	1.30334	9.63 ± 0.20	2%
au37.2q.bas.3h.txt	1	30	0.23203 ± 0.000309	0.10549 ± 0.000342	0.00036 ± 0.000005	0.32889 ± 0.001150	0.000321 ± 0.000007	1.58E-15	59.1%	1.29926	9.60 ± 0.19	2%
au37.2q.bas.3i.txt	1.1	30	0.21348 ± 0.000228	0.09934 ± 0.000315	0.00036 ± 0.000007	0.33869 ± 0.001727	0.000296 ± 0.000006	1.45E-15	59.1%	1.26984	9.38 ± 0.18	2%
au37.2q.bas.3j.txt	1.2	30	0.19411 ± 0.000226	0.08884 ± 0.000168	0.00035 ± 0.000005	0.32837 ± 0.001033	0.000284 ± 0.000007	1.32E-15	56.8%	1.24176	9.18 ± 0.23	3%
au37.2q.bas.3k.txt	1.3	30	0.17854 ± 0.000534	0.07980 ± 0.000209	0.00034 ± 0.000008	0.31676 ± 0.001314	0.000276 ± 0.000006	1.21E-15	54.4%	1.21657	8.99 ± 0.25	3%
au37.2q.bas.3l.txt	1.4	30	0.16521 ± 0.000491	0.06923 ± 0.000263	0.00038 ± 0.000008	0.29111 ± 0.001431	0.000276 ± 0.000008	1.12E-15	50.7%	1.20997	8.94 ± 0.33	4%
au37.2q.bas.3m.txt	1.5	30	0.15568 ± 0.000426	0.05702 ± 0.000256	0.00027 ± 0.000007	0.25830 ± 0.001096	0.000282 ± 0.000008	1.06E-15	46.5%	1.26886	9.38 ± 0.40	4%
au37.2q.bas.3n.txt	1.7	30	0.18793 ± 0.000348	0.05800 ± 0.000234	0.00034 ± 0.000008	0.28291 ± 0.001152	0.000405 ± 0.000008	1.28E-15	36.3%	1.17597	8.69 ± 0.37	4%
au37.2q.bas.3o.txt	1.8	30	0.17983 ± 0.000401	0.05295 ± 0.000186	0.00031 ± 0.000006	0.25573 ± 0.001428	0.000390 ± 0.000008	1.22E-15	35.8%	1.21698	8.99 ± 0.43	5%
au37.2q.bas.3p.txt	2	30	0.31222 ± 0.000364	0.06623 ± 0.000321	0.00049 ± 0.000007	0.41089 ± 0.000750	0.000795 ± 0.000009	2.12E-15	24.8%	1.16915	8.64 ± 0.40	5%
au37.2q.bas.3q.txt	2.2	30	0.34344 ± 0.000519	0.06224 ± 0.000173	0.00052 ± 0.000008	0.53139 ± 0.001328	0.000910 ± 0.000009	2.34E-15	21.7%	1.19625	8.84 ± 0.42	5%
au37.2q.bas.3r.txt	2.3	20	0.28582 ± 0.000802	0.05357 ± 0.000261	0.00037 ± 0.000009	0.44849 ± 0.001971	0.000740 ± 0.000017	1.94E-15	23.5%	1.25393	9.27 ± 0.87	9%
au37.2q.bas.3s.txt	2.4	20	0.24510 ± 0.000347	0.04995 ± 0.000198	0.00039 ± 0.000009	0.39765 ± 0.001569	0.000626 ± 0.000009	1.67E-15	24.5%	1.20403	8.90 ± 0.50	6%
au37.2q.bas.3t.txt	2.5	20	0.21714 ± 0.000202	0.04231 ± 0.000150	0.00033 ± 0.000010	0.37106 ± 0.001438	0.000570 ± 0.000010	1.48E-15	22.4%	1.14867	8.49 ± 0.64	7%
au37.2q.bas.3u.txt	2.6	20	0.15827 ± 0.000561	0.02842 ± 0.000127	0.00026 ± 0.000009	0.27975 ± 0.000989	0.000411 ± 0.000010	1.08E-15	23.2%	1.29080	9.54 ± 0.96	10%

Age = 9.089±0.095 Ma
(1σ, including J-error of .125%)
MSWD = 0.64, probability = 0.81
67.8% of the 39Ar, steps 9 through 21

Sample	P	t	40Ar (*+atm)	39 ArK	38 (atm+Cl)	37 (Ca)	36 (atm)	Moles 40Ar*	%Rad	R	Age (Ma)	%-sd
Label: DE16-001												
au37.2n.bas.2a.txt	0.6	30	0.04096 ± 0.000290	0.00301 ± 0.000044	0.00003 ± 0.000009	0.01342 ± 0.000174	0.000107 ± 0.000010	2.79E-16	22.7%	3.08623	22.72 ± 7.72	34%
au37.2n.bas.2b.txt	0.7	30	0.07204 ± 0.000322	0.00529 ± 0.000049	0.00001 ± 0.000006	0.03184 ± 0.000323	0.000209 ± 0.000011	4.90E-16	14.3%	1.94910	14.38 ± 4.71	33%
au37.2n.bas.2c.txt	0.7	30	0.09334 ± 0.000325	0.01058 ± 0.000057	0.00007 ± 0.000009	0.06621 ± 0.000446	0.000264 ± 0.000010	6.35E-16	16.3%	1.43678	10.61 ± 2.25	21%
au37.2n.bas.2d.txt	0.8	30	0.12274 ± 0.000358	0.02110 ± 0.000150	0.00019 ± 0.000015	0.16387 ± 0.001022	0.000302 ± 0.000010	8.35E-16	27.3%	1.58608	11.71 ± 1.28	11%
au37.2n.bas.2e.txt	0.8	30	0.09968 ± 0.000440	0.02172 ± 0.000187	0.00004 ± 0.000004	0.19621 ± 0.001155	0.000255 ± 0.000010	6.78E-16	24.5%	1.12398	8.31 ± 1.32	16%
au37.2n.bas.2g.txt	1	30	0.23576 ± 0.000293	0.03672 ± 0.000185	0.00026 ± 0.000010	0.44867 ± 0.001591	0.000636 ± 0.000011	1.60E-15	20.3%	1.30351	9.63 ± 0.83	9%
au37.2n.bas.2h.txt	1.1	30	0.25020 ± 0.000328	0.04591 ± 0.000257	0.00020 ± 0.000008	0.49153 ± 0.001355	0.000668 ± 0.000027	1.70E-15	21.1%	1.14883	8.49 ± 1.58	19%
au37.2n.bas.2i.txt	1.2	30	0.14495 ± 0.000602	0.06723 ± 0.000322	0.00015 ± 0.000004	0.47561 ± 0.001611	0.000205 ± 0.000011	9.86E-16	58.3%	1.25648	9.28 ± 0.64	7%
au37.2n.bas.2j.txt	1.3	30	0.12565 ± 0.000409	0.08170 ± 0.000298	0.00025 ± 0.000006	0.43875 ± 0.001213	0.000101 ± 0.000006	8.55E-16	76.2%	1.17191	8.66 ± 0.36	4%
au37.2n.bas.2k.txt	1.4	30	0.10188 ± 0.000411	0.07201 ± 0.000262	0.00018 ± 0.000006	0.32289 ± 0.000953	0.000024 ± 0.000002	6.93E-16	93.0%	1.31518	9.72 ± 0.29	3%
au37.2n.bas.2l.txt	1.5	30	0.06818 ± 0.000205	0.04869 ± 0.000176	0.00015 ± 0.000006	0.17443 ± 0.000764	0.000017 ± 0.000005	4.64E-16	92.5%	1.29503	9.57 ± 0.97	10%
au37.2n.bas.2m.txt	1.7	30	0.07879 ± 0.000225	0.05221 ± 0.000199	0.00023 ± 0.000009	0.18471 ± 0.000937	0.000048 ± 0.000012	5.36E-16	82.1%	1.23938	9.16 ± 1.05	11%
au37.2n.bas.2n.txt	1.8	30	0.09456 ± 0.000300	0.05211 ± 0.000280	0.00028 ± 0.000011	0.28583 ± 0.001573	0.000078 ± 0.000012	6.43E-16	75.7%	1.37297	10.14 ± 1.05	10%
au37.2n.bas.2o.txt	2	30	0.09506 ± 0.000410	0.04741 ± 0.000078	0.00032 ± 0.000009	0.45245 ± 0.002099	0.000118 ± 0.000010	6.47E-16	63.2%	1.26760	9.37 ± 1.01	11%
au37.2n.bas.2p.txt	2.2	30	0.14752 ± 0.000310	0.05607 ± 0.000190	0.00035 ± 0.000011	0.77111 ± 0.001596	0.000267 ± 0.000014	1.00E-15	46.5%	1.22265	9.04 ± 1.03	11%
au37.2n.bas.2q.txt	2.3	20	0.14415 ± 0.000347	0.04962 ± 0.000190	0.00035 ± 0.000013	0.73518 ± 0.001696	0.000284 ± 0.000014	9.81E-16	41.8%	1.21461	8.98 ± 1.06	12%
au37.2n.bas.2r.txt	2.4	20	0.07708 ± 0.000269	0.02819 ± 0.000090	0.00021 ± 0.000010	0.43750 ± 0.001305	0.000124 ± 0.000010	5.24E-16	52.4%	1.43386	10.59 ± 1.57	15%
au37.2n.bas.2s.txt	2.5	20	0.06373 ± 0.000328	0.02491 ± 0.000092	0.00015 ± 0.000008	0.34343 ± 0.001274	0.000098 ± 0.000012	4.34E-16	54.4%	1.39249	10.29 ± 2.13	21%
au37.2n.bas.2t.txt	2.6	20	0.05768 ± 0.000203	0.02243 ± 0.000181	0.00014 ± 0.000009	0.29070 ± 0.001423	0.000092 ± 0.000011	3.92E-16	53.1%	1.36466	10.08 ± 2.15	21%

Age = 9.40±0.18 Ma
(1σ, including J-error of .125%)
MSWD = 0.88, probability = 0.60
100% of the 39Ar, steps 1 through 19

Sample	P	t	40Ar (*+atm)	39 ArK	38 (atm+Cl)	37 (Ca)	36 (atm)	Moles 40Ar*	%Rad	R	Age (Ma)	%-sd
SW19-DD01												
au37.3b.mat.4a.txt	0.6	30	0.13686 ± 0.000448	0.00360 ± 0.000045	0.00011 ± 0.000021	0.01438 ± 0.000169	0.000458 ± 0.000016	9.31E-16	1.1%	0.42666	3.14 ± 11.11	354%
au37.3b.mat.4b.txt	0.7	30	0.06473 ± 0.000248	0.00446 ± 0.000048	0.00004 ± 0.000013	0.01813 ± 0.000245	0.000183 ± 0.000015	4.40E-16	16.3%	2.36551	17.35 ± 7.52	43%
au37.3b.mat.4c.txt	0.7	30	0.03959 ± 0.000275	0.00521 ± 0.000047	0.00005 ± 0.000012	0.02199 ± 0.000195	0.000118 ± 0.000014	2.69E-16	12.2%	0.92363	6.79 ± 6.19	91%
au37.3b.mat.4d.txt	0.8	30	0.05510 ± 0.000209	0.00980 ± 0.000061	0.00005 ± 0.000008	0.04161 ± 0.000277	0.000149 ± 0.000013	3.75E-16	20.1%	1.12964	8.30 ± 3.20	39%
au37.3b.mat.4e.txt	0.8	30	0.03377 ± 0.000205	0.00934 ± 0.000054	0.00001 ± 0.000003	0.03875 ± 0.000310	0.000082 ± 0.000013	2.30E-16	28.3%	1.02225	7.52 ± 3.38	45%
au37.3b.bas.4a.txt	0.9	30	0.04211 ± 0.000277	0.01451 ± 0.000085	0.00003 ± 0.000003	0.06223 ± 0.000414	0.000072 ± 0.000010	2.86E-16	49.1%	1.42586	10.48 ± 1.90	18%
au37.3b.bas.4b.txt	1	30	0.07671 ± 0.000287	0.02869 ± 0.000129	0.00004 ± 0.000003	0.14848 ± 0.000964	0.000127 ± 0.000010	5.22E-16	51.1%	1.36512	10.03 ± 1.04	10%
au37.3b.bas.4c.txt	1.1	30	0.10017 ± 0.000417	0.03459 ± 0.000245	0.00011 ± 0.000006	0.25563 ± 0.001121	0.000187 ± 0.000010	6.81E-16	44.9%	1.30137	9.56 ± 0.91	10%
au37.3b.bas.4d.txt	1.1	30	0.04068 ± 0.000185	0.02018 ± 0.000110	0.00006 ± 0.000004	0.10351 ± 0.000356	0.000046 ± 0.000009	2.77E-16	66.7%	1.34521	9.88 ± 1.61	16%
au37.3b.bas.4e.txt	1.2	30	0.06631 ± 0.000173	0.03773 ± 0.000206	0.00010 ± 0.000004	0.18650 ± 0.001087	0.000056 ± 0.000007	4.51E-16	74.9%	1.31702	9.68 ± 0.76	8%
au37.3b.bas.4f.txt	1.3	30	0.08744 ± 0.000348	0.05414 ± 0.000170	0.00011 ± 0.000004	0.24998 ± 0.001882	0.000057 ± 0.000006	5.95E-16	80.7%	1.30303	9.58 ± 0.55	6%
au37.3b.bas.4g.txt	1.4	30	0.08039 ± 0.000400	0.05454 ± 0.000141	0.00013 ± 0.000005	0.23048 ± 0.001211	0.000048 ± 0.000006	5.47E-16	82.4%	1.21426	8.93 ± 0.57	6%
au37.3b.bas.4h.txt	1.5	30	0.09139 ± 0.000269	0.06300 ± 0.000246	0.00018 ± 0.000004	0.25925 ± 0.000698	0.000036 ± 0.000005	6.22E-16	88.3%	1.28042	9.41 ± 0.54	6%
au37.3b.bas.4i.txt	1.7	30	0.11479 ± 0.000400	0.08002 ± 0.000266	0.00025 ± 0.000007	0.31349 ± 0.000769	0.000037 ± 0.000004	7.81E-16	90.5%	1.29769	9.54 ± 0.42	4%
au37.3b.bas.4j.txt	1.8	30	0.13885 ± 0.000467	0.09781 ± 0.000248	0.00025 ± 0.000007	0.36506 ± 0.001740	0.000079 ± 0.000007	9.45E-16	83.2%	1.18145	8.68 ± 0.35	4%
au37.3b.bas.4k.txt	2	30	0.14130 ± 0.000313	0.09208 ± 0.000237	0.00028 ± 0.000005	0.33113 ± 0.000969	0.000099 ± 0.000008	9.61E-16	79.3%	1.21629	8.94 ± 0.40	4%
au37.3b.bas.4l.txt	2.2	30	0.14982 ± 0.000394	0.08708 ± 0.000285	0.00034 ± 0.000008	0.29832 ± 0.001477	0.000164 ± 0.000009	1.02E-15	67.7%	1.16545	8.57 ± 0.34	4%
au37.3b.bas.4m.txt	2.4	30	0.13627 ± 0.000382	0.07604 ± 0.000167	0.00032 ± 0.000009	0.25378 ± 0.001126	0.000137 ± 0.000008	9.27E-16	70.2%	1.25797	9.25 ± 0.37	4%
au37.3b.bas.4n.txt	2.5	30	0.09646 ± 0.000251	0.05110 ± 0.000252	0.00032 ± 0.000015	0.17345 ± 0.001234	0.000118 ± 0.000008	6.56E-16	63.8%	1.20346	8.85 ± 0.51	6%
au37.3b.bas.4o.txt	2.6	20	0.06323 ± 0.000315	0.03416 ± 0.000167	0.00020 ± 0.000011	0.11429 ± 0.000734	0.000042 ± 0.000011	4.30E-16	80.4%	1.48859	10.94 ± 1.32	12%
au37.3b.bas.4p.txt	2.7	20	0.06571 ± 0.000297	0.03443 ± 0.000143	0.00019 ± 0.000014	0.12712 ± 0.000850	0.000097 ± 0.000009	4.47E-16	56.4%	1.07616	7.91 ± 0.80	10%

Age = 9.06±0.13 Ma
(1σ, including J-error of .125%)
MSWD = 0.75, probability = 0.78
100% of the 39Ar, steps 1 through 21

Result of Broken Pieces Plagioclase $^{40}Ar/^{39}Ar$ Dating

Sample	P	t	40Ar (*+atm)	39 ArK	38 (atm+Cl)	37 (Ca)	36 (atm)	Moles 40Ar*	%Rad	R	Age (Ma)	%-sd
Label: LEB-001												
au37.2h.plg.5a.txt	0.6	30	0.01469 ± 0.000177	0.00076 ± 0.000043	-0.00004 ± 0.000021	0.01574 ± 0.000144	0.000007 ± 0.000008	9.99E-17	85.8%	16.66004	119.44 ± 39.84	33%
au37.2h.plg.5b.txt	0.7	30	0.01235 ± 0.000151	0.00098 ± 0.000042	0.00000 -± 0.000002	0.02178 ± 0.000159	0.000037 ± 0.000007	8.40E-17	11.9%	1.50615	11.12 ± 17.94	161%
au37.2h.plg.5c.txt	0.7	30	0.01504 ± 0.000188	0.00135 ± 0.000047	0.00001 ± 0.000009	0.04152 ± 0.000570	0.000041 ± 0.000006	1.02E-16	18.5%	2.06903	15.26 ± 13.13	86%
au37.2h.plg.5d.txt	0.8	30	0.02083 ± 0.000185	0.00262 ± 0.000036	0.00000 ± 0.000001	0.08846 ± 0.000521	0.000060 ± 0.000006	1.42E-16	14.7%	1.17256	8.67 ± 6.81	79%
au37.2h.plg.5e.txt	0.8	30	0.01935 ± 0.000124	0.00310 ± 0.000045	-0.00002 -± 0.000019	0.11871 ± 0.000456	0.000047 ± 0.000005	1.32E-16	27.9%	1.74114	12.85 ± 5.73	45%
au37.2h.plg.5f.txt	0.9	30	0.04131 ± 0.000254	0.00623 ± 0.000051	-0.00003 -± 0.000021	0.24287 ± 0.001063	0.000106 ± 0.000005	2.81E-16	24.5%	1.62398	11.99 ± 2.82	24%
au37.2h.plg.5g.txt	1	30	0.03983 ± 0.000192	0.00763 ± 0.000053	0.00001 ± 0.000003	0.32272 ± 0.000915	0.000072 ± 0.000003	2.71E-16	46.5%	2.42976	17.91 ± 2.32	13%
au37.2h.plg.5h.txt	1.1	30	0.07183 ± 0.000317	0.01325 ± 0.000071	0.00004 ± 0.000004	0.52370 ± 0.002290	0.000083 ± 0.000005	4.89E-16	65.8%	3.56487	26.22 ± 2.21	8%
au37.2h.plg.5i.txt	1.2	30	0.06785 ± 0.000198	0.01477 ± 0.000130	0.00005 ± 0.000005	0.57574 ± 0.001947	0.000071 ± 0.000003	4.62E-16	69.0%	3.17214	23.35 ± 1.39	6%
au37.2h.plg.5j.txt	1.3	30	0.06112 ± 0.000217	0.01477 ± 0.000066	0.00005 ± 0.000005	0.61318 ± 0.001647	0.000056 ± 0.000002	4.16E-16	73.1%	3.02712	22.29 ± 1.43	6%
au37.2h.plg.5k.txt	1.4	30	0.05520 ± 0.000178	0.01158 ± 0.000150	0.00002 ± 0.000002	0.47192 ± 0.000750	0.000050 ± 0.000003	3.76E-16	73.0%	3.47855	25.59 ± 1.90	7%
au37.2h.plg.5l.txt	1.5	30	0.06453 ± 0.000227	0.01520 ± 0.000071	0.00003 ± 0.000004	0.65113 ± 0.002489	0.000075 ± 0.000002	4.39E-16	65.6%	2.78307	20.50 ± 1.25	6%
au37.2h.plg.5m.txt	1.7	30	0.07464 ± 0.000202	0.01675 ± 0.000071	0.00003 ± 0.000003	0.69248 ± 0.001533	0.000052 ± 0.000002	5.08E-16	79.3%	3.53238	25.98 ± 1.37	5%
au37.2h.plg.5n.txt	1.8	30	0.12345 ± 0.000527	0.02149 ± 0.000137	0.00009 ± 0.000006	0.78463 ± 0.002223	0.000090 ± 0.000003	8.40E-16	78.6%	4.51469	33.14 ± 1.28	4%
au37.2h.plg.5o.txt	2	30	0.19831 ± 0.000454	0.03021 ± 0.000077	0.00012 ± 0.000006	1.12161 ± 0.003131	0.000111 ± 0.000003	1.35E-15	83.5%	5.48067	40.16 ± 0.83	2%
au37.2h.plg.5p.txt	2.2	30	0.05003 ± 0.000266	0.01543 ± 0.000096	0.00004 ± 0.000004	0.74037 ± 0.001721	0.000055 ± 0.000002	3.40E-16	67.5%	2.18727	16.13 ± 1.47	9%
au37.2h.plg.5q.txt	2.4	30	0.08613 ± 0.000400	0.02815 ± 0.000129	0.00008 ± 0.000005	1.48325 ± 0.001875	0.000084 ± 0.000002	5.86E-16	71.1%	2.17617	16.05 ± 0.87	5%
au37.2h.plg.5r.txt	2.5	20	0.05163 ± 0.000293	0.02080 ± 0.000109	0.00006 ± 0.000005	1.08677 ± 0.001558	0.000027 ± 0.000001	3.51E-16	84.4%	2.09581	15.46 ± 1.20	8%
au37.2h.plg.5s.txt	2.6	20	0.03585 ± 0.000142	0.01454 ± 0.000084	0.00002 ± 0.000002	0.78196 ± 0.001998	0.000008 ± 0.000000	2.44E-16	93.3%	2.30164	16.97 ± 1.35	8%
au37.2h.plg.5t.txt	2.7	20	0.04677 ± 0.000203	0.02233 ± 0.000113	0.00006 ± 0.000004	1.23499 ± 0.002371	0.000019 ± 0.000001	3.18E-16	87.7%	1.83795	13.57 ± 1.00	7%

Discordant spectrum:
Minimum ~10 Ma, max ~35 at 50% 39ArK

Sample	P	t	40Ar (*+atm)	39 ArK	38 (atm+Cl)	37 (Ca)	36 (atm)	Moles 40Ar*	%Rad	R	Age (Ma)	%-sd
Label: LEB-003												
au37.2r.plg.7a.txt	0.6	30	0.01745 ± 0.000171	0.00045 ± 0.000039	0.00001 ± 0.000014	0.00637 ± 0.000129	0.000063 ± 0.000009	1.19E-16	-6.0%	-2.35018	-17.49 -± 58.93	337%
au37.2r.plg.7b.txt	0.7	30	0.02405 ± 0.000123	0.00140 ± 0.000072	-0.00001 -± 0.001626	0.03343 ± 0.000121	0.000081 ± 0.000008	1.64E-16	0.3%	0.05327	0.39 ± 16.47	4174%
au37.2r.plg.7c.txt	0.7	30	0.02165 ± 0.000235	0.00238 ± 0.000043	0.00000 ± 0.000003	0.08171 ± 0.000401	0.000061 ± 0.000006	1.47E-16	16.2%	1.46751	10.84 ± 7.55	70%
au37.2r.plg.7d.txt	0.8	30	0.02238 ± 0.000189	0.00359 ± 0.000039	0.00000 -± 0.000001	0.15165 ± 0.000699	0.000055 ± 0.000005	1.52E-16	27.6%	1.71996	12.70 ± 5.45	43%
au37.2r.plg.7e.txt	0.8	30	0.02004 ± 0.000146	0.00430 ± 0.000038	0.00002 ± 0.000006	0.19413 ± 0.000936	0.000057 ± 0.000005	1.36E-16	15.7%	0.73236	5.42 ± 4.75	88%
au37.2r.plg.7f.txt	0.9	30	0.02305 ± 0.000204	0.00598 ± 0.000050	-0.00001 -± 0.000002	0.28743 ± 0.001035	0.000045 ± 0.000004	1.57E-16	42.9%	1.65252	12.20 ± 4.10	34%
au37.2r.plg.7g.txt	1	30	0.03303 ± 0.000166	0.00907 ± 0.000050	0.00000 ± 0.000001	0.45081 ± 0.001482	0.000052 ± 0.000003	2.25E-16	53.8%	1.95870	14.45 ± 2.56	18%
au37.2r.plg.7h.txt	1.1	30	0.03883 ± 0.000243	0.01078 ± 0.000045	-0.00001 -± 0.000002	0.53891 ± 0.001955	0.000031 ± 0.000003	2.64E-16	76.3%	2.74722	20.24 ± 3.90	19%
au37.2r.plg.7i.txt	1.2	30	0.03602 ± 0.000201	0.01145 ± 0.000083	0.00001 ± 0.000002	0.59311 ± 0.000946	0.000051 ± 0.000002	2.45E-16	58.3%	1.83448	13.54 ± 1.98	15%
au37.2r.plg.7j.txt	1.3	30	0.09065 ± 0.000206	0.01135 ± 0.000051	0.00003 ± 0.000005	0.57274 ± 0.001893	0.000017 ± 0.000002	6.17E-16	94.5%	7.55063	55.10 ± 3.15	6%
au37.2r.plg.7k.txt	1.4	30	0.05799 ± 0.000303	0.01302 ± 0.000055	0.00001 ± 0.000002	0.67458 ± 0.002384	0.000058 ± 0.000003	3.95E-16	70.7%	3.14691	23.17 ± 2.07	9%
au37.2r.plg.7l.txt	1.5	30	0.04308 ± 0.000229	0.01322 ± 0.000075	0.00004 ± 0.000005	0.70029 ± 0.001579	0.000044 ± 0.000002	2.93E-16	69.6%	2.26656	16.71 ± 1.51	9%
au37.2r.plg.7m.txt	1.7	30	0.06481 ± 0.000283	0.01827 ± 0.000152	0.00004 ± 0.000004	0.94898 ± 0.002025	0.000073 ± 0.000002	4.41E-16	66.6%	2.36315	17.42 ± 1.45	8%
au37.2r.plg.7n.txt	1.8	30	0.07253 ± 0.000248	0.02161 ± 0.000136	0.00001 ± 0.000001	1.13244 ± 0.002136	0.000110 ± 0.000003	4.93E-16	55.0%	1.84597	13.62 ± 1.21	9%
au37.2r.plg.7o.txt	2	30	0.07450 ± 0.000274	0.02736 ± 0.000140	0.00006 ± 0.000004	1.45018 ± 0.001979	0.000049 ± 0.000001	5.07E-16	80.6%	2.19481	16.19 ± 0.96	6%
au37.2r.plg.7p.txt	2.2	30	0.05651 ± 0.000227	0.02323 ± 0.000109	0.00005 ± 0.000004	1.21690 ± 0.002582	0.000040 ± 0.000001	3.84E-16	78.9%	1.91859	14.16 ± 1.02	7%
au37.2r.plg.7q.txt	2.4	20	0.04204 ± 0.000310	0.02068 ± 0.000107	0.00006 ± 0.000005	1.11377 ± 0.002590	0.000010 ± 0.000000	2.86E-16	93.3%	1.89588	13.99 ± 1.04	7%
au37.2r.plg.7r.txt	2.5	20	0.01752 ± 0.000136	0.00862 ± 0.000043	0.00001 ± 0.000003	0.46309 ± 0.001878	-0.000003 ± 0.000000	1.19E-16	104.5%	2.12453	15.67 ± 2.46	16%
au37.2r.plg.7s.txt	2.6	20	0.01566 ± 0.000155	0.00766 ± 0.000051	-0.00001 -± 0.000003	0.41872 ± 0.000949	0.000003 ± 0.000000	1.07E-16	95.0%	1.94194	14.33 ± 2.62	18%
au37.2r.plg.7t.txt	2.7	20	0.02656 ± 0.000189	0.01283 ± 0.000043	0.00002 ± 0.000002	0.71796 ± 0.001298	-0.000006 ± 0.000000	1.81E-16	106.3%	2.20081	16.23 ± 1.49	9%

Age = 15.20±0.43 Ma
(1σ, including J-error of .125%)
MSWD = 1.14, probability = 0.33
67.5% of the 39Ar, steps 12 through 20

Sample	P	t	40Ar (*+atm)	39 ArK	38 (atm+Cl)	37 (Ca)	36 (atm)	Moles 40Ar*	%Rad	R	Age (Ma)	%-sd
Label: DE16-001												
au37.2m.plg.6a.txt	0.6	30	0.24368 ± 0.000196	0.00079 ± 0.000036	0.00015 ± 0.000020	0.09797 ± 0.000584	0.000805 ± 0.000011	1.66E-15	2.4%	7.49415	55 ± 139	255%
au37.2m.plg.6b.txt	0.7	30	0.01696 ± 0.000169	0.00069 ± 0.000046	0.00000 ± 0.000001	0.03693 ± 0.000362	0.000044 ± 0.000007	1.15E-16	23.7%	5.79713	42.45 ± 31.97	75%
au37.2m.plg.6c.txt	0.7	30	0.02939 ± 0.000285	0.00086 ± 0.000050	0.00002 ± 0.000013	0.04512 ± 0.000335	0.000089 ± 0.000009	2.00E-16	10.5%	3.61158	26.56 ± 31.70	119%
au37.2m.plg.6d.txt	0.8	30	0.04093 ± 0.000146	0.00151 ± 0.000056	0.00000 ± 0.000003	0.14802 ± 0.000900	0.000121 ± 0.000008	2.78E-16	12.7%	3.45930	25.45 ± 18.51	73%
au37.2m.plg.6e.txt	0.8	30	0.04599 ± 0.000197	0.00149 ± 0.000040	0.00000 -± 0.000010	0.22756 ± 0.000682	0.000123 ± 0.000006	3.13E-16	20.7%	6.38294	46.69 ± 14.47	31%
au37.2m.plg.6f.txt	0.9	30	0.04651 ± 0.000205	0.00226 ± 0.000040	0.00002 ± 0.000010	0.35520 ± 0.000949	0.000104 ± 0.000005	3.16E-16	33.7%	6.94225	50.72 ± 9.68	19%
au37.2m.plg.6g.txt	1	30	0.04346 ± 0.000244	0.00243 ± 0.000038	0.00000 ± 0.000001	0.50899 ± 0.001284	0.000098 ± 0.000004	2.96E-16	33.6%	6.00806	43.98 ± 8.33	19%
au37.2m.plg.6h.txt	1.1	30	0.06762 ± 0.000231	0.00310 ± 0.000053	0.00003 ± 0.000010	0.61628 ± 0.001637	0.000194 ± 0.000006	4.60E-16	15.1%	3.28736	24.19 ± 8.38	35%
au37.2m.plg.6i.txt	1.2	30	0.07524 ± 0.000196	0.00290 ± 0.000057	0.00004 ± 0.000011	0.75415 ± 0.002618	0.000164 ± 0.000008	5.12E-16	35.4%	9.18817	66.83 ± 13.53	20%
au37.2m.plg.6j.txt	1.3	30	0.12160 ± 0.000439	0.00470 ± 0.000083	0.00007 ± 0.000013	0.88538 ± 0.002563	0.000300 ± 0.000011	8.27E-16	27.1%	7.00869	51.20 ± 9.73	19%
au37.2m.plg.6k.txt	1.4	30	0.07760 ± 0.000292	0.00722 ± 0.000040	0.00003 ± 0.000009	0.86374 ± 0.001758	0.000184 ± 0.000004	5.28E-16	30.1%	3.23482	23.81 ± 2.93	12%
au37.2m.plg.6l.txt	1.5	30	0.06770 ± 0.000316	0.00744 ± 0.000051	0.00005 ± 0.000010	0.94332 ± 0.001694	0.000151 ± 0.000004	4.61E-16	34.0%	3.09053	22.75 ± 3.42	15%
au37.2m.plg.6m.txt	1.7	30	0.06836 ± 0.000404	0.00786 ± 0.000046	0.00003 ± 0.000006	0.95211 ± 0.002799	0.000140 ± 0.000003	4.65E-16	39.3%	3.42392	25.19 ± 2.87	11%
au37.2m.plg.6n.txt	1.8	30	0.13156 ± 0.000545	0.01120 ± 0.000063	0.00008 ± 0.000008	0.90801 ± 0.001623	0.000325 ± 0.000007	8.95E-16	27.0%	3.17219	23.35 ± 2.50	11%
au37.2m.plg.6o.txt	2	30	0.05720 ± 0.000226	0.01866 ± 0.000070	0.00005 ± 0.000005	1.00700 ± 0.002014	0.000045 ± 0.000001	3.89E-16	76.7%	2.35166	17.34 ± 1.08	6%
au37.2m.plg.6p.txt	2.2	30	0.03177 ± 0.000201	0.01093 ± 0.000090	0.00000 ± 0.000000	0.62465 ± 0.001616	-0.000049 -± 0.000006	2.16E-16	145.4%	4.22770	31.05 ± 3.09	10%
au37.2m.plg.6q.txt	2.4	20	0.05242 ± 0.000185	0.01604 ± 0.000084	0.00005 ± 0.000006	0.93872 ± 0.001968	0.000049 ± 0.000002	3.57E-16	72.3%	2.36484	17.44 ± 1.53	9%
au37.2m.plg.6r.txt	2.5	20	0.01758 ± 0.000144	0.00813 ± 0.000049	0.00000 ± 0.000000	0.46619 ± 0.001498	-0.000047 -± 0.000007	1.20E-16	178.4%	3.86080	28.38 ± 3.87	14%
au37.2m.plg.6s.txt	2.6	20	0.02435 ± 0.000146	0.00944 ± 0.000043	-0.00001 -± 0.000001	0.57056 ± 0.001966	-0.000020 -± 0.000002	1.66E-16	123.9%	3.19470	23.52 ± 3.57	15%
au37.2m.plg.6t.txt	2.7	20	0.01633 ± 0.000166	0.00879 ± 0.000056	0.00000 ± 0.000000	0.52383 ± 0.002225	-0.000056 -± 0.000010	1.11E-16	201.6%	3.74373	27.53 ± 4.34	16%

Discordant spectrum:
Minimum ~17 Ma at 50% 39ArK

Sample	P	t	40Ar (*+atm)	39 ArK	38 (atm+Cl)	37 (Ca)	36 (atm)	Moles 40Ar*	%Rad	R	Age (Ma)	%-sd
Label: SW19-DD01												
au37.3f.plg.6a.txt	0.6	30	0.02585 ± 0.000138	0.00134 ± 0.000045	0.00000 -± 0.000003	0.00752 ± 0.000196	0.000035 ± 0.000022	1.76E-16	59.8%	11.54706	83.16 ± 37.52	45%
au37.3f.plg.6b.txt	0.7	30	0.01224 ± 0.000180	0.00043 ± 0.000041	0.00002 ± 0.000028	0.00676 ± 0.000095	-0.000007 ± 0.000030	8.33E-17	115.8%	29.69784	206.70 ± 99.71	48%
au37.3f.plg.6c.txt	0.7	30	0.00896 ± 0.000158	0.00034 ± 0.000041	0.00011 ± 0.000035	0.00931 ± 0.000215	0.000043 ± 0.000012	6.09E-17	-40.3%	-10.67669	-80.41 -± 92.24	115%
au37.3f.plg.6d.txt	0.8	30	0.00764 ± 0.000141	0.00060 ± 0.000030	0.00001 ± 0.000013	0.01594 ± 0.000222	0.000016 ± 0.000009	5.20E-17	36.2%	4.56989	33.37 ± 41.75	125%
au37.3f.plg.6e.txt	0.8	30	0.00572 ± 0.000125	0.00066 ± 0.000027	-0.00001 ± 0.000083	0.02250 ± 0.000279	0.000011 ± 0.000008	3.89E-17	41.9%	3.61129	26.42 ± 40.66	154%
au37.3f.plg.6f.txt	0.9	30	0.00938 ± 0.000142	0.00154 ± 0.000042	-0.00009 ± 0.000025	0.05186 ± 0.000491	-0.000003 -± 0.000002	6.38E-17	108.3%	6.58958	47.92 ± 14.24	30%
au37.3f.plg.6g.txt	1	30	0.01019 ± 0.000193	0.00213 ± 0.000036	-0.00003 ± 0.000061	0.08553 ± 0.000355	-0.000028 ± 0.000338	6.93E-17	180.4%	8.38097	60.73 ± 19.76	33%
au37.3f.plg.6h.txt	1.1	30	0.01153 ± 0.000162	0.00279 ± 0.000031	-0.00002 -± 0.000087	0.12453 ± 0.000623	0.000031 ± 0.000005	7.85E-17	20.6%	0.85085	6.26 ± 8.09	129%
au37.3f.plg.6i.txt	1.2	30	0.01173 ± 0.000145	0.00352 ± 0.000040	-0.00005 ± 0.000083	0.16002 ± 0.000531	-0.000016 -± 0.000006	7.98E-17	139.8%	4.66562	34.06 ± 7.37	22%
au37.3f.plg.6j.txt	1.3	30	0.01134 ± 0.000173	0.00407 ± 0.000034	0.00000 ± 0.000001	0.18943 ± 0.001244	0.000016 ± 0.000002	7.71E-17	58.0%	1.61427	11.86 ± 5.29	45%
au37.3f.plg.6k.txt	1.4	30	0.01422 ± 0.000188	0.00471 ± 0.000031	0.00009 ± 0.000023	0.22851 ± 0.001664	0.000064 ± 0.000010	9.67E-17	-32.7%	-0.98860	-7.30 -± 8.94	123%
au37.3f.plg.6l.txt	1.5	30	0.01220 ± 0.000199	0.00463 ± 0.000050	-0.00002 -± 0.000010	0.21947 ± 0.001026	0.000102 ± 0.000011	8.30E-17	-146.0%	-3.84548	-28.56 -± 8.49	30%
au37.3f.plg.6m.txt	1.7	30	0.01398 ± 0.000165	0.00551 ± 0.000039	-0.00001 -± 0.000002	0.26148 ± 0.001620	0.000077 ± 0.000009	9.51E-17	-62.6%	-1.58767	-11.74 -± 7.09	60%
au37.3f.plg.6n.txt	1.8	30	0.02481 ± 0.000239	0.00839 ± 0.000066	0.00001 ± 0.000001	0.39813 ± 0.001460	0.000098 ± 0.000010	1.69E-16	-17.3%	-0.51175	-3.77 -± 5.78	153%
au37.3f.plg.6o.txt	2	30	0.02486 ± 0.000245	0.00925 ± 0.000065	-0.00001 -± 0.000002	0.42657 ± 0.002112	0.000102 ± 0.000008	1.69E-16	-21.5%	-0.57804	-4.26 -± 4.28	100%
au37.3f.plg.6p.txt	2.2	30	0.02241 ± 0.000145	0.00846 ± 0.000056	0.00001 ± 0.000001	0.41554 ± 0.002751	0.000040 ± 0.000005	1.52E-16	47.1%	1.24762	9.17 ± 5.16	56%
au37.3f.plg.6q.txt	2.4	30	0.05933 ± 0.000290	0.01224 ± 0.000055	0.00004 ± 0.000006	0.60979 ± 0.002314	0.000061 ± 0.000005	4.04E-16	69.8%	3.38224	24.75 ± 3.62	15%
au37.3f.plg.6r.txt	2.5	30	0.04970 ± 0.000156	0.01293 ± 0.000051	0.00008 ± 0.000009	0.64960 ± 0.002039	0.000099 ± 0.000007	3.38E-16	41.3%	1.58899	11.67 ± 3.37	29%
au37.3f.plg.6s.txt	2.6	20	0.02274 ± 0.000174	0.00630 ± 0.000047	0.00004 ± 0.000011	0.31485 ± 0.001278	0.000039 ± 0.000006	1.55E-16	49.8%	1.79569	13.18 ± 6.96	53%
au37.3f.plg.6t.txt	2.7	20	0.01771 ± 0.000233	0.00574 ± 0.000054	-0.00001 -± 0.000002	0.29015 ± 0.000942	0.000059 ± 0.000008	1.20E-16	1.2%	0.03787	0.28 ± 7.41	2657%

Discordant spectrum:
Minimum ~10 Ma, max ~35 at 50% 39ArK

Result of Single Megacryst Plagioclase $^{40}Ar/^{39}Ar$ Dating

Sample	P	t	40Ar (*+atm)	39 ArK	38 (atm+Cl)	37 (Ca)	36 (atm)	Moles 40Ar*	%Rad	R	Age (Ma)	%-sd
Label: LEBC-1												
au37.2f.plg.2a.txt	0.6	30	0.02173 ± 0.000137	0.00012 ± 0.000035	0.00000 ± 0.000013	0.00424 ± 0.000121	0.000042 ± 0.000014	1.48E-16	43.3%	78.96323	507.61 ± 447.50	88%
au37.2f.plg.2b.txt	0.7	30	0.02477 ± 0.000242	0.00060 ± 0.000031	0.00001 ± 0.000016	0.01915 ± 0.000181	0.000072 ± 0.000014	1.69E-16	14.3%	5.88264	43.07 ± 57.78	134%
au37.2f.plg.2c.txt	0.7	30	0.02145 ± 0.000172	0.00073 ± 0.000050	0.00000 -± 0.000018	0.02780 ± 0.000154	0.000123 ± 0.000019	1.46E-16	-68.9%	-20.20275	-156.14 -± 67.97	44%
au37.2f.plg.2d.txt	0.8	30	0.02786 ± 0.000199	0.00132 ± 0.000034	0.00003 ± 0.000019	0.04937 ± 0.000292	0.000104 ± 0.000013	1.90E-16	-10.7%	-2.24889	-16.74 -± 25.28	151%
au37.2f.plg.2e.txt	0.8	30	0.02736 ± 0.000178	0.00191 ± 0.000055	0.00001 ± 0.000010	0.07747 ± 0.000706	0.000085 ± 0.000012	1.86E-16	8.3%	1.18919	8.79 ± 17.07	194%
au37.2f.plg.2f.txt	0.9	30	0.03220 ± 0.000199	0.00342 ± 0.000040	0.00002 ± 0.000009	0.13793 ± 0.000741	0.000096 ± 0.000010	2.19E-16	11.5%	1.08464	8.02 ± 9.07	113%
au37.2f.plg.2g.txt	1	30	0.04574 ± 0.000333	0.00667 ± 0.000031	0.00000 ± 0.000000	0.26045 ± 0.001079	0.000167 ± 0.000017	3.11E-16	-7.7%	-0.52636	-3.90 -± 8.04	206%
au37.2f.plg.2h.txt	1.1	30	0.04018 ± 0.000247	0.00733 ± 0.000038	0.00004 ± 0.000010	0.29661 ± 0.001739	0.000120 ± 0.000009	2.73E-16	11.6%	0.63867	4.73 ± 4.45	94%
au37.2f.plg.2i.txt	1.2	30	0.03521 ± 0.000189	0.00757 ± 0.000047	0.00001 ± 0.000003	0.29546 ± 0.001959	0.000036 ± 0.000007	2.40E-16	70.2%	3.26123	24.00 ± 7.14	30%
au37.2f.plg.2j.txt	1.3	30	0.03571 ± 0.000168	0.00864 ± 0.000053	0.00001 ± 0.000002	0.34581 ± 0.001856	0.000064 ± 0.000006	2.43E-16	47.1%	1.94588	14.36 ± 3.87	27%
au37.2f.plg.2k.txt	1.4	30	0.03558 ± 0.000219	0.00855 ± 0.000063	-0.00001 -± 0.000005	0.34263 ± 0.001760	0.000051 ± 0.000005	2.42E-16	57.2%	2.38178	17.56 ± 3.48	20%
au37.2f.plg.2l.txt	1.5	30	0.03529 ± 0.000136	0.01011 ± 0.000044	0.00003 ± 0.000005	0.39471 ± 0.001500	0.000019 ± 0.000002	2.40E-16	84.4%	2.94624	21.70 ± 3.30	15%
au37.2f.plg.2m.txt	1.7	30	0.05093 ± 0.000320	0.01562 ± 0.000112	-0.00003 -± 0.000012	0.61750 ± 0.001459	0.000068 ± 0.000003	3.46E-16	60.7%	1.97746	14.59 ± 1.82	12%
au37.2f.plg.2n.txt	1.8	30	0.07182 ± 0.000263	0.02069 ± 0.000146	0.00006 ± 0.000005	0.80180 ± 0.002267	0.000161 ± 0.000008	4.89E-16	33.9%	1.17713	8.70 ± 2.11	24%
au37.2f.plg.2o.txt	2	30	0.08370 ± 0.000345	0.02881 ± 0.000178	0.00010 ± 0.000008	1.13486 ± 0.001114	0.000103 ± 0.000003	5.69E-16	63.7%	1.84995	13.65 ± 1.10	8%
au37.2f.plg.2p.txt	2.2	30	0.06729 ± 0.000250	0.02323 ± 0.000195	0.00005 ± 0.000004	0.89122 ± 0.002974	0.000102 ± 0.000007	4.58E-16	55.0%	1.59383	11.77 ± 2.25	19%

Age = 13.71±0.74 Ma
(1σ, including J-error of .125%)
MSWD = 2.3, probability = 0.027
84.8% of the 39Ar, steps 9 through 16

Sample	P	t	40Ar (*+atm)	39 ArK	38 (atm+Cl)	37 (Ca)	36 (atm)	Moles 40Ar*	%Rad	R	Age (Ma)	%-sd
Label: DE16-CY												
au37.2l.plg.1a.txt	0.6	30	0.02343 ± 0.000265	0.00022 ± 0.000033	-0.00004 ± 0.000023	0.00395 ± 0.000079	0.000077 ± 0.000014	1.59E-16	2.5%	2.61642	19.28 ± 209.56	1087%
au37.2l.plg.1b.txt	0.7	30	0.03556 ± 0.000239	0.00069 ± 0.000029	0.00000 ± 0.000006	0.01852 ± 0.000077	0.000114 ± 0.000014	2.42E-16	5.0%	2.58314	19.04 ± 49.48	260%
au37.2l.plg.1c.txt	0.7	30	0.02642 ± 0.000231	0.00076 ± 0.000034	-0.00002 ± 0.000049	0.03728 ± 0.000198	0.000115 ± 0.000012	1.80E-16	-28.9%	-10.01458	-75.74 -± 43.62	58%
au37.2l.plg.1d.txt	0.8	30	0.01552 ± 0.000176	0.00103 ± 0.000033	0.00000 ± 0.000005	0.04741 ± 0.000185	0.000052 ± 0.000010	1.06E-16	1.0%	0.15009	1.11 ± 27.62	2485%
au37.2l.plg.1e.txt	0.8	30	0.01412 ± 0.000191	0.00135 ± 0.000024	-0.00004 ± 0.000036	0.06430 ± 0.000651	0.000027 ± 0.000008	9.60E-17	43.5%	4.56055	33.48 ± 20.89	62%
au37.2l.plg.1f.txt	0.9	30	0.01855 ± 0.000223	0.00138 ± 0.000028	0.00005 ± 0.000018	0.06266 ± 0.000264	-0.000004 -± 0.000007	1.26E-16	106.3%	14.26630	102.75 ± 37.93	37%
au37.2l.plg.1g.txt	1	30	0.03037 ± 0.000163	0.00348 ± 0.000046	0.00005 ± 0.000014	0.16545 ± 0.000894	0.000073 ± 0.000007	2.07E-16	29.0%	2.53781	18.70 ± 7.64	41%
au37.2l.plg.1h.txt	1.1	30	0.03394 ± 0.000197	0.00556 ± 0.000034	0.00006 ± 0.000014	0.26761 ± 0.001244	0.000070 ± 0.000006	2.31E-16	39.0%	2.37920	17.54 ± 4.85	28%
au37.2l.plg.1i.txt	1.2	30	0.03477 ± 0.000225	0.00690 ± 0.000045	0.00007 ± 0.000009	0.34170 ± 0.001050	0.000094 ± 0.000006	2.37E-16	20.2%	1.01807	7.53 ± 3.85	51%
au37.2l.plg.1j.txt	1.3	30	0.03709 ± 0.000370	0.00843 ± 0.000058	0.00007 ± 0.000008	0.41771 ± 0.001491	0.000068 ± 0.000004	2.52E-16	45.8%	2.01608	14.87 ± 3.11	21%
au37.2l.plg.1k.txt	1.4	30	0.04508 ± 0.000205	0.01141 ± 0.000066	0.00008 ± 0.000011	0.57282 ± 0.002764	0.000056 ± 0.000005	3.07E-16	63.2%	2.49600	18.40 ± 4.12	22%
au37.2l.plg.1l.txt	1.5	30	0.02668 ± 0.000203	0.00825 ± 0.000041	0.00001 ± 0.000004	0.41995 ± 0.001049	0.000066 ± 0.000004	1.81E-16	26.7%	0.86271	6.38 ± 3.06	48%
au37.2l.plg.1m.txt	1.7	30	0.03385 ± 0.000234	0.01014 ± 0.000119	0.00005 ± 0.000005	0.50009 ± 0.001317	0.000068 ± 0.000004	2.30E-16	40.5%	1.35075	9.98 ± 2.68	27%
au37.2l.plg.1n.txt	1.8	30	0.05027 ± 0.000226	0.01490 ± 0.000058	0.00005 ± 0.000006	0.76614 ± 0.002333	0.000106 ± 0.000004	3.42E-16	37.7%	1.27157	9.40 ± 1.74	19%
au37.2l.plg.1o.txt	2	30	0.07657 ± 0.000230	0.02041 ± 0.000098	0.00010 ± 0.000007	1.02052 ± 0.002595	0.000163 ± 0.000005	5.21E-16	37.0%	1.38769	10.25 ± 1.61	16%
au37.2l.plg.1p.txt	2.2	30	0.07852 ± 0.000266	0.02274 ± 0.000140	0.00009 ± 0.000010	1.12652 ± 0.004518	0.000144 ± 0.000004	5.34E-16	45.8%	1.58294	11.69 ± 1.31	11%
au37.2l.plg.1q.txt	2.3	30	0.04889 ± 0.000385	0.01613 ± 0.000141	0.00002 ± 0.000003	0.80716 ± 0.001878	0.000073 ± 0.000004	3.33E-16	55.6%	1.68445	12.44 ± 2.12	17%
au37.2l.plg.1r.txt	2.4	30	0.04014 ± 0.000314	0.01409 ± 0.000080	0.00000 ± 0.000001	0.70324 ± 0.002845	0.000063 ± 0.000003	2.73E-16	53.5%	1.52424	11.26 ± 1.89	17%
au37.2l.plg.1s.txt	2.5	20	0.04492 ± 0.000306	0.01366 ± 0.000058	0.00006 ± 0.000009	0.68623 ± 0.002050	0.000053 ± 0.000003	3.06E-16	65.0%	2.13729	15.77 ± 2.50	16%
au37.2l.plg.1t.txt	2.6	20	0.02284 ± 0.000187	0.00805 ± 0.000070	0.00004 ± 0.000007	0.41080 ± 0.002478	0.000037 ± 0.000003	1.55E-16	51.6%	1.46552	10.82 ± 3.20	30%

Age = 11.45±0.62 Ma
(1σ, including J-error of .125%)
MSWD = 1.4, probability = 0.11
100% of the 39Ar, steps 1 through 20